

Nanyang Technological University



Biodegradable Ocular Implant for Sustained Drug Delivery

Peng Yan

School of Materials Science and Engineering (MSE)

2011

Biodegradable Ocular Implant for Sustained Drug Delivery

A thesis submitted to the Nanyang Technological University
in partial fulfillment of the requirement for the degree of
Doctor of Philosophy

by

Peng Yan

School of Materials Science and Engineering (MSE)

2011

Acknowledgements

I would like to extend my sincere gratitude to my immediate thesis advisor, Prof. Subbu S. Venkatraman for his continuous supervision until the completion of my PhD project. His advice and guidance saw the materializing of this research work.

My heart-felt thanks is extended to my co-supervisor Dr. Tina Wong, ophthalmological expert of Singapore National Eye Centre (SNEC) and Singapore Eye Research Institute (SERI), for her great vision and support in terms of ophthalmic knowledge, practical clinical application and *in vivo* studies. Her knowledge and expertise have been a great source of inspiration.

My gratefulness also goes to my co-supervisor Prof. Zbigniew Stachurski of Australia National University, Canberra, Australia, for his encouragement and patient guidance throughout the PhD study.

Special thanks to Dr. Marcus Ang, Selin Foo and the rest of research staff from SERI (Singapore Eye Research Institute) and SNEC (Singapore National Eye Center) for conducting the *in vivo* studies. Thanks to Ms. Ma Zhen for the method development of HPLC; Dr. Luan Deyan for her help in writing the MATLAB codes for modelling; Mr. Au Jun Duan Reuben for verifying some of the experimental results.

Many thanks also to all the technical staff in School of Materials Science & Engineering to provide warmest help when I was doing the experiment works. I would like to thank all the research staffs and students who have helped in one way or another.

Lastly, I am grateful to Singapore National Research Foundation-Funded Translational & Clinical Research (TCR) Programme Grant for sponsoring my PhD research study.

Table of Contents

Acknowledgements	i
Table of Contents	ii
List of Figures	v
List of Tables	xii
List of Abbreviations	xiii
Abstract	xiv
Chapter 1 Introduction	
1.1 Background	1
1.2 Problem statement	3
1.3 Hypothesis	4
1.4 Objectives	4
1.5 Novelty	5
1.6 Scope	6
1.7 Overviews	6
Chapter 2 Literature Review	8
2.1 Background of ocular drug delivery	8
2.1.1 <i>Anatomy of human eye</i>	8
2.1.2 <i>Introduction to glaucoma</i>	9
2.1.3 <i>Current challenges of drug delivery systems for glaucoma treatment</i>	10
2.1.4 <i>Current approaches in ocular drug delivery</i>	11
2.2 Biodegradable polymers and biodegradation	14
2.2.1 <i>Lactide-based polymers</i>	15
2.2.2 <i>Hydrolytic biodegradation of lactide-based polymers</i>	17
2.2.3 <i>Fick's law of diffusion</i>	21
2.3 Drug delivery systems	25
2.3.1 <i>Diffusion-controlled systems</i>	25
2.3.2 <i>Degradation-controlled systems</i>	25
2.4 Drug release kinetics and mathematical models	26
2.4.1 <i>Models of non-degradable release system</i>	26

2.4.2 <i>Models of degradable release system</i>	29
2.5 Conclusion	31
Chapter 3 Materials and Methods	32
3.1 Materials	32
3.1.1 <i>Polymers</i>	32
3.1.2 <i>Solvents and reagents</i>	32
3.2 Experimental Methods	33
3.2.1 <i>Sample preparation</i>	33
3.2.2 <i>In vitro degradation study</i>	34
3.2.3 <i>In vivo degradation study</i>	35
3.2.4 <i>Measurement of water sorption in PLC7030</i>	37
3.2.5 <i>In vitro drug release study</i>	38
3.2.6 <i>Quantification of PA loaded in the PLC film and released in buffer</i>	39
3.2.7 <i>In vivo drug release study</i>	39
3.2.8 <i>Statistical analysis</i>	40
Chapter 4 Characterization of Candidate Materials	41
4.1 Experimental results	42
4.1.1 <i>In vitro degradation study</i>	42
4.1.2 <i>In vivo degradation study</i>	51
4.2 Discussions	55
4.2.1 <i>Degradation period of PLGA5347 and PLC7030</i>	55
4.2.2 <i>Bulk degradation or surface erosion?</i>	56
4.3 Conclusions	58
Chapter 5 Study of Degradation Behaviours of PLC7030	60
5.1 Results and Discussions	61
5.1.1 <i>Effect of sample shape</i>	61
5.1.2 <i>Effect of film thickness</i>	70
5.1.3 <i>Effect of degradation media</i>	79
5.2 Mathematical Modelling and Experiments on Degradation	84
5.2.1 <i>Calculation of N</i>	85

5.2.2 Calculation of λ	86
5.2.3 Diffusion coefficient of water D_{eff}	86
5.2.4 Analysis on degradation behaviour of PLC7030 with thickness 500 μ m	89
5.2.5 Prediction of critical thickness of PLC7030	91
5.3 Conclusions	94
Chapter 6 Study of Drug Release from PLC7030 Films	96
6.1 Results and Discussion	97
6.1.1 In vitro degradation study of drug loaded films (250 μ m)	98
6.1.2 In vitro drug release - Effect of drug loading	103
6.1.3. In vitro drug release - Effect of film thickness	115
6.1.4 In vitro and in vivo drug release- 20%-loaded PLC7030 film (80 μ m)	124
6.2 Mathematical Modeling of Drug Release	127
6.2.1 Effect of drug loading	129
6.2.2 Comparison of in vitro and in vivo release	132
6.2.3 Summary	134
6.3 Conclusions	135
Chapter 7 Conclusions and Future Recommendations	136
7.1 Final Conclusions	136
7.1.1 Characterization and selection of candidate material	136
7.1.2 Degradation study of PLC7030	137
7.1.3 Drug release study from PLC7030	138
7.2 Future Recommendations	140
7.2.1 In vitro degradation study of PLC7030	140
7.2.2 Various types of drug loaded for drug release study	140
7.2.3 Multi-layers design to achieve multiple drug release	141
References	142

List of Figures

Figure 2.1	Anatomy of the anterior segment of the human eye	8
Figure 2.2	The classical treatment paradigm for glaucoma	9
Figure 2.3	Schematic demonstration of laser trabeculoplasty	10
Figure 2.4	Synthesis of (A) poly lactic acid and (B) poly glycolic acid by poly-condensation	16
Figure 2.5	Synthesis of poly lactide-co-glycolide (A) and poly lactide-co- ϵ -caprolactone (B)	16
Figure 2.6	Schematic illustrations of surface erosion and bulk erosion	19
Figure 2.7	Schematic presentation of one-dimensional diffusion of a specimen exposed on both sides to moisture	22
Figure 2.8	Schematic demonstration of mass uptake for film in an infinite medium (Case I)	24
Figure 3.1	Demonstration of AS-OCT graph	36
Figure 4.1(I)	<i>In vitro</i> water absorption of PLGA5347 and PLC7030 (500 μ m)	44
Figure 4.1(II)	<i>In vitro</i> water absorption of PLC7030 (500 μ m) (expanded Y-axis)	44
Figure 4.2(I)	<i>In vitro</i> mass loss of PLGA5347 and PLC7030 (500 μ m)	45
Figure 4.2(II)	<i>In vitro</i> mass loss of PLC7030 (500 μ m) (Expanded Y-axis)	46
Figure 4.2(III)	Dependence of mass loss of polymers on degradation time, pH7.4, 37°C	46
Figure 4.3	Monitoring of Mw for PLGA5347 and PLC7030 in vitro (500 μ m)	47

Figure 4.4	Monitoring of PDI for PLGA5347 and PLC7030 <i>in vitro</i> (500µm)	48
Figure 4.5(I)	SEM images of cross-section (left column) and morphology (right column) of PLC7030 films (500µm)	49
Figure 4.5(II)	Change of film thickness of PLGA5347 and PLC7030 <i>in vitro</i> (500µm)	50
Figure 4.6	Slit-lamp photographs of PLGA5347 and PLC7030 microfilms after surgical insertion into the subconjunctival space of rabbits eyes at 1, 3 and 6 months (500µm)	51
Figure 4.7	AS-OCT scans of PLGA5347 and PLC7030 microfilms after subconjunctival implantation in rabbits' eyes at 0, 1, 3 and 6 months (500µm)	52
Figure 4.8	Serial AS-OCT thickness measurements of PLGA5347 and PLC7030 microfilms in subconjunctival space (500µm)	53
Figure 4.9	Change of thickness for PLGA and PLC microfilms, <i>in vitro</i> and <i>in vivo</i> (500µm)	54
Figure 4.10(I)	Demonstration of homogeneous degradation behavior	57
Figure 4.10 (II)	Demonstration of heterogeneous degradation behavior	57
Figure 4.10 (III)	Schematic illustration of surface erosion and bulk erosion	58
Figure 5.1	Mass losses of PLC7030 square, rectangle and disk samples (250µm), pH7.4, 37°C	62
Figure 5.2	Monitoring of weight average molecular mass of PLC7030 square, rectangle and disk samples (250µm), pH7.4, 37°C	63
Figure 5.3	Monitoring of number average molecular mass of PLC7030 square, rectangle and disk samples (250µm), pH7.4, 37°C	64

Figure 5.4	Changes of polydispersity index with time of PLC7030 square, rectangle and disk samples (250 μ m), pH7.4, 37°C	64
Figure 5.5	Slit lamp photographs of rectangle and disk samples in the rabbit eyes	66
Figure 5.6	Observation and measurement of film thickness (rectangle and disk) by AS-OCT	66
Figure 5.7	Comparison of rectangle and disk film thicknesses <i>in vivo</i> (rabbit eyes)	67
Figure 5.8	Monitoring of M_w of PLC7030 rectangle and disk samples (250 μ m), <i>in vivo</i>	68
Figure 5.9	Monitoring of M_n of PLC7030 rectangle and disk samples (250 μ m), <i>in vitro</i>	69
Figure 5.10	Changes of polydispersity index with time of PLC7030 rectangle and disk samples (250 μ m), <i>in vivo</i>	69
Figure 5.11	Mass loss of PLC7030 films, 500, 250 and 80 μ m, <i>in vitro</i> , pH7.4, 37°C	71
Figure 5.12	Monitoring of M_w for PLC7030 films, 500, 250 and 80 μ m, <i>in vitro</i> , pH7.4, 37°C	72
Figure 5.13	Monitoring of M_n for PLC7030 films, 500, 250 and 80 μ m, <i>in vitro</i> , pH7.4, 37°C	73
Figure 5.14	List of λ for rectangle PLC7030 films, 500, 250 and 80 μ m, <i>in vitro</i> , pH7.4, 37°C	73
Figure 5.15	SEM images of cross-section 250 μ m (left column) and 500 μ m (right column) thick PLC7030 films <i>in vitro</i> , pH7.4, 37°C	75

Figure 5.16	Monitoring of thickness for PLC7030 films, 500, 250 and 80 μm , <i>in vitro</i> , pH7.4, 37°C	76
Figure 5.17	Slit lamp and AS-OCT photographs of PLC7030 after subconjunctival implantation in rabbits' eyes at 0, 1 and 3 months (250 μm , scale bar=500 μm)	77
Figure 5.18	Monitoring of thickness change, PLC7030 (500 μm and 250 μm) <i>in vivo</i>	78
Figure 5.19	Monitoring of M_w of PLC7030 rectangle film in PBS buffer (pH7.4) and in subconjunctival space of rabbit eyes (250 μm)	80
Figure 5.20	Monitoring of M_n of PLC7030 rectangle film in PBS buffer (pH7.4) and in subconjunctival space of rabbit eyes (250 μm)	80
Figure 5.21	Monitoring of change in thickness of PLC7030 rectangle film in PBS buffer (pH7.4) and in subconjunctival space of rabbit eyes (250 μm)	81
Figure 5.22	Monitoring of M_w of PLC7030 disk sample in PBS buffer (pH7.4) and subconjunctival space of rabbit eyes (250 μm)	82
Figure 5.23	Monitoring of M_n of PLC7030 disk sample in PBS buffer (pH7.4) and subconjunctival space of rabbit eyes (250 μm)	83
Figure 5.24	Monitoring of change in thickness of PLC7030 disk film in PBS buffer (pH7.4) and in subconjunctival space of rabbit eyes (250 μm)	84
Figure 5.25	Water sorption curves for PLC7030 (250 μm) samples in PBS	87
Figure 5.26	Dependence of critical thickness (L_{critical}) on the diffusion coefficient of water (D_{eff}) and degradation rate constant (λ) for PLC7030	92

Figure 5.27	Determination of $L_{critical}$ with different De_{eff} and λ values for PLC7030	93
Figure 6.1	Water absorption of PLC7030 films (250 μ m), with 0%, 5%, 10% and 20% PA (PBS pH7.4, 37°C)	98
Figure 6.2	Mass loss from PLC7030 films (250 μ m), with 0%, 5%, 10% and 20% PA (PBS pH7.4, 37°C)	99
Figure 6.3	A two-dimensional representation of random distributed drug particles in polymer matrix (filled squares) (Idea adopted from Ctierke and Hsu)	100
Figure 6.4	SEM images of 250 μ m 5%, 10% and 20% prednisolone acetate-loaded PLC7030 films in PBS buffer at 0 day, 30 day and 63 day(PBS pH7.4, 37°C)	101
Figure 6.5	Monitoring of M_w of PLC7030 films (250 μ m), with 0, 5%, 10% and 20% PA (PBS pH7.4, 37°C)	102
Figure 6.6	Monitoring of M_n of PLC7030 films (250 μ m), with 0, 5%, 10% and 20% PA(PBS pH7.4, 37°C)	102
Figure 6.7	MDSC curves of pure prednisolone acetate drug powder and PLC7030 film loaded with 20% prednisolone acetate	103
Figure 6.8	Comparison of theoretical loading and actual loading of PA-loaded PLC7030	104
Figure 6.9	Cumulative release (weight) of PA from 5%, 10% and 20% loaded PLC films (250 μ m, PBS pH7.4, 37°C)	105
Figure 6.10	Rate of release (weight) of PA from 5%, 10% and 20% loaded PLC films (250 μ m, PBS pH7.4, 37°C)	106
Figure 6.11	Schematic demonstration of drug release from PA-loaded	106

	PLC7030 films in the first 30 days	
Figure 6.12	Cumulative release (%) of PA from 5%, 10% and 20% loaded PLC films (250 μ m, PBS pH7.4, 37°C)	108
Figure 6.13	Rate of release (weight percentage) of PA from 5%, 10% and 20% loaded PLC films (250 μ m, PBS pH7.4, 37°C)	108
Figure 6.14	Cumulative release of PA from 5%, 10% and 20% loaded PLC7030 films (500 μ m, PBS pH7.4, 37°C) , (A) is the cumulative weight, (B) is the cumulative weight fraction	111
Figure 6.15	Schematic demonstration of drug release from PA-loaded PLC7030 films	112
Figure 6.16	Cumulative drug released and residual drug in the remaining films	113
Figure 6.17	Rate of release of PA from 5%, 10% and 20% loaded PLC7030 films (500 μ m, PBS pH7.4, 37°C) , (A) is the weight per day, (B) is the weight fraction per day	114
Figure 6.18	Cumulative releases (weight) of PA-loaded PLC7030 films with thickness 40 μ m, 80 μ m, 250 μ m and 500 μ m (PBS pH7.4, 37°C), (A) 5%, (B) 10% and (C) 20%	120
Figure 6.19	Release rates (weight) of PA-loaded PLC7030 films with thickness 40 μ m, 80 μ m, 250 μ m and 500 μ m (PBS pH7.4, 37°C), (A) 5%, (B) 10% and (C) 20%	121
Figure 6.20	Cumulative releases (%) of PA-loaded PLC7030 films with thickness 40 μ m, 80 μ m, 250 μ m and 500 μ m (PBS pH7.4, 37°C), (A) 5%, (B) 10% and (C) 20%	122
Figure 6.21	Release rates (%) of PA-loaded PLC7030 films with	123

thickness 40µm, 80µm, 250µm and 500µm (PBS pH7.4, 37°C), (A) 5%, (B) 10% and (C) 20%

Figure 6.22	Cumulative releases of 20% PA-loaded PLC7030 films with thickness 80µm, <i>in vitro</i> and <i>in vivo</i> (A) weight and (B) weight percentage	125
Figure 6.23	Cumulative releases of 20% PA-loaded PLC7030 films with thickness 80µm, <i>in vitro</i> and <i>in vivo</i>	126
Figure 6.24	Experimental and model data fitting of prednisolone acetate release from PLC7030 films (80µm thick) with (A) 5%, (B) 10% and (C) 20% loadings	131
Figure 6.25	Experimental and model data fitting of <i>in vivo</i> prednisolone acetate release from PLC7030 films (80µm thick) 20% loadings	133

List of Tables

Table 2.1	Current commercially available ocular drug delivery systems	12
Table 4.1	Physical properties of PLGA5347 and PLC7030 (500 μm)	42
Table 5.1	Parameters of PLC7030 degradation study	60
Table 5.2	List of λ for square, rectangle and disk PLC7030 films in the <i>in vitro</i> degradation	65
Table 5.3	List of λ for rectangle and disk PLC7030 films in the <i>in vivo</i> degradation	70
Table 5.4	List of calculated parameters for 250 μm <i>in vitro</i> and <i>in vivo</i> PLC7030 samples	88
Table 6.1	Physical properties of prednisolone acetate and prednisolone	97
Table 6.2	Actual loading of PA-loaded PLC7030 films with different thicknesses	116
Table 6.3	List of first order degradation rate constant for PA-loaded PLC7030	129
Table 6.4	Model parameters for prednisolone acetate release from PLC7030 80 μm thick films	132
Table 6.5	Model parameters for prednisolone acetate release from PLC7030 80 μm thick films, <i>in vitro</i> and <i>in vivo</i>	134

List of Abbreviations

PLGA5347	Poly d,l-lactide-co-glycolide 53/47
PLC7030	Poly d,l-lactide-co- ϵ -caprolactone 70/30
GFS	Glaucoma Filtration Surgery
PA	Prednisolone Acetate
IOP	Intraocular Pressure
ROP	Ring Opening Polymerization
AS-OCT	Anterior Segment Optical Coherence Tomography
DSC	Differential Scanning Calorimetry
MDSC	Modulated Differential Scanning Calorimetry
PCL	Poly ϵ -caprolactone
PLLA	Poly lactide
HPLC	High Performance Liquid Chromatography
PBS	Phosphate Buffer Saline
TGA	Thermo- Gravimetical Analysis
GPC	Gel Permeation Chromatography
SEM	Scanning Electron Microscope
PDI	Polydispersity Index
M_w	Weight Average Molecular Mass
M_n	Number Average Molecular Mass
ETO	Ethylene Oxide
ARVO	Association for Research in Vision and Ophthalmology
T_g	Glass Transition Temperature
T_m	Melting Temperature

Abstract

This thesis is aimed to develop a drug loaded microfilm, which can release drug in a controlled manner sustainably, with comparable or better therapeutic effect to that seen with drug loaded eye drops. This thesis presents the development progress of the drug releasing microfilm, which includes the investigation of the degradation behaviour of the candidate biomaterials and the drug release performance from the biomaterial as effects of diffusion and degradation.

Microfilms, which were made of two candidate materials, poly [d,l-lactide-co-glycolide] with lactide/glycolide ratio of 53/47 (mol %/mol %) PLGA5347 and poly[d,l lactide-co-caprolactone] with lactide/caprolactone ratio of 70/30 (mol %/mol %) PLC7030 were developed and evaluated for their degradation behaviour *in vitro* and *in vivo*. PLGA5347 and PLC7030 both exhibited bulk degradation mechanism *in vitro*, with exponentially decaying molecular weight (M_w) and unchanged film thicknesses. *In vivo*, PLGA5347 degraded homogeneously and became non-visible in the rabbit eyes three months after the study; whereas PLC7030 persisted throughout 6 months, with unchanged width and length, but linearly decreasing film thickness. This is the first time reporting that biodegradable polymers hydrolyze homogeneously *in vitro* but heterogeneously *in vivo*.

Subsequently, the degradation behaviour of PLC7030 was further investigated. The effects of sample shape and thickness and degrading media were evaluated. Experimental results revealed that the samples (250 μ m) with sharp edges (square and rectangle) seem to degrade faster compared to round samples (disk). And this difference became more pronounced *in vivo* than *in vitro*. Though bulk degradation is said to be homogeneous, the thickness of sample was found to have an impact on the degradation rate of PLC7030. Thinner films demonstrated slower *in vitro* degradation rate but higher mass loss than the thicker films. The degradation behavior of PLC7030 *in vitro* and in the subconjunctival

space of rabbit eyes differed; the disparity became larger when the film thickness increased from 250 μm to 500 μm . Additionally, PLC7030 with a thickness of 250 μm demonstrated homogeneous degradation *in vitro* and *in vivo*, whereas PLC7030 with a thickness of 500 μm seemed to degrade homogeneously *in vitro*, but heterogeneously *in vivo*. From the calculation by using an existing mathematical model, the critical thickness was found greatly dependent on the ratio of degradation rate constant and water diffusivity ($\frac{\lambda}{D_{\text{eff}}}$).

Prednisolone acetate was loaded into PLC7030 films at different loadings (5%, 10% and 20%). There were two stages observed in the drug release profiles, which are diffusion-controlled stage (0~ 56 days approximately) and degradation-controlled stage (after 56 days). The effect of drug loading and effect of film thickness on the drug release were studied. The fractional drug release (both cumulative and rate of release) decreased with drug loading, and increased with the decreased film thickness. 20% PA-loaded PLC7030 films (80 μm) was inserted in the subconjunctival space of rabbit eyes after glaucoma filtration surgery for *in vivo* drug release study over a period of 90 days. The amount and percentage of drug released *in vivo* are higher than those obtained *in vitro*. The amount released daily kept comparatively higher than the therapeutic level throughout the 90 days of study. Finally, the release profiles were expressed mathematically by modifying an existing model. The modified model was able to predict the experimental results well.

In conclusion, degradation of microfilms made from PLC7030 is affected by shape and thickness of the samples, as well as the degrading media. The drug release behavior from PLC7030 is affected by drug loading, film thickness and the releasing media (*in vitro* and *in vivo*). Additionally, 20% prednisolone acetate loaded PLC7030 microfilms are able to achieve sustain release over a period of 90 days with equal therapeutical effects compared to the eye drop *in vivo*.

Chapter 1 Introduction

1.1 Background

The eye is an important organ for sight and unique due to its anatomical and immunological privileges. Physiologically, the eye is protected by several layers of tissues, which are also resistant to penetration by drugs. Post-operative inflammation is a very important risk factor for excessive subconjunctival scarring following ophthalmic surgeries clinically, such as glaucoma filtration surgery (GFS) [1]. It has been reported that early postoperative failures of less than 6 months on glaucoma patients show a noticeable inflammatory response and excessive conjunctival scarring [2]. Topical corticosteroids such as prednisolone acetate (PA) are often administered post-operatively as an anti-inflammatory drug [3]. However, due to the poor bioavailability of eye drops [4-7], patients often require administration of the corticosteroid drug intensively and frequently for several months to ensure the inflammation resolves in the early stages after surgery [8]. Patient non-compliance however, is a major issue that may compromise surgical outcome. To improve patient compliance, drug delivery from a sustained release carrier would improve on optimizing drug delivery to the targeted site.

Polymeric biomaterials are proven vehicles for sustained drug delivery [9] due to their ease of fabrication, predictable degradation kinetics as well as proven biocompatibility [10-13]. Polymeric biomaterials such as poly-d,l-lactide-co-glycolide (PLGA) or poly-d,l-lactide-co-caprolactone (PLC), degrade through hydrolysis of their ester bonds into lactic acids, glycolic acids and caproic acid [14, 15], and release sustained levels of drugs to exert effects locally without systemic side effects [16-18]. The polymeric biomaterials may be fabricated with varying geometry, size with different kinds of drugs at various loading to modulate the amount and duration of drug released [19-21]. Moreover, the

polymer matrix not only offers protection of the drugs, preventing from rapid washout by the surrounding fluids, but also allows for slow release of a large amount of drug sustainably [22].

Recently, the development of biodegradable polymeric ocular drug delivery devices has been actively researched to overcome the limitations of the existing ocular drug delivery systems. However, most of the research reports only on targeting delivery to the posterior segment of the eye [22-24]. There is a lack of data on a controlled drug delivery device to the anterior segment, where disease like glaucoma, cataract and corneal transplant are all associated. Additionally, the degradation behavior of biodegradable polymers have not been investigated in the anterior segment of the eye before, which may potentially have a different performance as in other parts of the body [10, 25, 26].

Due to the delicate and complex nature of the anterior segment of the eye, majority of the ocular drug-delivery devices targeting the anterior segment are designed either very soft such as gels [27] or tiny in size, such as microparticles [28], liposomes [29] and nanoparticles [30, 31]. However, these designs are associated with some unsolved problems, such as limited drug loading capability, relatively limited period of release, as well as agglomeration and stability issue for micro- and nano- scaled carriers [32]. Comparatively, biodegradable microfilms are easy to fabricate and reproducible, well dimension-controlled (shape, size, thickness etc.), as well as potentially higher loading amount. Nevertheless, only limited numbers of this geometry for a drug loaded device was investigated in the anterior segment of the eye [33]. Thus there is a huge potential to study the drug release performance from microfilms in the anterior segment of the eye.

1.2 Problem Statement

As mentioned earlier, topical administration of corticosteroids for post-operative treatment needs to be frequent, and non-compliance by patients leads to serious problems such as subconjunctival fibrosis, corneal surface impairment, epithelial apoptosis, and the potential risk of glaucoma surgery failure [34]. Therefore, it would be an advantage to design a biodegradable drug loaded device, such that it is able to release the loaded drug in a controlled manner sustainably. The challenge lies on controlling and adjusting the release rate of the drug and degradation behavior of the drug carrier material to suit the therapy requirements.

Since majority of ocular drug release research has been targeting in the posterior segment of the eye, there is a gap in the literature for controlled drug delivery to the anterior segment. A controlled drug release device, applied through the anterior segment (in the subconjunctival space), directly after ophthalmic surgeries for postoperative care, is aimed to be developed.

To solve the drug loading efficiency and stability issues of micro- and nano- sized drug carrier, microfilms have been selected as the drug-loading matrix. In this work, a single layer biodegradable microfilm has been developed from poly d,l-lactide-co-glycolide 53/47 (PLGA5347) with 53% (mole) of d,l-lactide and 47% (mole) of glycolide, and poly d,l-lactide-co- ϵ -caprolactone 70/30 (PLC7030) with 70% (mole) of d,l-lactide and 30% (mole) of ϵ -caprolactone. From past studies and technical data (provided by the manufacturer), firstly, the glass transition temperatures of PLC7030 and PLGA5347 are below or around body temperature (37°C), which made the materials soft under body temperature to accommodate the delicate nature of the eye; secondly, PLGA5347 and PLC7030 demonstrate different degradation periods, which potentially provide tailored period of the implant in the body. Furthermore, these two biomaterials also demonstrated

biocompatibility to some extent from various sites of the body [12, 25, 35, 36]. Therefore, PLGA5347 and PLC7030 were selected initially as the candidate materials to be further studied.

Degradation behaviour of biodegradable microfilms in the anterior segment of the eye has not been well-established in the literature; especially no one has studied the effect of film thickness and film geometry on the degradation in the subconjunctiva of the eye. In this study, the degradation behaviour of both of the two polymers have been investigated *in vitro* and in the eye, with further investigation on the effect of thickness, shape of the film, as well as co-relation of *in vitro/in vivo* environment on the degradation of PLC7030.

1.3 Hypothesis

It is hypothesized that the biodegradable microfilms with predicted degradation behaviour can control the release of corticosteroid sustainably in the anterior segment of the eye for postoperative treatment with equal or better therapeutical effects compared to the eye drop.

1.4 Objectives

Experiments to prove the hypothesis can be divided into three major phases.

Objective 1:

The first phase is to develop and characterize biodegradable microfilms made from two different polymeric biomaterials (poly (d,l-lactide-co-glycolide) with lactide/glycolide ratio of 53/47 (mol %/mol %) PLGA5347 and poly (d,l lactide-co-caprolactone) with lactide/caprolactone ratio of 70/30 (mol %/mol %) PLC7030 for their potential application as vehicles for intraocular drug delivery (without drugs), specifically on surgical insertion into the subconjunctival space, as well as the *in vitro/in vivo*

degradation behaviours of both polymers. The most suitable polymeric biomaterial is selected for subsequent studies.

Objective 2:

The second phase is to further investigate the degradation behaviour of the selected polymeric biomaterial. The focus of the study is on the effect of shape of the sample, thickness of sample and degrading media (*in vitro* and *in vivo*) on the degradation kinetics. The effects of selected parameters on degradation will be considered in the subsequent drug release studies.

Objective 3:

The third phase is to develop the drug (corticosteroid) loaded microfilms with the selected biomaterial and exploit the drug release potential of a single layer polymeric microfilm. The release mechanism is examined as an effect of drug loading percentages, film thickness, as well the *in vitro/in vivo* media. The experimental *in vitro/in vivo* release results are correlated with mathematical drug release models.

1.5 Novelty

The first novelty of the work is investigating different degradation mechanisms of PLC7030 and PLGA5347 *in vivo* (in the subconjunctival space of the rabbit eye) as compared to in the *in vitro* environment. Moreover, it is the first time that the difference in the degradation mechanism is reported of one material (film) *in vitro* and *in vivo* for the same thickness. *i.e.* the critical thickness (of PLC7030) which determines the degradation mode was found to be different in the *in vitro* and *in vivo* environments.

It is the first time to employ AS-OCT (anterior segment optical coherence tomography) as the non-destructive technique to quantitatively examine the samples in the eye.

This is the first time to study drug loaded microfilm, which can be applied in the anterior segment of the eye that can release corticosteroid (anti-inflammatory drug) over at least 90 days with effective therapy.

1.6 Scope

In this work, single layer film configuration of PLGA5347 and PLC7030 has been studied. The range of film thickness for the samples in this study is in microns. A single corticosteroid, which is prednisolone acetate, is loaded as the anti-inflammatory and anti-scarring agent into the selected polymeric material for drug release study. The *in vivo* degradation and drug release study is conducted in the subconjunctival space of rabbit eyes. The *in vivo* degradation studies are monitored mainly by slit-lamp microscopy and anterior segment optical coherence tomography (AS-OCT). Finally the mathematical model employed to predict the drug release behaviour is modified from existing ones, without self-construction.

1.7 Overviews

This thesis is separated into seven chapters. The motivation, hypothesis and rationale that initiated this project; the scope of the work and novel contributions have been highlighted in the first chapter. Chapter 2 summarizes reported works, including background information, related theories, existing challenges as well as current approaches. It is the foundation of the work which leads to the direction of this project. Chapter 3 describes the methodology of all the experiments conducted in this thesis. Chapter 4, Chapter 5 and Chapter 6 are the experimental results and discussions. Chapter 4 focuses on developing and characterizing the drug carrier made from two candidate materials-PLGA5347 and PLC7030 microfilms, including their degradation behaviors both *in vitro* and *in vivo*. Then a more suitable material, which is PLC7030, has been chosen for further studies in

the next chapters. The degradation behavior of PLC7030 as an effect of sample shape, film thickness and degradation media is evaluated in Chapter 5. Chapter 6 examines the drug release performance as an effect of drug loading, film thickness, as well the *in vitro/in vivo* media. The experimental *in vitro/in vivo* release results are co-related with mathematical drug release models. Chapter 7, which is the last chapter gives final conclusions of all the work done in the thesis, and recommends some of future research directions.

Chapter 2 Literature Review

2.1 Background of ocular drug delivery

Eye is a vital organ for sight and unique due to its anatomical and immunological privilege. However, ocular diseases, such as glaucoma, viral retinitis, age related macular degeneration (AMD), and diabetic retinopathy, which damage vision and even cause blindness, threaten millions of people's health worldwide [37, 38].

2.1.1 Anatomy of human eye

Generally speaking, the anatomic structure of the eye can be divided into two segments, namely anterior segment and posterior segment. There are two chambers in the anterior segment, the anterior chamber (between the cornea and iris, as seen in Figure 2.1) and the posterior chamber (between iris and lens). The tissues in the anterior segment are cornea, lens, pupil, ciliary body, iris and aqueous humor, where the iris blends into the sclera via a mesh-like fibrillar structure called the trabecular meshwork.

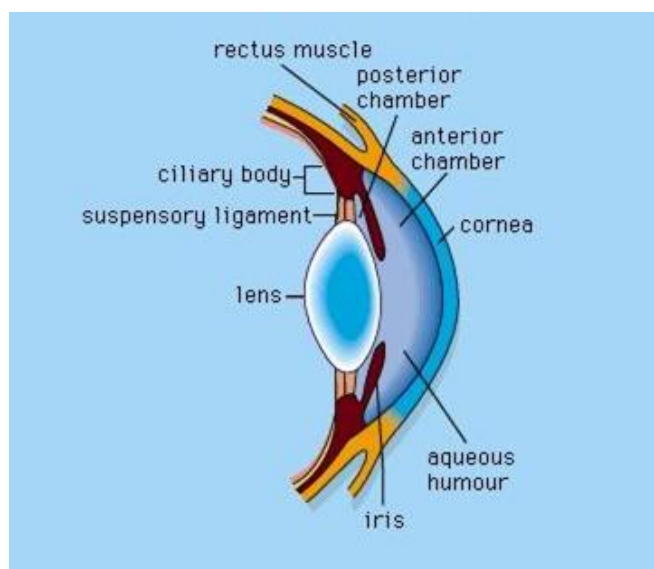


Figure 2.1 Anatomy of the anterior segment of the human eye [39]

While in the posterior segment, tissues comprise sclera, choroid, retinal pigment epithelium (RPE), neural retina and vitreous humor. A thin protective membrane layer covers the eyeball, the conjunctiva, which is inside of the eyelids and anterior sclera [37].

2.1.2 Introduction to glaucoma

Despite of the complex structure of the eye, its important functionality may be deteriorated by the ocular diseases, such as glaucoma. The ocular disease-glaucoma, which is one of the leading causes to irreversible blindness, is going to be introduced in the following section. And glaucoma will be the main focus relating to the research work done by the author.

Glaucoma is a physiological disorder defined by gradual loss of vision associated with damaged optic nerves. There are two major types of glaucoma, which are Open Angle Glaucoma (OAG) and Closed Angle Glaucoma (CAG). In OAG, progressive blockage of aqueous outflow is observed in the eye, though the space in the anterior chamber seems to be open. And in CAG, the angle gets narrower, restricting the flow of fluid, thus blocks the channel (angle) that normally allows drainage of the aqueous fluid. If blockage happens, a rapid rise in intraocular pressure may occur [40]. In both cases, the increased intraocular pressure (IOP) is the common factor that is believed to contribute to the damage to the optic nerve [39].



Figure 2.2 The classical treatment paradigm for glaucoma [41]

Current treatment for glaucoma (Figure 2.2) involves medical therapy (normally topical application of eye drops and intra-vitreous injection), laser trabeculoplasty (tiny holes are created by laser in the filtration angle of the eye- Figure 2.3), trabeculectomy (removing part of the eye's trabecular meshwork and adjacent structures) [41], where tube shunt (glaucoma drainage device) is the last strategy.

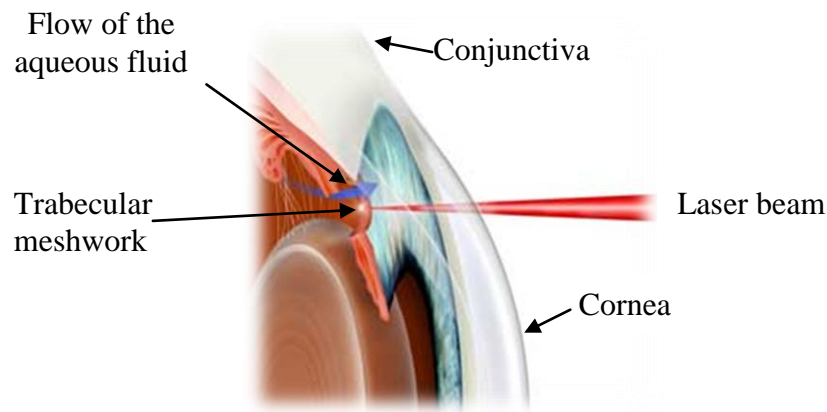


Figure 2.3 Schematic demonstration of laser trabeculoplasty (revised from ref [42])

2.1.3 Current challenges of drug delivery systems for glaucoma treatment

Among all the treatments, topical application is still the most preferred methods due to ease of administration and low cost [9]. However, there are quantities of experimental and clinical evidences show that prolonged application of eye drops potentially induces various side effects, such as change of ocular surface, causing conjunctival inflammation and subconjunctival fibrosis, etc. Patients who receive anti-glaucoma topical treatment for long period of time were reported to have chronic inflammation [34]. In addition, majority of the drug following topical administration is lost through lacrimation, tear dilution, tear turnover and nasolacrimal drainage [43] due to very low bioavailability of the administered drug, typically less than 5% [9, 44], which prompts the ophthalmologists searching for alternative routes of drug administration.

Intravitreal injections, which involves direct injection of drug into the vitreous, have attracted much attention in the past two decades [9]. Since it by-passes the barrier of cornea and conjunctiva, and offers higher drug concentration as compared to topical administration. However, this method has strict requirements for drug, such as the molecular weight, and chain structure [45]. Though intravitreal administration often offers higher concentration of drug solution, which may cause various short term complications, thus patients need to be monitored carefully by doctors after the injection.

When the patients' case is more severe, glaucoma filtration surgeries (GFS) such as trabeculoplasty, trabeculectomy and glaucoma drainage device are required. It is known that scarring and failure of the filtering bleb are the two main complications after GFS, therefore, postoperative treatments are very important parameters that determine whether an operation is a success or a failure [46]. There are two ways to provide positive effect on the postoperative conjunctival wound healing, one is apply anti-inflammatory treatment preoperatively, and the other one is discontinuation of topical medication after the surgery [47]. In order to further increase the success rate of GFS and minimize the side effects, more research on wound healing to prevent scarring are urged to be done. Thus postoperative wound healing is still a big challenge for all the ophthalmologists.

2.1.4 Current approaches in ocular drug delivery

Limitations of topical and intravitreal routes of ocular drug administration greatly challenged the scientist and ophthalmologists for postoperative care, especially for glaucoma patients [47]. There are several intraocular drug delivery systems using biodegradable polymers, such as intraocular implants, ocular insert, microspheres, liposome injection, etc (Table 2.1), which are further elaborated in the following sub-sections. These approaches may achieve targeted delivery, which potentially bypass the barriers in the eye, thus increase the bioavailability of drugs.

Table 2.1 Current commercially available ocular drug delivery systems

System	Product	Component	Targeted diseases
Gels	Gelrite® (Merk)	0.5% timoptic-XE	Glaucoma
	Nyogel® (Novartis AG, Basel)	0.1% timolol melete	Glaucoma
Surgical implants	Ozurdex® (Lomb)	0.7mg dexamethasone	Chronic non-infectious uveitis
Biodegradable ocular implant	Surodex™ (Oculex Pharmaceuticals, Inc.)	Dexamethasone with PLGA	Postsurgical inflammation

i. Gels

One of the approaches is using gels to reduce the number of doses everyday and several gel formulations have been developed. Merck marketed its controlled-release product Gelrite® consists of 0.5% Timoptic-XE® for glaucoma patients by taking a gellan gum consists of glucose, glucuronic acid and rhamnose as the drug excipient [33]. Another in-situ formation gels for short term intravitreal injection is Nyogel® (Novartis AG, Basel) by researchers in Switzerland [30]. The gels did reduce the doses required daily; even so, the delivery period is still too short to fulfil the actual application, and they were found to cause blur vision [48].

ii. Surgical implants

Surgical implants can deliver active agents potentially for longer period of time in the eye. Allergan developed a dexamethasone implant which delivers the steroid intravitreally for

6 months (Ozurdex®) [30]. Another intravitreal implant developed by Lomb, USA, which has the capability to deliver fluocinolone acetonide for up to 30 months for chronic uveitis [30]. Additionally, a triamcinolone acetonide coated helical screw (Surmodics, USA), which can deliver drug intravitreally over 3 years [30]. Despite of the effectiveness and the long period of releasing capability, the initial invasive surgery as well as subsequent implant removal surgery would cause serious adverse effects, which deter the glaucoma patients from using them widely.

iii. Biodegradable ocular implant

Due to the extremely slow degradation or non-degradation of the surgical implants, removal surgery was required to be done after the device is exhausted of active agents. For an ideal drug delivery system for the glaucoma patients would able to deliver drug for 3-4 months at a controlled manner. Patient non-compliance can be improved by using biodegradable polymers devices, providing the drug release kinetics is controllable, and the amount of drug released can maintain in the therapeutical level. Biodegradable SurodexTM (Oculex Pharmaceuticals, Inc.) is a PLGA rod containing dexamethasone, which is implanted during the cataract surgery for treatment of postsurgical inflammation [49, 50].

iv. Microspheres, nanoparticles and liposomes

Transport drug at targeted site has generated great interest in the field due to its potential to overcome many barriers in the current therapy, though most of the approaches are still at the research stage.

Microspheres can be administered in to the vitreous cavity by injection as suspension. This method is an advantage for drug administration, but it can also be disadvantageous

as large quantity of microspheres may cause a temporary disturbance in the vitreous transparency [51].

In contrast, the nanoparticles reach the targeted area by taking an intracellular route through the corneal epithelium. DeCampo and co-workers [52] studied the role of charges on the nanoparticles administered topically in the eye. It was reported that the neutral nanoparticles are able to deliver greater drugs than the negatively charged one. Another approach was done by formulating nanocapsules consist of a di-block copolymer with both a hydrophobic block and a hydrophilic block, which can release the loaded agent promptly or fuse in the cell membranes [30].

Liposomes are tiny vesicles that can be formulated from natural non-toxic phospholipids and cholesterol. It was reported that the trans-corneal permeability of ofloxacin can be greatly enhanced by ofloxacin loaded liposomal hydrogel than it is in the aqueous solution [30]. Most recently, a group of researchers had successfully developed latanoprost-loaded liposomes, which was efficaciously deliver drug to the anterior segment of the eye over 50 days [53].

Therefore, there is not adequate research done focusing on the anterior segment of the eye, nor on desired sustained release of active agents to the anterior segment of the eye at an equal or better therapeutical effect as compared to eye drops.

2.2 Polymeric biomaterials and biodegradation

In the past decades, polymeric biomaterials have received tremendous attention for the administration of pharmaceutical and biomedical applications. These types of biomaterials are able to degrade and removed/metabolized in the body after preset duration, thus become especially attractive when only temporary interventions are required [54]. Being degradable is one criterion for polymeric biomaterial, while several

other pre-requisites have to be met. Firstly, the material should not invoke non-tolerable inflammation or toxic responses. Secondly, it has to match the mechanical, physical and biological properties with the intended application. Lastly, it has to be easily manufactured into final products with acceptable storage life and capability of sterilization [55]. Therefore, one family of polyesters-the poly lactide based polymers became more and more popular among several types of available degradable polymers. Several medical devices made from these degradable polyesters have been approved by Food and Drug Administration (FDA) for clinical uses [56]. The biocompatibility of poly lactide-based polymers (such as poly lactide-co-glycolide and poly lactide-co- ϵ -caprolactone) has been demonstrated in many biological sites [12, 25, 35, 36, 57, 58].

2.2.1 Lactide-based polymers

2.2.1.1 Synthesis

Poly lactide-based polymers are synthesized mainly by two ways, namely poly-condensation and ring-opening-polymerization (ROP) of lactides and other co-monomers, such as glycolide and ϵ -caprolactone [59]. Poly-condensation applies normally to low molecular weight polymers (M_w ~a few thousand Daltons) by simple direct condensation of lactic acid and/or glycolic acid (Figure 2.4) with water removal process, whereas ROP method (chain-growth polymerization) is employed to synthesize high molecular weight polymers ($M_w > 10,000$ Daltons) without dehydration. A high temperature of around 130 °C -190 °C is required, sometimes catalysts are added. Copolymerization of LA with glycolide and ϵ -caprolactone will yield different tactic structure of isomers, such as block-copolymer and random-copolymers (Figure 2.5).

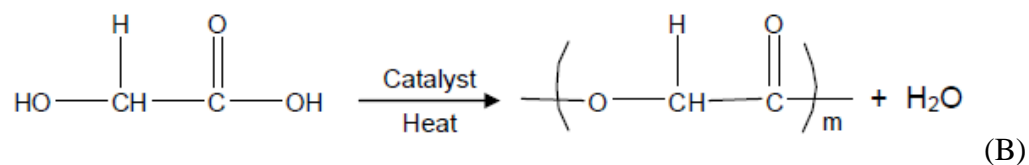
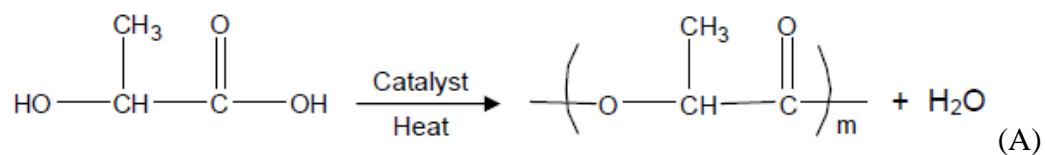


Figure 2.4 Synthesis of (A) poly lactic acid and (B) poly glycolic acid by poly-condensation

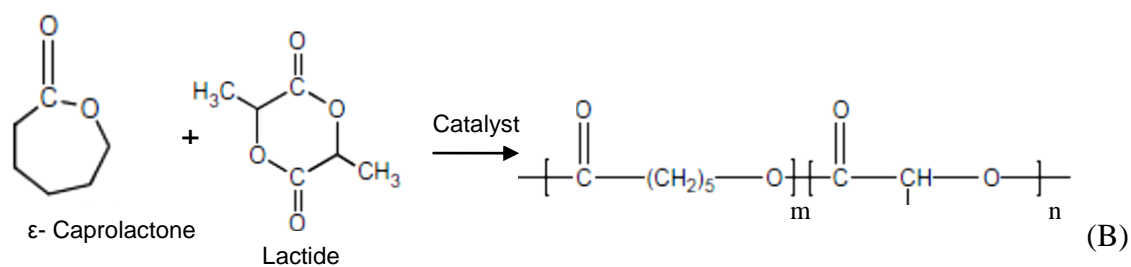
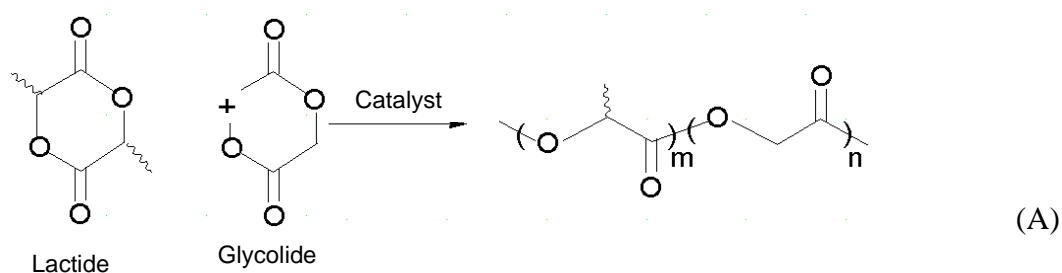


Figure 2.5 Synthesis of poly lactide-co-glycolide (A) and poly lactide-co-ε-caprolactone (B)

2.2.1.2 Poly lactide-co-glycolide polymers

Poly lactide-co-glycolide is a copolymer consists of lactide segments and glycolide segments. Amorphous copolymers of d, l-lactide and glycolide can be synthesized in the range of 0% to 70% glycolide.

The polymer composition does not only indicate the crystallinity, but also the rate of degradation. Generally, the glass transition temperature of the PLGA copolymers range from 40°C to 65°C [60, 61] and increase with increased lactide contents, as well as the molecular weight.

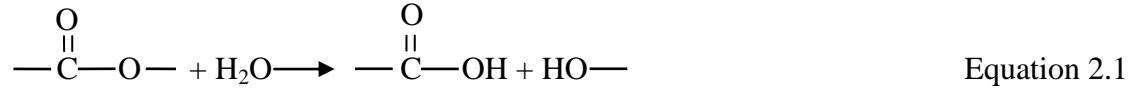
2.2.1.3 Poly lactide-co- ϵ -caprolactone polymers

Poly-lactide-co- ϵ -caprolactone (PLC) is a relatively new material in the class of biodegradable polymers. Structurally, PCL makes up the flexible segment of the copolymeric backbone as its chains are amorphous. PLLA, on the other hand, is stiffer semi-crystalline linear aliphatic polyester. It acts as the hard blocks of the copolymer due to its high tensile strength, modulus and low elongation [62]. Therefore, it possesses several desirable properties such as enhanced elasticity (with shape memory effect)[63], high flexibility (lower glass transition temperature), and superior extendibility (elongation at break can be up to a few hundred times). PLC is fundamentally a copolymer of ductile poly (ϵ -caprolactone) (PCL) and brittle poly (L-lactic Acid) (PLLA), with better biodegradation and mechanical properties than the two [64].

2.2.2 Hydrolytic biodegradation of lactide-based polymers

Though there are many kinds of degradation, such as mechanical degradation, thermal degradation, light deterioration and enzymatic degradation, the only focus here will be chemically hydrolytic degradation. The lactide-based copolymers belong to the aliphatic

polyester family, thus in the presence of water, the ester bonds will be hydrolytically degraded as follows:



2.2.2.1 Parameters on degradation

There are numerous parameters that determine degradation of poly lactide-based polymers, such as molecular weight, composition of the copolymer, tactic structure, crystallinity, molecular orientation, porosity, pH, temperature and etc. Generally, higher temperature, increasing or decreasing pH will accelerate the hydrolysis reaction; while higher molecular weight, crystallinity and degree of orientation will reduce the hydrolytic rate [59].

2.2.2.2 Mechanisms of hydrolytic degradation

In the early 1980s, the hydrolytic degradation of polymers was classified into bulk degradation and surface erosion [14]. Then what crucial factors govern the modes of degradation? Generally speaking, there are two processes dominating hydrolytic degradation, one is water uptake (R_w), and the other is hydrolysis rate of the polymer backbone (R_h). The hydrolysis process starts with ingress of water into the polymer matrix. If the water uptake is slow compared to hydrolysis ($R_w < R_h$), the polymer is surface eroding/heterogeneous degraded, as the water diffused in the polymer matrix is consumed at the surface before entering into the bulk. On the other hand, if hydrolysis is slow compared to water ingress ($R_h < R_w$), there will be abundant of water inside the polymer matrix, which results in homogeneous hydrolysis, *i.e.* surface erosion.

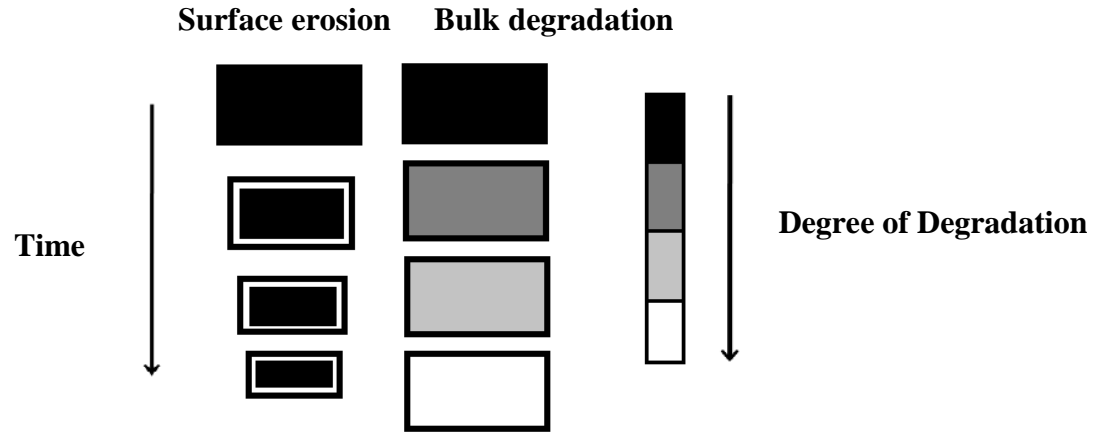


Figure 2.6 Schematic illustrations of surface erosion and bulk erosion [65]

Friederike *et al.* developed a theoretical model that allows predicting whether a polymer matrix undergoes homogeneous or heterogeneous degradation [65]. Before further elaboration, a few assumptions were made to allow better forecasting.

- i. The polymer matrix is insoluble in water
- ii. Hydrolysis is the only trigger to degradation
- iii. Other process has no effect on the degradation process

Therefore, two major processes during degradation will be concerned, which are diffusion of water into the polymer (R_w) and hydrolysis of the polymer backbone (R_h).

By applying the diffusion theory, the time t_{diff} , that water travels a mean distance $\langle x \rangle$, can be calculated by random motion of water in polymer.

$$t_{\text{diff}} = \frac{\langle x \rangle^2 \pi}{D_{\text{eff}}} \quad \text{Equation 2.2 [65]}$$

where D_{eff} is the effective diffusion coefficient of water into the polymer. Equation 2.2 is equivalent to the measure of rate of water ingress (R_w).

By assuming the hydrolytic degradation is a process of scission of bond in the polymer backbone, Poisson kinetics with zero-order was applied, and finally the rate of hydrolysis can be expressed in Equation 2.3 as below:

$$E(t_n) = \frac{1}{\lambda} \left\{ \ln\langle x \rangle - \ln \left[\sqrt[3]{\frac{\overline{M}_n}{N_A(N-1)\rho}} \right] \right\} \quad \text{Equation 2.3 [65]}$$

where $E(t_n)$ is the time that on average required to degrade n ester bonds; λ is the rate constant in the reaction kinetics and directly related to a ester bond's half-life; \overline{M}_n is the number average molecular weight; N is the average degree of polymerization, *i.e* number of monomers per polymer chain; N_A is the Avogadro's number and ρ is the polymer density.

The two rates can be compared by dividing Equation 2.2 by Equation 2.3, and denote ratio of $t_{\text{diff}}/E(t_n)$ as ε . The ratio can be rewritten as

$$\varepsilon = \frac{\langle x \rangle^2 \lambda \pi}{4D_{\text{eff}} \left\{ \ln\langle x \rangle - \ln \left[\sqrt[3]{\overline{M}_n / N_A (N-1)\rho} \right] \right\}} \quad \text{Equation 2.4}$$

where ε is dimensionless. The calculated value for ε falls into three cases:

- i. $\varepsilon > 1$
- ii. $\varepsilon < 1$
- iii. $\varepsilon = 1$

2.2.3 Fick's law of diffusion

Diffusion is a spontaneous movement of molecules/particles from high concentration region to low concentration region [66]. This phenomenon was analyzed and expressed mathematically by Adolph Fick in the year 1855 [67]. His work has been well established through two fundamental equations, which are named Fick's laws of diffusion [66].

Fick's first law states that the flux in the x-direction (J) is proportional to the concentration gradient

$$J = -D \frac{\partial C}{\partial x} \quad \text{Equation 2.5}$$

Flux (J) is the amount of substance diffusing across unit area in unit time, and D is the diffusion coefficient. This first law can be only applied to diffusion in the steady state, where concentration is not changing with time. C is concentration of the diffusing substance, and x is position that is normal to the central plane/axis; the minus sign means that diffusion takes place down the concentration gradient.

Fick's second law describes the continually changing state diffusion (non-steady state), i.e., when the concentration within the diffusion region changes with respect to time and position. In a planar geometry, this can be written as

$$\frac{\partial C}{\partial t} = D \frac{\partial^2 C}{\partial x^2} \quad \text{Equation 2.6}$$

If assume a piece of polymeric film is placed in an infinite medium of diffusant, the concentration C at point within the film at time t are given by Equation 2.7 [68], which is the solution to equation 2.2.

$$\frac{C}{C_1} = 1 - \frac{4}{\pi} \sum_{n=0}^{\infty} \frac{(-1)^n}{(2n+1)} \exp\left(-\frac{D(2n+1)^2 \pi^2 t}{4l^2}\right) \cos\left(\frac{(2n+1)\pi x}{2l}\right) \quad \text{Equation 2.7}$$

Where l is half the thickness and C_1 is the concentration at the surfaces of the film, which is established instantaneously. By integrating Equation 2.3, the mass uptake by film, M_t can be obtained in Equation 2.8.

$$\frac{M_t}{M_\infty} = 1 - \sum_{n=0}^{\infty} \frac{8}{(2n+1)^2 \pi^2} \exp\left(\frac{-D (2n+1)^2 \pi^2 t}{4l^2}\right) \quad \text{Equation 2.8}$$

Here M_∞ is the mass uptake at equilibrium, and l is half the film thickness.

In general, diffusion and transport in glassy polymers have been classified according to the relative rates of mobility of the penetrant and of the polymer segments. There are 3 basic categories of behaviour as follows:

- i. Case I (Fickian diffusion). The rate of diffusion is much less than the polymer segment mobility. Thus sorption equilibrium is rapidly reached, which leads to time-independent boundary condition without dependence on swelling.
- ii. Case II. The diffusion and penetrant mobility are much greater than the segment relaxation process, which leads to strong dependence on swelling kinetics.
- iii. Non-Fickian diffusion. When the rate of diffusion & penetrant mobility and polymer segment relaxation are comparable, the diffusion is observed in hard and glassy polymers, but this will vanish as long as the temperature is at and above the glass transition temperature.

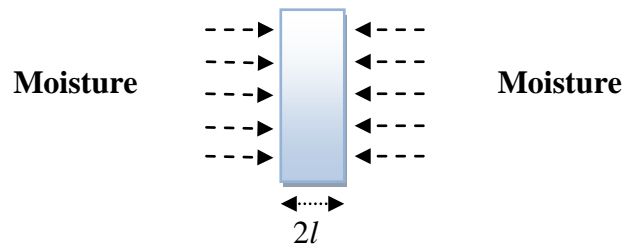


Figure 2.7 Schematic presentation of one dimensional diffusion of a specimen exposed on both sides to moisture [66]

Case I and Case II are two types of limiting transport process with anomalous diffusion being between them. The sorption-time curve can be expressed by Equation 2.9.

$$\frac{M_t}{M_\infty} = k t^n \quad \text{Equation 2.9}$$

Where M_t is the relative weight gain at time t , M_∞ is the relative weight gain at equilibrium and k , n are constants. When $n = 1/2$, it is Fickian diffusion (Case I), while for Case II, $n=1$, and for non-Fickian systems, $1/2 < n < 1$. As shown schematically in Figure 2.7, a film with thickness of $2l$, exposing on both sides to the same environment, the mass uptake related to time can be expressed in a simple way as Equation 2.10, only if the value nl/\sqrt{Dt} is large enough [69].

$$\frac{M_t}{M_\infty} = \frac{2}{l} \left(\frac{Dt}{\pi} \right)^{1/2} \quad \text{Equation 2.10}$$

Following are some of the characteristic features of Fickian diffusion:

- i. Both sorption and desorption curves as functions of the square root of time are linear in the initial stage
- ii. Above the linear portion both absorption and desorption curves are concave to the abscissa
- iii. The sorption behaviour obeys the film thickness scaling law, *i.e.* reduced sorption curves for films of different thicknesses are all super-imposable.
- iv. When D is a constant and absorption and desorption curves coincide over the entire range of t .

v. The temperature dependence of D can be expressed by the Arrhenius equation $D = D_0 \exp (-E_a/RT)$, where D_0 is the permeability index, E_a is the activation energy of diffusion process and R is the gas constant.

The moisture diffusion coefficient can be determined by exposing a thin dry specimen to a constant moisture environment, monitoring and plotting its mass uptake versus $t^{1/2}$. The slope of the linear early stage can be employed to calculate the diffusion coefficient by Equation 2.11 below:

$$k = \frac{2}{l} \sqrt{\frac{D}{\pi}} \quad \text{Equation 2.11}$$

Thus D can be obtained as

$$D = \frac{k^2 l^2 \pi}{4} \quad \text{Equation 2.12}$$

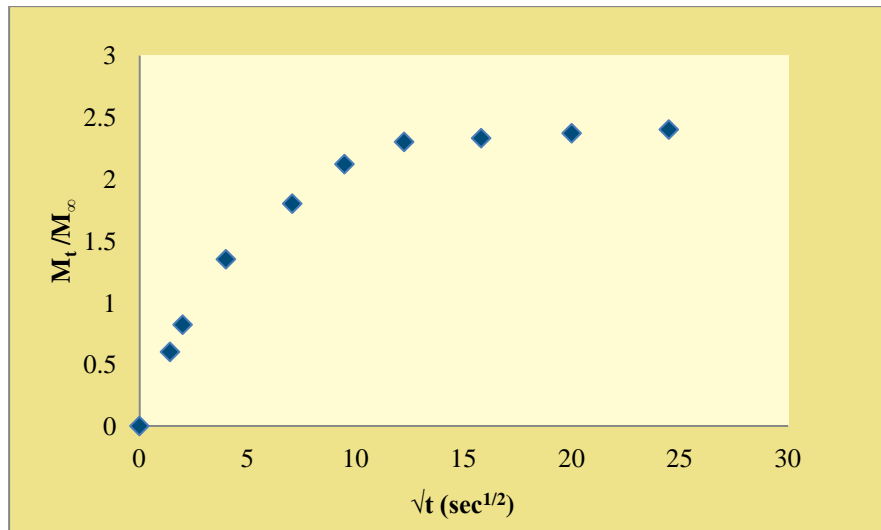


Figure 2.8 Schematic demonstration of mass uptake for film in an infinite medium (Case I)

2.3 Drug delivery systems

There is plenty of literature on the types of drug delivery systems. However, the characterization of drug delivery systems is based on the basic mechanism of release. Generally, there are two focuses, namely diffusion-controlled systems, degradation-controlled systems.

2.3.1 Diffusion-controlled systems

The simplest diffusion-controlled system is a reservoir device, which comprises of an inert membrane, encapsulating the agent to be released. The release kinetics of reservoir highly depends on the membrane thickness, area, partition coefficient, as well as the permeability [67, 70]. The most serious problem associated with the reservoir system is due to catastrophic failure of the membrane. Another diffusion-controlled system is the matrix type, the drug is uniformly distributed throughoutly and is released at a uniform as drug particles dislodge from the polymer network [18, 70].

2.3.2 Degradation-controlled systems

The degradation-controlled systems may be differentiated by the modes of hydrolytic degradation, which are heterogeneous degradation and homogeneous degradation. Drug release from heterogeneous degrading device is simply dependent on the degradation rate, due to the layer-by-layer erosion mechanism. Whereas homogeneous degrading devices are more complex, which normally produce a degradation-controlled monolithic system, which incorporate both diffusion and degradation. Generally, there are four principle biodegradable devices, which are degradation-controlled monolithic system, diffusion-controlled monolithic system, diffusion-controlled reservoir system and erodible poly-agent system [70].

2.4 Drug release kinetics and mathematical models

2.4.1 Models of non-degradable release system

For non-degradable drug devices, the drug release is mainly dominated by diffusion; thus the rate of diffusion of the drug in the device into the surrounding media governs the rate of release. Higuchi model is well accepted to predict the drug release from a non-degradable monolithic system, where the drug particles are uniformly dispersed throughout the rate controlling polymeric matrix [70].

There are two principal categories of monolithic systems, namely monolithic solution and monolithic dispersion. In monolithic solution systems, the active agent (drugs) is fully dissolved in the polymer matrix. Where in monolithic dispersion systems, the active agent is in solid form and dispersed uniformly throughout the polymer matrix. In both systems, the governing theory is Fick's law of diffusion (discussed in the earlier sections). In this project, due to high drug loading requirement, only mathematical model for monolithic dispersion system will be covered.

Assume the geometry of the device is a slab, with initial drug loading of C_0 , with thickness l .

The model starts from Fick's first law, and Equation 2.5 can be rewritten as

$$R = -AD \frac{dC}{dx} \quad \text{Equation 2.13}$$

where R is the rate of release (g/s), A is the diffusion cross-sectional area (cm^2), D is the diffusion coefficient of drug in the polymer (cm^2/s), C is the concentration of drug in the polymer (g/cm^3), and x is the diffusional distance measured from the medium-polymer interface (cm).

Two boundary conditions:

a) When $x=0$, $C=C_bK$

b) When $x=f(t)$, $C=C_{ss}$

C_b is the concentration of drug in the releasing medium, C_{ss} is the solubility of the drug in the polymer matrix, and K is the partition coefficient of drug between the matrix and medium.

Assume a pseudo-steady state is established, in which the concentration of drug in the diffusion region varies with time linearly, and then Equation 2.13 can be integrated and rewritten as

$$R(t) = -AD \frac{(C - C_bK)}{f(t)} \quad \text{Equation 2.14}$$

In the diffusion region, mass conservation principle holds, thus the rate of release can also be represented by

$$R(t) = \frac{dM_t}{dt} = AD \frac{d}{dt} \left[C_o^{-\frac{1}{2}} (C_{ss} + C_bK) f(t) \right] \quad \text{Equation 2.15}$$

Substitute Equation 2.14 into Equation 2.15, and followed by a series of integration, the final expression can be written as

$$M_t = A[D(C_{ss} - C_bK)(2C_o - C_{ss} - C_bK)t]^{1/2} \quad \text{Equation 2.16}$$

In an infinite “sink” condition, C_b is very low, and approximately close to zero. Thus

$$M_t = A[DC_{ss}(2C_o - C_{ss})t]^{1/2} \quad \text{Equation 2.17}$$

And also for monolithic dispersion systems, the drug loading is much higher than the solubility of drug in the polymer, thus $C_o \gg C_{ss}$. Therefore, Equation 2.16 can be simplified as

$$M_t = A(2DC_{ss}C_o t)^{1/2} \quad \text{Equation 2.18}$$

Thus the amount of drug released is proportional to square root of time.

Taking derivative of M_t over time t , the release rate at any time is given by

$$\frac{dM_t}{dt} = \frac{A}{2} \left(\frac{2DC_{ss}C_o}{t} \right)^{1/2} \quad \text{Equation 2.19}$$

Subsequently, the mathematical expression for total release and rate of release in terms of percentage will be analyzed and expressed.

Initially, the total amount of drug present in the polymer matrix can be expressed as

$$M_o = AC_o l/2 \quad \text{Equation 2.20}$$

Then the fraction of the drug released is expressed by taking ratio of M_t/M_o :

$$\frac{M_t}{M_o} = \left[\frac{(8DC_{ss}t)^{1/2}}{l} \right] C_o^{-1/2} \quad \text{Equation 2.21}$$

And the fractional rate of release is

$$\frac{d}{dt} \left(\frac{M_t}{M_o} \right) = \frac{(2DC_{ss})^{1/2}}{l(C_o t)^{1/2}} \quad \text{Equation 2.22}$$

This model is a good prediction of monolithic system with $C_o \gg C_{ss}$ by assuming a pseudo-steady state is achieved. There was slightly more than 11% discrepancy was observed by this assumption, and the exact solution was derived by Paul and McSpadden [71].

Worth noting that from the prediction of the Higuchi model, in a monolithic dispersion system with slab geometry, the amount of drug released is proportional to $t^{1/2}$. For dissolved agent, the fraction released is independent of initial loading, whereas for dispersed agent, the fractional release decreases with increased loading. The relationship between the release rate and loading falls to a $t^{-1/2}$ rule.

2.4.2 Models of degradable release system

There are numerous drug release models from surface eroding as well as bulk degrading systems reported in the literature. A review of the more useful mathematical model for both degradation modes was summarized by Siepmann and Gopferich [72].

In general, it is easier to model drug release from surface-eroding systems because the drug is released concurrently with the erosion and mainly controlled by the erosion rate from the outermost surface of the matrix. Mathematical models for drug release from bulk degrading polymer usually employ the well-established Higuchi model for diffusion-controlled non-degradable systems. Charlie *et al.* [73] demonstrated that the diffusion coefficient D is time-dependent, instead of being a constant as Higuchi model applied. The first order of polymer degradation follows Equation 2.23

$$M_w(t) = M_{wo} e^{-kt} \quad \text{Equation 2.23}$$

And the instantaneous value of $D(t)$ is inversely dependent on the molecular weight (M_w) of the polymer matrix. $D(t)$ increases exponentially with time and can be expressed as

$$D(t) = D_o e^{kt} \quad \text{Equation 2.24}$$

where k is the degradation rate constant. Finally the $D(t)$ was substituted into the Higuchi model, and integrated and re-generated the model at pseudo-steady state as below

$$M_t = A(2D_o C_{ss} C_o)^{1/2} [(e^{kt} - 1)/k] \quad \text{Equation 2.25}$$

Arfin and co-workers developed another method that can determine the initial burst and lag period before Fickian release for microspheres [74], which implemented the release that cannot be predicted from Higuchi model. Later, Rothstein *et al.* developed a unified model which predicted the drug release from a biodegradable polymer matrix transition from surface erosion to bulk degradation, and whether the drug release undergo dissolution limited or degradation-controlled release [75].

Another model was developed by Lao *et al.* [76, 77], which interpreted the drug release of a hydrophobic drug from the PLGA matrix. The model counted tri-phase release of paclitaxel, which were initial burst, following by relaxational release, and diffusion of the drug was in the last stage. This model is more close to the system used in the current study, due to the hydrophobic nature of drug and geometry of the drug loaded device (film). The equation of the model developed is in Equation 2.26 below:

$$\frac{M_t}{M_\infty} = \varphi_b(1 - e^{-k_b t}) + \varphi_r[e^{k_r(t-t_b)} - 1] + \varphi_d \left\{ 1 - \sum_{n=0}^{\infty} \frac{8}{(2n+1)^2 \pi^2} \exp \left[\frac{-D(2n+1)^2 \pi^2 (t-t_r)}{4l^2} \right] \right\}$$

-Equation 2.26

where $\varphi_b + \varphi_r + \varphi_d = 1$

M_t/M_∞ is the cumulative fraction release, which consists of three parts. The first component is burst release, φ_b is the fraction released due to initial burst, k_b is the burst constant; the second component is release due to relaxation/degradation of the polymer matrix, φ_r is the fraction released from relaxation/degradation, k_r is the degradation relaxation rate constant, t_b is time taken that burst release ends; while the last component is contributed from diffusion of the drug from the polymer matrix, φ_d is fraction release

due to diffusion, D is the diffusion coefficient of drug in the polymer matrix, l is the half thickness of the film sample, and t_r is the time that relaxation ends.

Most recently, Chen *et al.* [78] proposed a mathematical model that combines the hydrolytic biodegradation and mass transport of active agents to simulate the release behaviour. Additionally, the autocatalytic effect was also included in the consideration while developing the model. The diffusive transport was found to play an important role for the degradation pathway determination, whilst autocatalysis makes the homogeneous degradation size dependent. In the literature, the modelling agreed with the experimental data.

2.5 Conclusion

There is not adequate research done focusing on the sustained release of active agents to the anterior segment of the eye at an equal or better therapeutical effect as compared to eye drops. Additionally, the degradation mechanism of the polymeric biomaterials in the eye is still unclear, especially in subconjunctival space. Therefore, it is proposed that the biodegradable microfilms made from PLGA5347 or PLC7030 with predicted degradation behaviours can control the release of corticosteroid sustainably in the anterior segment of the eye for postoperative treatment with equal or better therapeutical effect compared to the eye drop.

Chapter 3 Materials and Methods

3.1 Materials

3.1.1 Polymers

The polymers used in the entire study are poly (lactide)-based aliphatic polyesters. Medical grade poly d,l-lactide-co-glycolide 53/47 (PLGA5347) with an intrinsic viscosity of 1.02dl/g, and poly d,l-lactide-co- ϵ -caprolactone 70/30 (PLC7030) with an intrinsic viscosity of 1.60dl/g were purchased from Purac Far East, Singapore. In PLGA5347, there are 53% (mole) of d,l-lactide and 47% (mole) of glycolide; vice versa for PLC7030, which has 70% (mole) of d,l-lactide and 30% (mole) of ϵ -caprolactone.

3.1.2 Solvents and reagents

HPLC-grade chloroform, dichloromethane, acetonitrile were obtained from Tedia. Phosphate buffer saline (PBS) tablets from Sigma-Aldrich, Singapore. PBS (pH 7.4) was prepared by dissolving PBS tablets into 1 litre deionized water for *in vitro* degradation studies. Tobradex® (tobramycin & dexamethasone) eye drop and PRED FORTE® eye drop were bought from Alcon Laboratories Inc., USA, and 10-0 Nylon sutures were from Ethilon, USA. Konnyaku gelly powder was obtained from Aces Foods and Beverage, Malaysia. Prednisolone 21-acetate ($\geq 97\%$) and prednisolone were purchased from Sigma-Aldrich, Singapore.

3.2 Experimental Methods

3.2.1 Sample preparation

3.2.1.1 Samples for degradation studies

Films of PLGA5347 (with thickness 500 μ m) and PLC7030 (with thickness 250 μ m and 500 μ m) were solution cast by weighing before dissolving the appropriate amount (film thickness is controlled by weight of polymers) in dichloromethane, and then poured into petri-dish. And the PLC7030 film with thickness of 80 μ m was cast on a glass plate using an automatic film applicator, which can move the casting knife at a preset speed (50mm/min). Following casting the samples were left in the fume hood for a day, followed by drying in a vacuum oven at 37°C until the solvent level was less than 1% of the total weight, as measured using a thermo-gravimetric analyzer (TGA, TA instruments Q500). After drying, all samples were cut manually into standard sized microfilms for testing.

3.2.1.2 Samples for drug release studies

Prednisolone acetate and PLC7030 with three predetermined drug loading percentages (5wt%, 10wt% and 20wt%) were dissolved in dichloromethane to form a polymer solution with the drug uniformly distributed in it. Drug loaded polymeric films with thickness of 500 μ m and 250 μ m were prepared through solution casting method, and 80 μ m-thick films were prepared by knife casting method (as described above). Subsequently, the films were placed under a fume hood for a day, followed by drying in a vacuum oven at 37°C until the solvent level was less than 1% of the total weight, as verified by a thermo-gravimetric analyzer (TGA, TA instruments Q500). After drying, the samples were cut manually into three standard sized microfilms for testing.

3.2.2 *In vitro* degradation study

Samples were immersed in closed vials containing 5ml PBS. All vials were incubated at 37°C throughout the study. The buffer was refreshed every week, and at every predetermined time point, samples were taken out, rinsed with deionized water and dried in 37°C vacuum oven for 7 days. Degradation of PLGA5347 and PLC7030 was monitored by film thickness (measured by Elcometer 456 and SEM-JSM6360A, JEOL), water absorption (defined below), weight loss (defined below), weight average molecular mass (M_w) and poly dispersity index (PDI). Dried samples were dissolved in chloroform (1-2mg/ml) and filtered through 0.22µm regenerated cellulose syringe driven filters before test. Weight average molar mass (M_w) and number average molar mass (M_n) of the sample were determined by gel permeation chromatography (GPC, Agilent 1100) at 35°C, using Agilent PLgel 5µm mixed-C column, under a flow rate of 1 ml chloroform per minute, using a Refractive Index Detector (RID).

i. Definition of water absorption

As these polymers degrade in the medium by simple hydrolysis, water absorption rates influence the hydrolysis rates. The amount of water absorbed by the sample was calculated as:

$$\text{Water absorption} = (W_w - W_d) / W_o \% \quad \text{Equation 3.1}$$

where W_w represents the weight of the wet sample after wiping by tissue, W_d represent the final weight of the dried samples, and W_o represent the sample's initial weight.

ii. Definition of mass loss

Mass loss was calculated as:

$$\text{Mass loss} = (W_o - W_d) / W_o \% \quad \text{Equation 3.2}$$

where W_d represent the final weight of the dried samples, and W_o represent the sample's initial weight.

iii. Definition of thickness change

Thickness change was calculated as

$$\text{Thickness change} = (T_d - T_o) / T_o \%$$

where T_d represent the final thickness of the dried samples, and T_o represent the sample's initial thickness.

3.2.3 *In vivo* degradation study

3.2.3.1 Surgical insertion of microfilms

All the samples were sterilized by ethylene oxide (ETO) at 37°C (used for normal medical device) in Tan Tock Seng Hospital (Singapore) prior insertion into animals. Rabbits were selected to be the *in vivo* testing animals, as it is ideally suited for ophthalmological researches, due to its similarity to human's eye, ease of handling, as well as being economical comparing with monkeys, etc.[79].

The *in vivo* study was conducted by doctors and researchers from Singapore National Eye Center/ Singapore Eye Research Institute. Approval from the SingHealth Institute Animal Care and Use Committee (IACUC Singhealth Approval Number 2009/SHS/478) was obtained and all procedures were performed in accordance with the ARVO Statement for the Use of Animals in Ophthalmic and Vision Research. New Zealand white rabbits aged 4-6 months old with a weight range of 2-2.5kg each were used. Each rabbit was adequately anaesthetized, and then the eye was cleaned and draped with sterile cloth. A

subconjunctival pocket was created via blunt dissection just at the limbus with a 5-6 mm incision in the superior-temporal aspect of the rabbit's eye. The microfilm was then inserted into the subconjunctival pocket 1mm from the limbus using a conjunctival forceps. Closure with 10-0 nylon sutures was done to ensure secure implantation of each microfilm. In Chapter 4, Characterization of Candidate Materials, in each rabbit, PLC7030 (n=9) microfilms were inserted into the right eye, whilst PLGA5347 (n=9) microfilms were inserted into the left eye. Whereas in Chapter 5, Study of Degradation Behavior of PLC7030, in each rabbit, PLC7030 rectangle microfilm samples (n=3) with thickness of 250 μ m were inserted into the right eye and disk microfilm samples (n=3) with thickness of 250 μ m were inserted into the left eye. Topical Tobradex (tobramycin & dexamethasone, Alcon Laboratories Inc., USA) was administered each eye 4 times a day for 5 days.

3.2.3.2 Characterization of *in vivo* degradation

The *in vivo* degradation of PLGA5347 and PLC7030 was monitored by measuring the film thickness using anterior segment optical coherence tomography (AS-OCT), as well as observation through the slit-lamp photography.

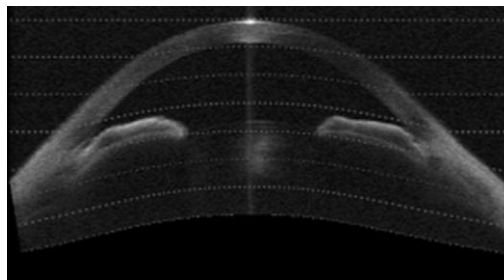


Figure 3.1 Demonstration of AS-OCT graph [80]

Anterior segment photographs and anterior segment optical coherence tomography (AS-OCT, Visante OCT, Carl Zeiss Meditec Inc., Germany) is an optical signal acquisition and processing method, which captures cross-sectional image of the eye without contact. AS-OCT of the implanted eyes was performed at monthly intervals. The Visante OCT is a high-resolution bio-microscopic device for anterior segment imaging (axial resolution = 18 μ m), based the principle of low coherence interferometry using a 1310 nm light emitting diode[81]. Due to the optical properties of different tissues, the AS-OCT image can help us identify internal structures of the eye, such as fluid, scarring or thinning of the sclera or conjunctiva[82]. A radial anterior segment line scan was chosen to include both the implanted microfilm and the surgical insertion site. The site of conjunctival elevation from the microfilm was determined by the location of a light reflex over the conjunctiva during image acquisition. This AS-OCT technique allowed us to image the layers of the eye, location of implant as well as obtaining standardized measurements of the implant, which was included microfilm thickness and length. The AS-OCT is calibrated internally to detect internal structures of the eye using high-resolution corneal and angle scans and pachymetry maps at a rate of up to 2048 A-scans per second, with an optical axial resolution of up to 18 μ m and optical transverse resolution of up to 60 μ m (Carl Zeiss Meditec Inc).

Besides those visual techniques, both PLC7030 rectangle and disk samples were retrieved from the animals at predetermined time point for weight average molecular mass (M_w) and number average molecular mass (M_n) measurement using the GPC method described above in section 3.3.2.

3.2.4 Measurement of water sorption in PLC7030

Two media were prepared to mimic the *in vitro* and *in vivo* environment for testing. The medium used for *in vitro* water sorption measurement is PBS buffer, pH7.4, at 37°C. We

also prepared hydrogel using Konnyaku with 70wt% water (PBS, pH7.4) by adding PBS buffer, heated to 90°C, into weighed Konnyaku powder with constant stirring until gelation while cooling down to room temperature. This is to mimic the *in vivo* water environment in the rabbit's eye [83]. Prior to each time interval, the samples were dried in 37°C vacuum oven for 1 hour. Subsequently, the dried samples (10×10mm², n=5) with thicknesses 250µm were immersed in the two prepared media (5mL PBS buffer and Konnyaku gel with dimension of 2×2×1 cm²) in closed vials at 37°C respectively.

The samples were removed from the media at pre-determined intervals, blotted on to tissue paper to remove surface moisture, and then water concentration in the samples was measured by Karl Fischer Method Moisture Meter (Mitsubishi, Japan). The sorption experiment was conducted for 7 days, assuming equilibrium water uptake has been established by then without any degradation.

3.2.5 *In vitro* drug release study

Three films of each drug-loading percentage (5%, 10% and 20%), with dimension 10×10mm², were weighed before testing. Each sample was then immersed in an individual amber vial containing 5ml PBS. Due to the poor solubility of prednisolone acetate in aqueous environment, buffer was refreshed everyday to maintain the “sink condition” in the first 7 days. Subsequently, at every predetermined time point, the film was taken out and put in 5ml fresh buffer. The amount of drug released was quantified by analyzing the remaining aliquot using high-performance liquid chromatography (HPLC). The concentration of drug in the buffer was determined by the HPLC (Agilent series 1200), at a wavelength of 240nm, using a ZORBAX 300SB-C18 column of pore size 5µm, acetonitrile/water 60/40 (v/v) as the mobile phase and flow rate of 1ml/min. The total amount of drug released is calculated by cumulative method, and release rate is calculated on daily basis.

3.2.6 Quantification of PA loaded in the PLC film and released in buffer

The actual drug loading was quantified by dissolving pre-weighed films (n=3) in acetonitrile at a ratio of 1mg (sample) to 5ml (acetonitrile). The concentration of drug in the solution was analyzed by HPLC, and then converted to weight. The drug loading was calculated by dividing the weight of drug detected over the weight of the film.

It was found that in PBS buffer (pH7.4), prednisolone acetate partially hydrolyzed into prednisolone gradually. When testing the drug in the aliquot during drug release, in order to achieve correct calibration and detection of prednisolone acetate in PBS, acetonitrile/PBS 1/1(v/v) was used as the medium for the drug to be tested. After taking out the film, 5ml of acetonitrile was added in the 5ml drug-containing aliquot, mixed uniformly before HPLC test. The total amount of prednisolone acetate released into buffer was calculated by adding moles of prednisolone acetate and prednisolone in each sample, following by converting the overall amount of drug in terms of mole to weight of prednisolone acetate.

3.2.7 *In vivo* drug release study

All the samples (6×3mm²) were sterilized by ethylene oxide (ETO) at 37°C (used for normal medical device) in Tan Tock Seng Hospital (Singapore) prior insertion into animals. Experimental filtration surgery was performed on the left eye of each rabbit using an established technique by ophthalmic surgeons [84]. All rabbits were firstly anesthetized. Subsequently a limited conjunctival dissection was performed and a 25-gauge cannula was passed from the limbus into the anterior chamber, trimmed and secured with 10/0 nylon to allow efflux of aqueous humor into the subconjunctival space. The film was then inserted in the subconjunctival space and sutured 2mm posterior to the site of the cannula with two 10/0 nylon sutures. Topical tetracycline ointment 1% was

administered daily post-operation for 5 days. All procedures were performed in accordance with the ARVO Statement for the Use of Animals in Ophthalmic and Vision Research. The drug loaded films were then retrieved from the animal at pre-determined time point. The residual drug in the retrieved films was analyzed by the method described in section 3.3.6, same as the drug loading test.

3.2.8 Statistical analysis

Statistical analysis included descriptive statistics, where the mean and standard deviation (SD) was calculated for the continuous variables, with sample size equal to or greater than 3. The student's t-test was used to analyze the results, where inter-comparison is required for two groups of data. The F-test (ANOVA) was employed if the comparison involves three or more groups of data. P-values of less than 0.05 were defined as statistically significant. All data was expressed as mean \pm SD unless otherwise stated.

Chapter 4 Characterization of Candidate Materials

The study aimed to develop and characterize biodegradable microfilms made from two different biomaterials for their potential application as vehicles for intraocular drug delivery, specifically on surgical insertion into the subconjunctival space.

Blank microfilms with controlled thickness, were fabricated from poly d,l-lactide-co-glycolide (PLGA5347) and poly d,l-lactide-co-caprolactone (PLC7030). From past studies and technical data (provided by the manufacturer), firstly, the glass transition temperatures of PLC7030 and PLGA5347 are below or around body temperature (37°C), which made the materials soft under body temperature to accommodate the delicate nature of the eye; secondly, PLGA5347 and PLC7030 demonstrate different degradation periods, which potentially provide tailored period of the implant in the body. Furthermore, these two biomaterials also demonstrated biocompatibility to some extent from various sites of the body, as discussed in the literature review. Therefore, PLGA5347 and PLC7030 were selected initially as the candidate materials to be further studied.

The degradation behaviour *in vitro* and *in vivo* of both types of microfilms was evaluated. Water absorption, mass loss, monitoring of M_w and M_n , as well as change in film thickness are the parameters that govern the *in vitro* degradation. And in the *in vivo* study involved using two complementary techniques: slit-lamp microscopy and anterior segment optical coherence tomography (AS-OCT). According to the similar work done in the lab previously, the initial film thickness was chosen to be 500 μm .

The size of samples for *in vitro* and *in vivo* degradation is $6 \times 3 \text{ mm}^2$. The physical properties of PLGA5347 and PLC7030 before and after sample preparation (both with thickness 500 μm) are listed in Table 4.1.

Table 4.1 Physical properties of PLGA5347 and PLC7030 (500 μ m)

Properties	PLGA5347		PLC7030	
	Film	As received	Film	As received
*Glass transition temperature, T_g ($^{\circ}$ C)	39.3 \pm 1.7	46.3 \pm 4.3	12.7 \pm 3	16.5 \pm 5
*Melting temperature, T_m ($^{\circ}$ C)	--	--	100 \pm 5	115 \pm 5
*Crystallinity	--	--	4~6%	6~9%
#Intrinsic viscosity, IV (dl/g)	1.05	1.05	1.66	1.66
^Weight average molecular weight, M_w (kDa)	148 \pm 5	160	180 \pm 5.8	210
^Number average molecular weight, M_n (kDa)	67 \pm 1.5	75	90 \pm 3.2	115
^Polydispersity index (M_w/M_n)	2.2	2.04	2	1.91

*As measured by Differential Scanning Calorimetry

#As indicated by certificate of analysis provided by manufacturer

^As measured by Gel Permeation Chromatography

PCL, $\Delta H_m^0 = 139.5$ J/g [85], PLLA, $\Delta H_m^0 = 93$ (J/g) [86]

PLC7030 (as received), $\Delta H_m = 8.35$ (J/g), PLC7030 (film), $\Delta H_m = 5.97$ (J/g)

4.1 Experimental results

4.1.1 *In vitro* degradation study

Various attributes of the PLGA5347 and PLC7030 were studied *in vitro*, including water absorption, mass loss, change in thickness, change in molar mass as well as change in polydispersity index, to characterize the degradation of both types of microfilms.

4.1.1.1 Water absorption

As these polymers degrade in the medium by simple hydrolysis, water absorption rates influence the hydrolysis rates. The amount of water absorbed in the microfilm increased with immersion time for both polymers (Figure 4.1). In the current study, PLGA5347 started to absorb significant amounts of water after a week, absorbing more than 50% by day 42, whereas PLC7030 absorbed only about 1% of water over 8 weeks. The results obtained are quite comparable with the previous studies done by H. Kranz [87] and Y. Zhang [88], who reported on water absorption in the study of degradation of PLGA5347 (approximately three times lower M_w compared with the PLGA5347 used in the current study): they showed that water absorption of PLGA5347 ($M_w=56,500\text{Da}$) reached 90% on the 21st day of study and 80% on the 30th day for PLGA5347 ($M_w=42,000\text{Da}$).

The difference between the two polymers (PLGA5347 and PLC7030) is primarily due to two factors: first, the PLGA5347 is completely amorphous with a T_g close to 40°C, and this allows quicker water penetration. The PLC7030 is semi-crystalline, and water absorption is limited to the amorphous phase. Second, the glycolide segment is more hydrophilic than either the lactide and caprolactone moiety, which results in a more hydrophilic PLGA5347 matrix. Moreover, once significant water absorption occurs, the hydrolysis is accelerated, resulting in oligomers that are increasingly more water-soluble.

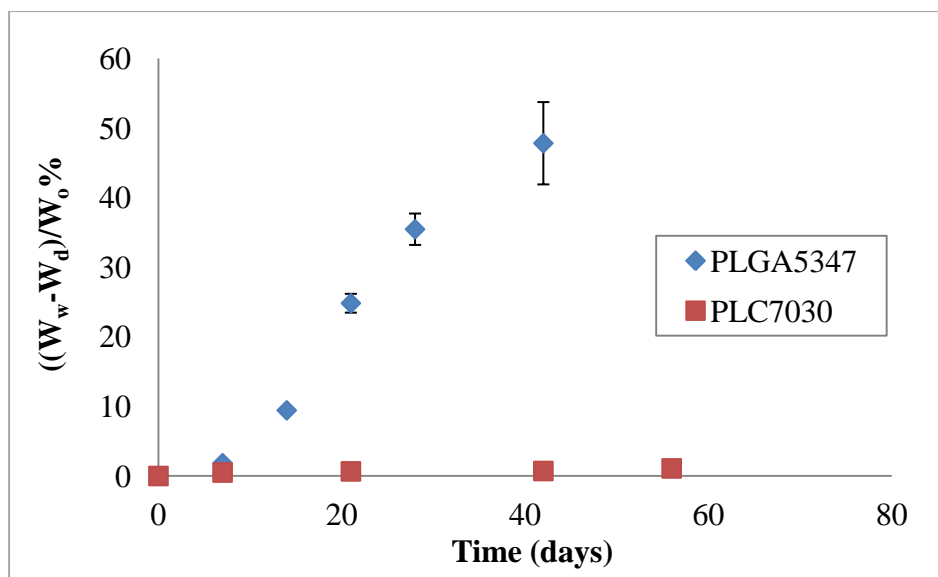


Figure 4.1(I) In vitro water absorption of PLGA5347 and PLC7030 (500µm)

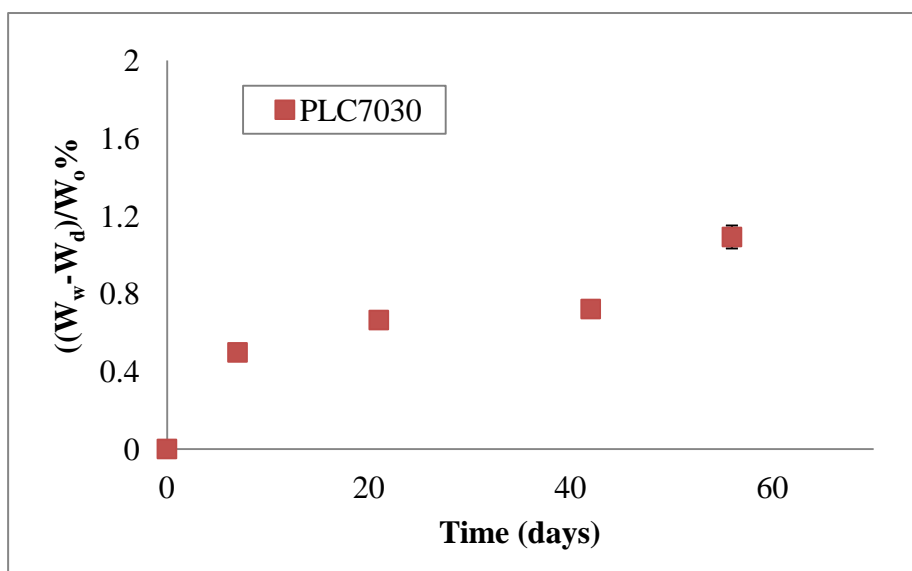


Figure 4.1(II) In vitro water absorption of PLC7030 (500µm) (expanded Y-axis)

Generally, this class of polymers (poly α -hydroxy esters) undergo what is called bulk (or homogeneous) hydrolysis. Water enters and fills the volume of the polymer sample; degradation proceeds throughout the bulk of the polymer. As more oligomers are produced by hydrolytic scission, the extent of water uptake does change with time.

Eventually, the oligomers are of low enough molar mass to be water-soluble, and hence leach out leading to the observed mass loss [54].

4.1.1.2 Mass loss

In conjunction with water absorption, mass loss started earlier for PLGA5347. At 3 weeks, PLGA5347 started to lose significant mass (lost almost 100% in the end of 42 days), whereas PLC7030 did not demonstrate any notable mass loss until after day 56 (Figure 4.2(I)). As water absorption increased, PLGA5347 started to degrade, with oligomers being produced with carboxylic end groups (-COOH). Such oligomers become increasingly water-soluble as molar mass decreases. In contrast, PLC7030 had absorbed very little water and hence the observed hydrolysis rate was low, with water-soluble oligomers not forming to any measurable extent until day 56. The mass loss results for PLC7030 are consistent with the study done by Lu *et al.*, which showed less than 3% mass loss for PCLA70 (400 μm thick), as seen in Figure 4.2(III) [63].

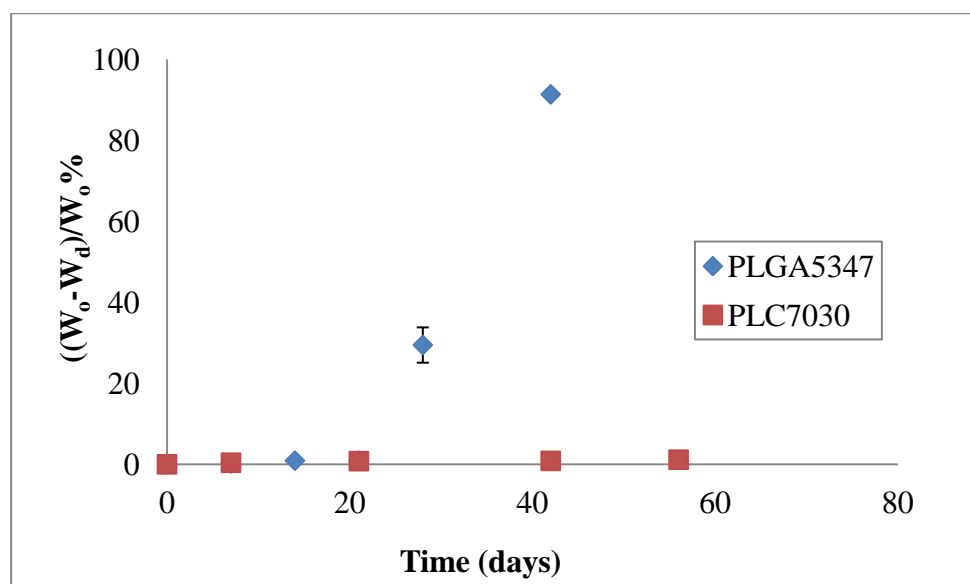


Figure 4.2 (I) In vitro mass loss of PLGA5347 and PLC7030 (500 μm)

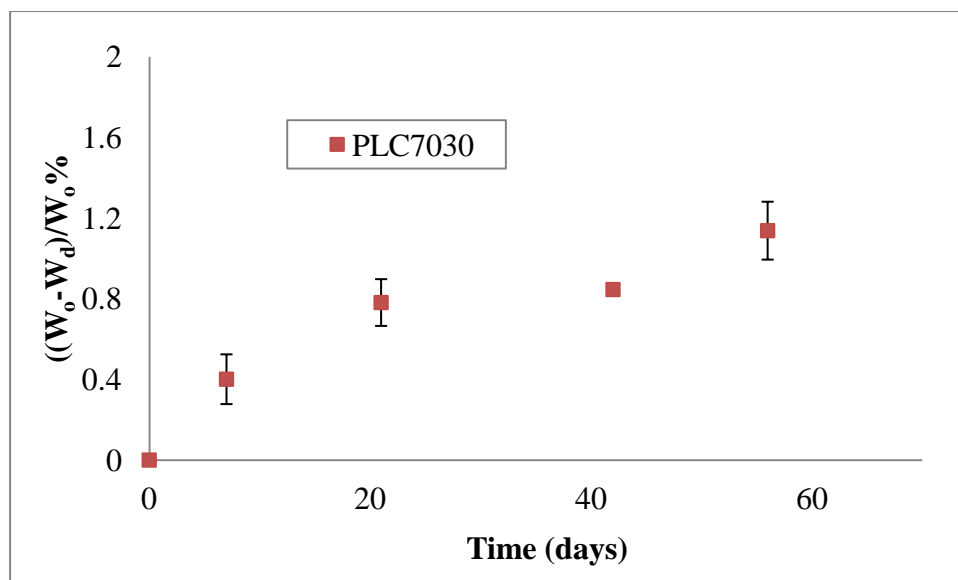


Figure 4.2(II) In vitro mass loss of PLC7030 (500 μm) (Expanded Y-axis)

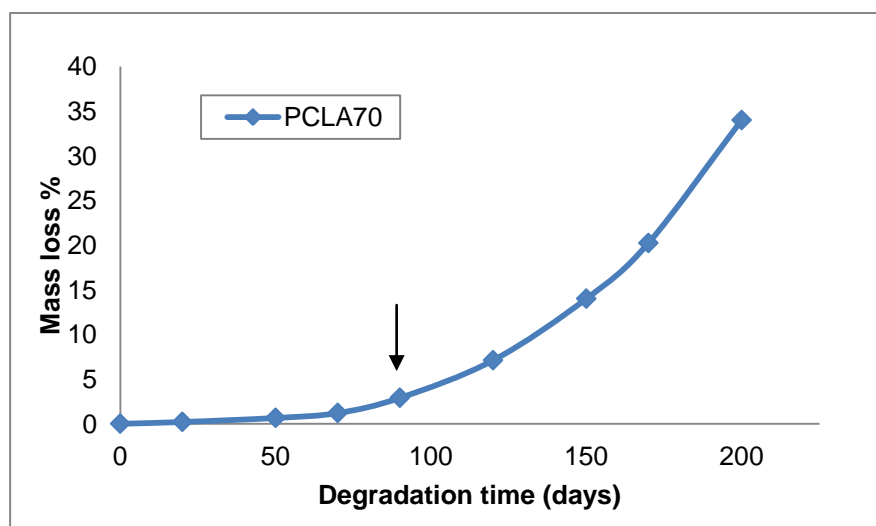


Figure 4.2 (III) Dependence of mass loss of polymers on degradation time, pH7.4, 37°C (redrawn from reference [63])

4.1.1.3 Change of molecular weight (M_w , M_n) and PDI

There was a notable decrease in weight molecular mass for both PLGA5347 (42 days) and PLC7030 (96 days) over the period of study (Figure 4.3). The M_w/M_0 versus time graph showed that both polymers demonstrated bulk degradation with a thickness of

500 μ m. PLGA5347 degraded faster than PLC7030, and the drop in M_w agreed with the corresponding water absorption and mass loss of these two materials.

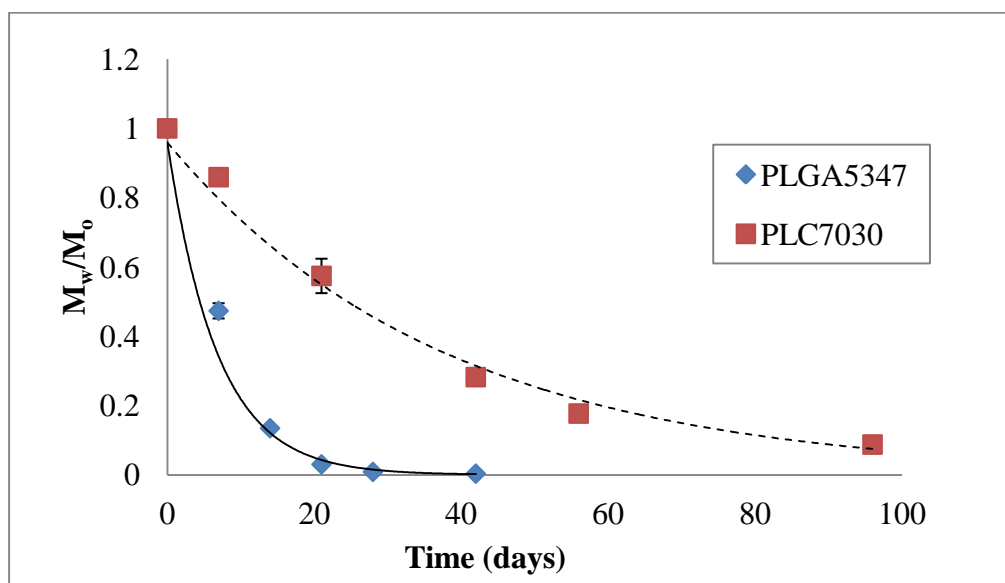


Figure 4.3 Monitoring of M_w for PLGA5347 and PLC7030 in vitro (500 μ m)

As shown in Figure 4.4, PDI of both polymer samples increased with time. PDI for PLGA5347 increased from week 2, but dropped to a lower value (lower than its initial PDI) on day 42, which shows it is fully degraded. PDI for PLC7030 increased slightly in the first 56 days of study, but increased drastically to 5 or more at the end of the study (not fully degraded at the end of the study period).

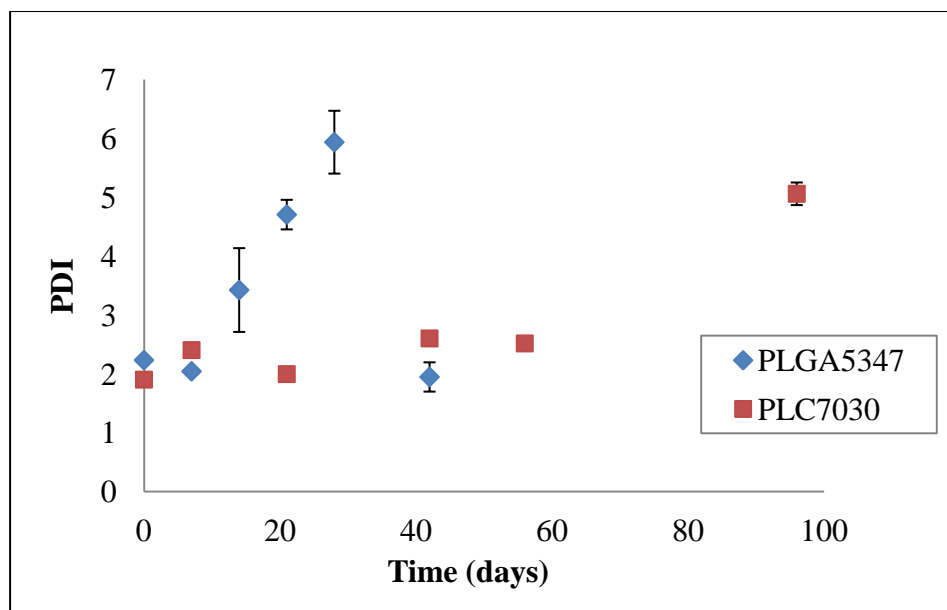


Figure 4.4 Monitoring of PDI for PLGA5347 and PLC7030 *in vitro* (500 μ m)

4.1.1.4 Thickness change with degradation

The thickness of PLGA5347 was unchanged (within 2%) in the first 14 days, and started to decrease on the 21st day, followed by a sudden drop of 60% which occurred on the day 42 (Figure 4.5(II)). From the observed changes on mass loss, PLGA5347 lost 90% of its initial weight on day 42, and corresponded to the change in film thickness. Furthermore, we observed the PLGA5347 film to become increasingly softer with time, and the film thickness was not measurable after 42 days. In contrast, PLC7030 maintained its shape throughout the entire duration of the study period, with minimal change in film thickness (Figure 4.5(I)).

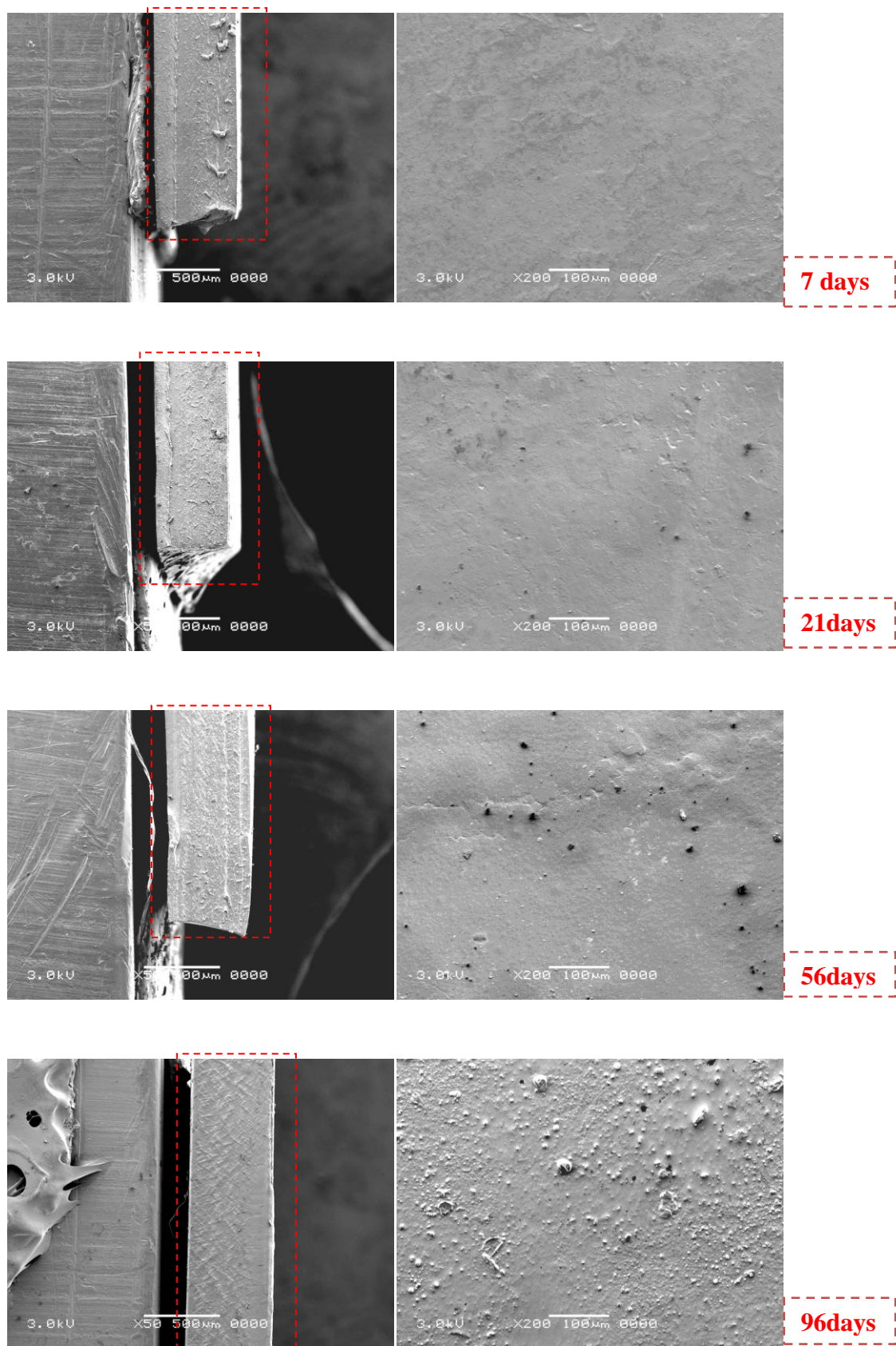


Figure 4.5 (I) SEM images of cross-section (left column) and morphology (right column) of PLC7030 films (500μm)

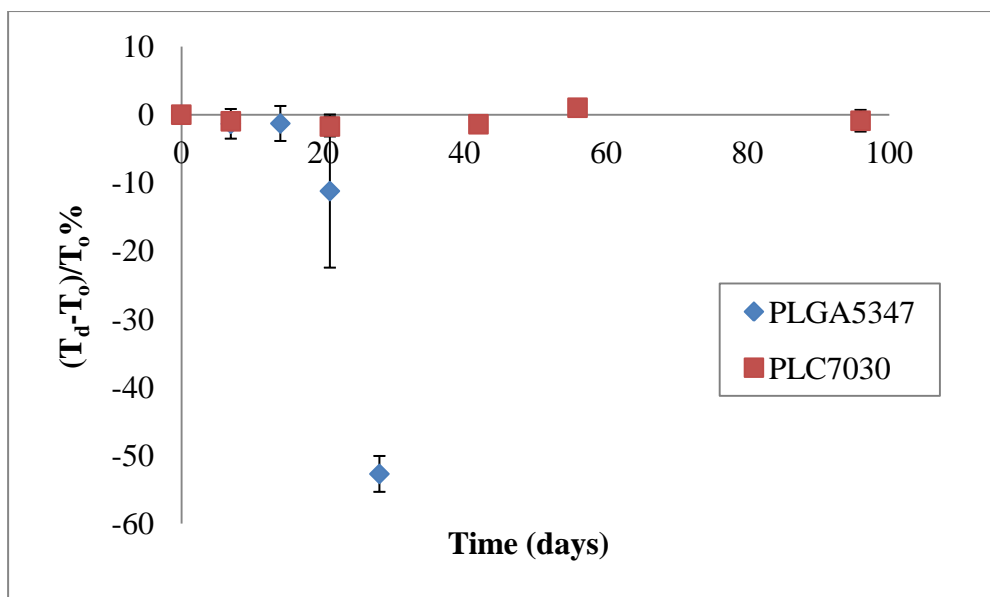


Figure 4.5 (II) Change of film thickness of PLGA5347 and PLC7030 *in vitro* (500 μm)

4.1.1.5 Summary of *in vitro* degradation results

PLGA5347 and PLC7030, which are poly α -hydroxy esters, both exhibited bulk degradation mechanism *in vitro*, with exponentially decaying molecular weight (M_w) and unchanged film thicknesses (before full disintegration). PLGA5347 started to absorb significant amount of water after the first week, and mass loss was initiated on the 3rd week of study. Moreover, the film thickness of PLGA5347 decreased from 3rd week onwards (which is consistent with the mass loss results) until it became immeasurable on the 42nd day. Full degradation was observed for PLGA5347 on the 42nd day. Not as evident, PLC7030 lost 90% of its initial average weight molecular mass at the end of the study (96th day), with minimal water absorption and mass loss (both are less than 2%), as well as almost unchanged dimensions. Both these polymers therefore appear to degrade by bulk degradation *in vitro*, as evident from the molar mass loss data alone.

4.1.2 *In vivo* degradation study

4.1.2.1 *Visual appearance of implanted microfilms observed by slit lamp*

From slit lamp photographs (Figure 4.6), it was noticed that the external ocular examination of the PLGA5347 microfilms appeared more pliable compared to the PLC7030 microfilms, which retained its original shape. The animals did not display any signs of ocular discomfort, nor was there any extrusion of any of the implants from either material. At month 3 onwards, the PLGA5347 microfilms had dissolved to such an extent that they were not grossly visible with slit-lamp examination. In contrast, PLC7030 microfilms persisted and visible up to 6 months with unchanged width and length.

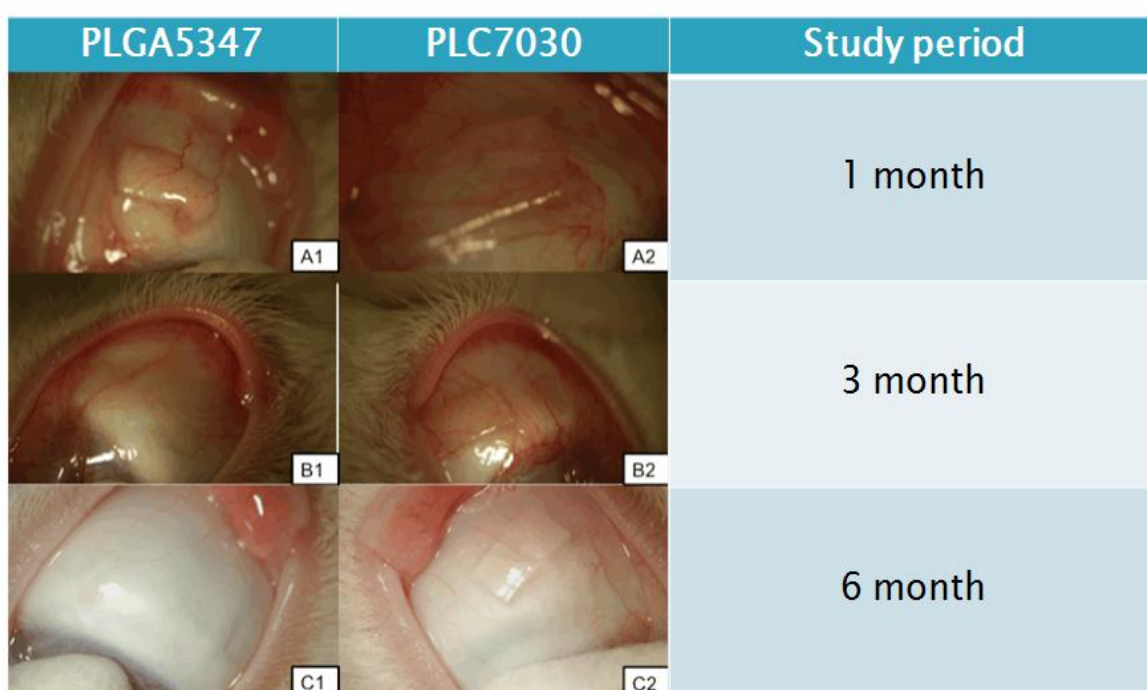


Figure 4.6 Slit-lamp photographs of PLGA5347 and PLC7030 microfilms after surgical insertion into the subconjunctival space of rabbits eyes at 1, 3 and 6 months (500 μ m)

4.1.2.2 Anterior segment optical coherence tomography (AS-OCT) scans

The AS-OCT images taken at monthly intervals revealed good anatomical placement of all microfilms implanted (n=18) in the subconjunctival space (Figure 4.7). The red-cross labelled area is the microfilm, inserted in between conjunctiva (denoted as C) and sclera (denoted as S), and the scale bar on the right top corners of each graph displays 500 μ m. No migration from the original surgically implanted site was seen in any of the implants.

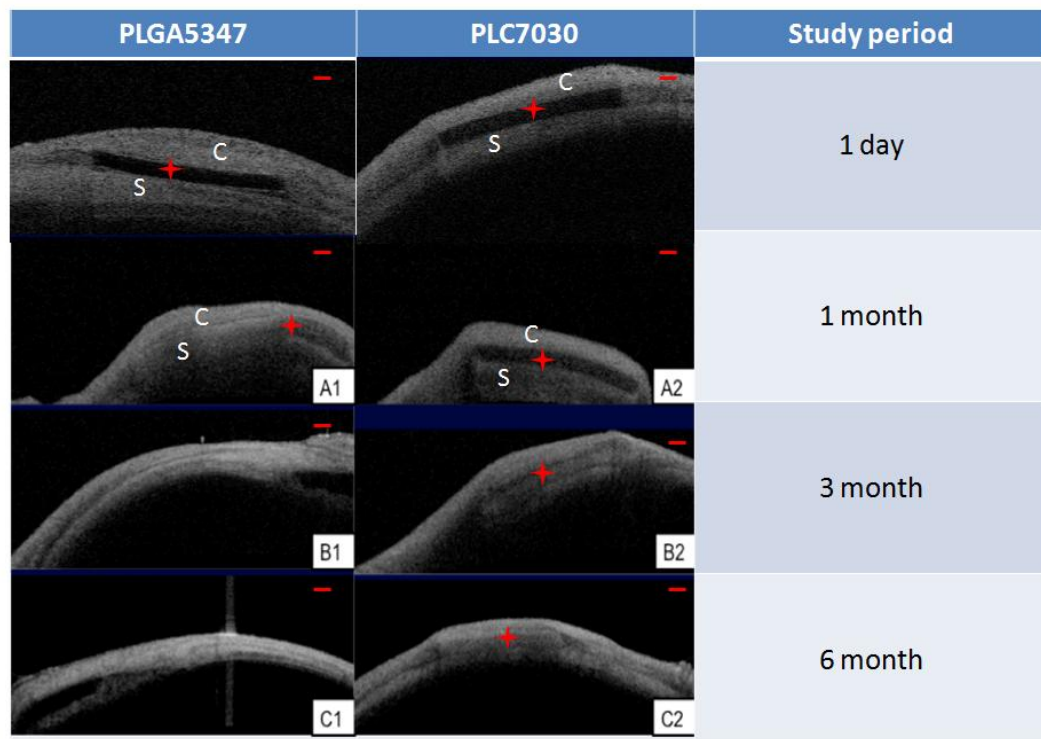


Figure 4.7 AS-OCT scans of PLGA5347 and PLC7030 microfilms after subconjunctival implantation in rabbits' eyes at 0, 1, 3 and 6 months (500 μ m)

Serial measurements were taken from the AS-OCT images that measured multiple sections of the implanted microfilms. We found that the thickness of both PLGA and PLC microfilms decreased, and PLC7030 decreased in a linear fashion ($R^2=0.8878$ for PLC7030), as measured by AS-OCT (Figure 4.8).

When change of thickness for PLGA5347 and PLC7030 were plotted, clearer *in vitro* and *in vivo* comparison can be made for PLGA5347 and PLC7030 respectively. Looking at PLGA5347 *in vitro* (blue colour) in Figure 4.9, the thickness was unchanged within 14 days, following a sudden drop of 50% in the subsequent 2 weeks, before becoming too soft to be measured at the 42nd day. Similarly, thickness of PLGA5347 microfilms *in vivo* decreased in a same manner as that *in vitro*, but at a faster rate; despite of the “missing points” within the first month (*in vivo* measurements were done by monthly basis).

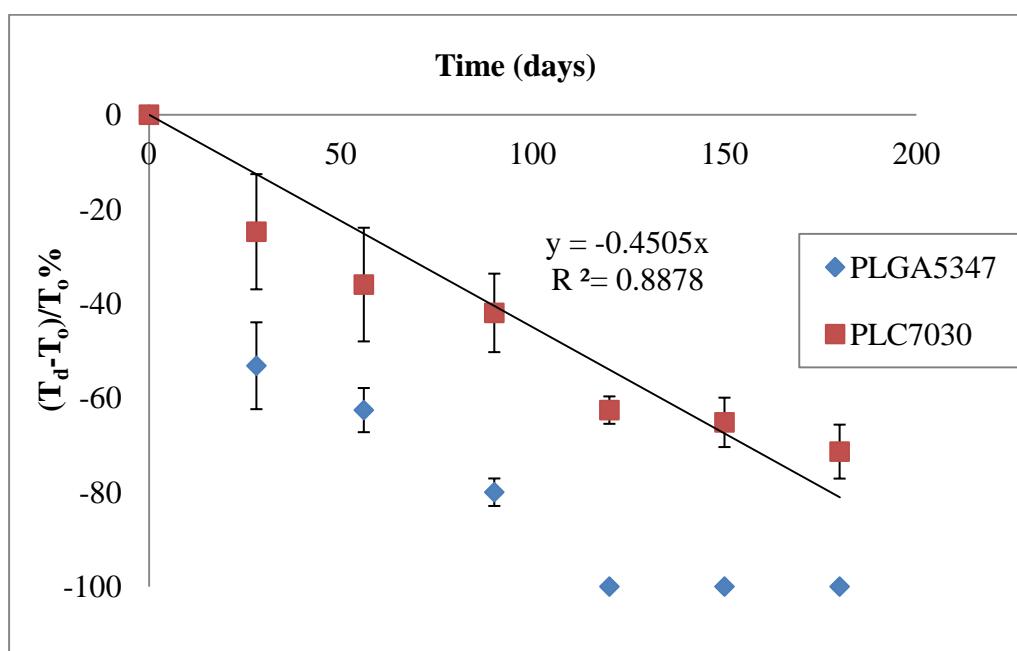


Figure 4.8 Serial AS-OCT thickness measurements of PLGA5347 and PLC7030 microfilms in subconjunctival space (500 μm)

However, PLC7030 demonstrated significantly different degradation mechanisms *in vitro* and *in vivo*, which can be seen from red colour dots and squares in Figure 4.9. *In vitro*, film thickness of PLC7030 samples did not change until the 96th day, nevertheless, the film thickness of PLC7030 samples *in vivo* decreased linearly over a period of 6 months, which is typically observed in surface erosion or heterogeneous degradation[65]. If

extrapolating the change of film thickness for PLC7030 *in vitro*, represented by red circles, it will maintain till a point when the whole matrix disintegrates, and then drop suddenly to zero (Figure 4.9).

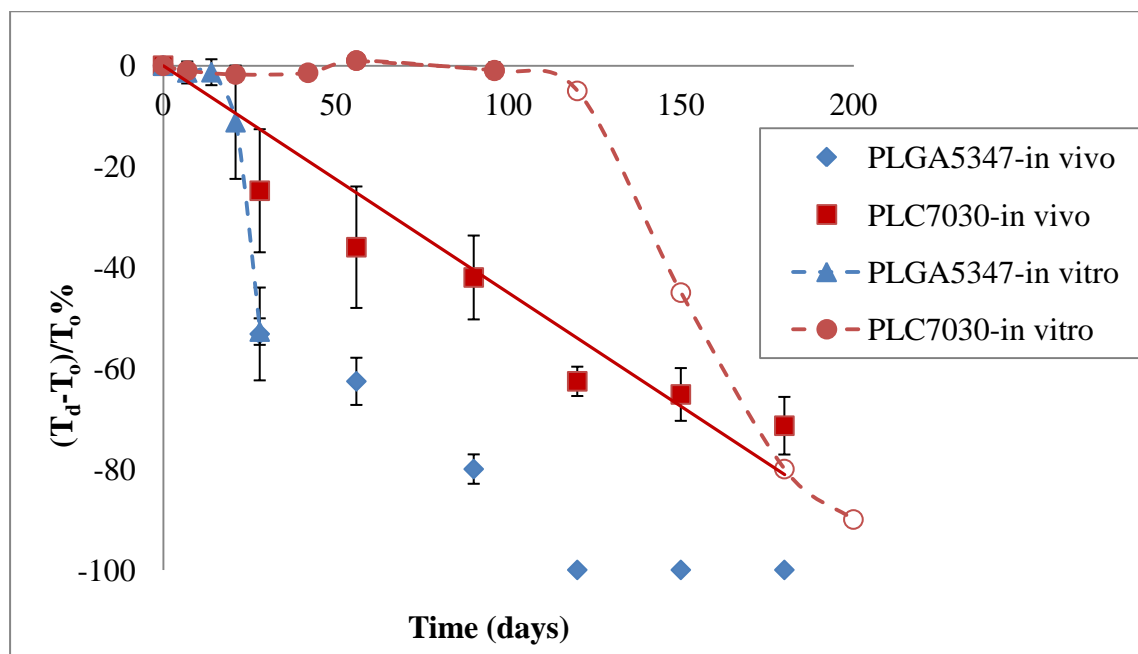


Figure 4.9 Change of thickness for PLGA and PLC microfilms, *in vitro* and *in vivo* (500 μm)

4.1.2.3 Summary of *in vivo* degradation results

PLGA5347 was degraded and non-visible in the rabbit eyes 3 months after the study; whereas PLC7030 persisted throughout 6 months of study, with unchanged width and length, but linearly decreasing film thickness, as observed from the slit-lamp microscopy and As-OCT graphs. *In vivo*, PLGA5347 degraded homogeneously also, but PLC7030 appears to degrade heterogeneously.

4.2 Discussions

4.2.1 Degradation period of PLGA5347 and PLC7030

The study shows that, for microfilms with thickness of 500 μm , both *in vitro* and *in vivo* degradation period of PLGA5347 is shorter (fully degraded in 42 days *in vitro*, grossly not visible after 3 months *in vivo*) as compared to PLC7030 (not fully degraded in 96 days *in vitro*). As discussed in Chapter 2, this difference between the two polymers is attributed to composition and crystallinity differences. Firstly, the glycolide segment is more hydrophilic than the lactide and caprolactone moiety, as caprolactone unit comprises five methylene groups in between two ester groups as compared to only one methylene group of an glycolide unit, which results in a more hydrophilic PLGA5347 matrix as compared to PLC7030 (water-air contact angle for PLGA5347 is 73 ± 2 degree [89], whereas water-air contact angle for PLC7030 is 83.4 ± 1.1 [90]). Once significant water absorption occurs, the hydrolysis is accelerated, resulting in oligomers (glycolic acid, lactic acid and caproic acid) that are increasingly more water-soluble, which will further increase water absorption, thus hydrolysis rate is faster for PLGA5347. Secondly, when hydrolysis takes place, the amorphous region will be attacked first. PLGA5347 is an amorphous polymer with a T_g close to 40°C , thus water can easily ingress into the polymer matrix. PLC7030 is a semi-crystalline polymer with a low but measurable degree of crystallinity [91], and water penetration is limited to the amorphous region.

4.2.2 Bulk degradation or surface erosion?

It is generally accepted that, in the class of polymers used (poly α -hydroxy esters), there may be two different modes of hydrolytic degradation. In the first mechanism, which is often referred to as homogeneous or bulk degradation, the polymers degrade slowly with no appreciable mass or volume loss until the degradation products become water-soluble and leach out of the matrix, when mass loss is then detectable (Figure 4.10(I) and Figure 4.10(III)). In the second mechanism, the polymer degrades first at the surface, and the surface molecules decrease in molecular weight to the point where the surface molecules leach out, without affecting the interior of the material. In this mode of degradation, which is sometimes referred to as heterogeneous degradation or surface erosion, there is continuous decrease in mass and in the material dimensions (Figure 4.10(II) and Figure 4.10(III)) [65], but no change in bulk molar mass

From the results, for thickness of 500 μ m, PLGA5347 films clearly exhibited bulk degradation *in vitro* and *in vivo*. Although not as evident (since no significant water absorption or mass loss has been detected up to day 56 – Figure 4.1(I) and Figure 4.2(II)), *in vitro*, PLC7030 also exhibited molar mass decrease (Figure 4.3) without much mass loss, which is also characteristic of bulk degradation. However, PLC7030 behaves differently when implanted into the rabbit eyes. PLC7030 microfilms underwent surface erosion in the subconjunctival space, as evidenced by the serial measurements using Slit-lamp microscopy and AS-OCT techniques, since the width and length of the microfilms did not change visually over 6 months (Figure 4.6), but thickness of the films (Figure 4.7) decreased continuously.

Usually, the polymer changes from a bulk degradation mode to a surface erosion mode when the intrinsic hydrolysis rate (R_h) becomes higher than the water ingress rate into the polymer (R_w). We hypothesize that in the *in vivo* situation, R_h is being increased relative

to R_w , most likely due to the influence of enzymes (esterases) or proteins present in the eye [92].

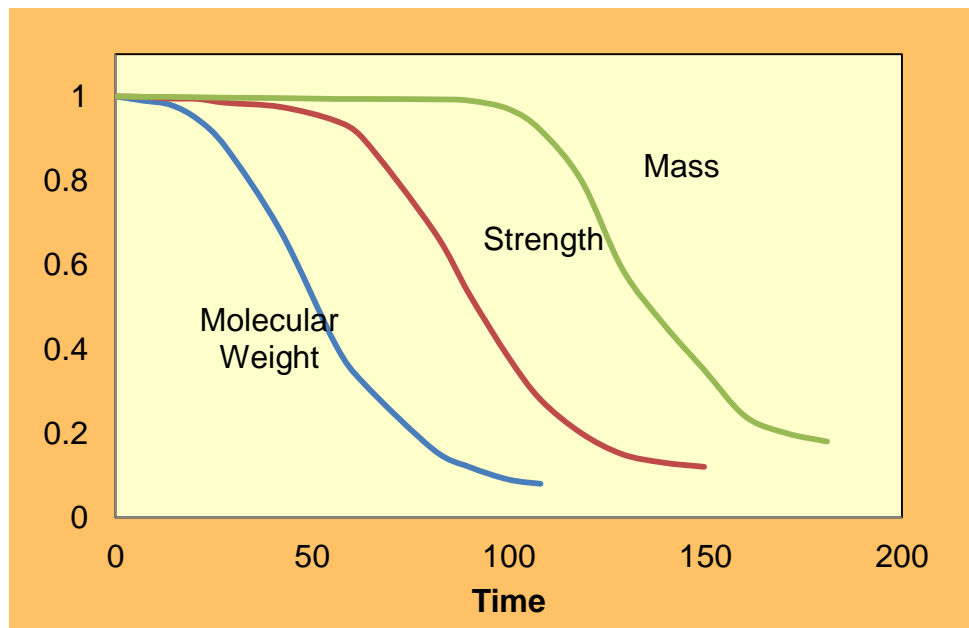


Figure 4.10 (I) Demonstration of homogeneous degradation behaviour

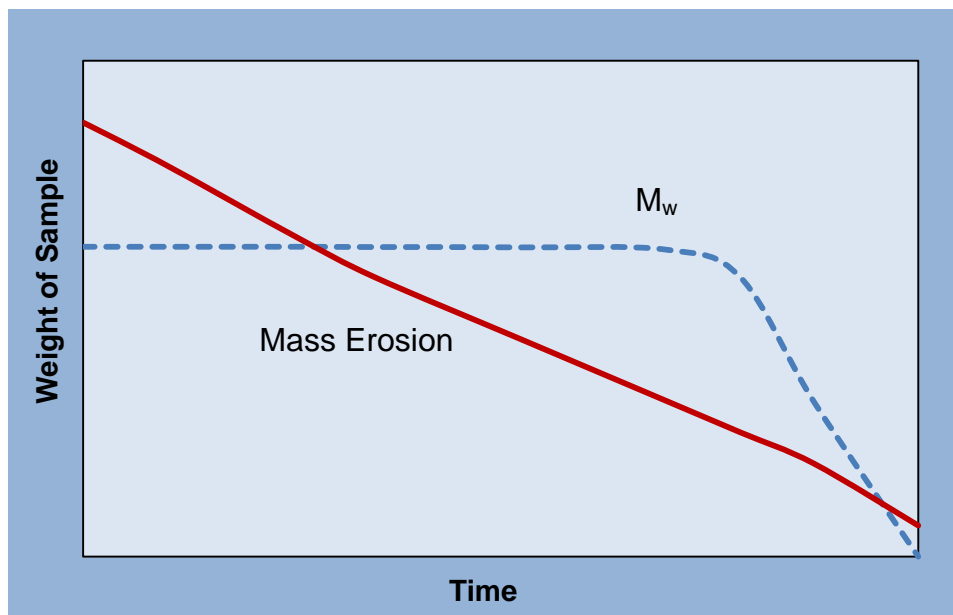


Figure 4.10 (II) Demonstration of heterogeneous degradation behaviour

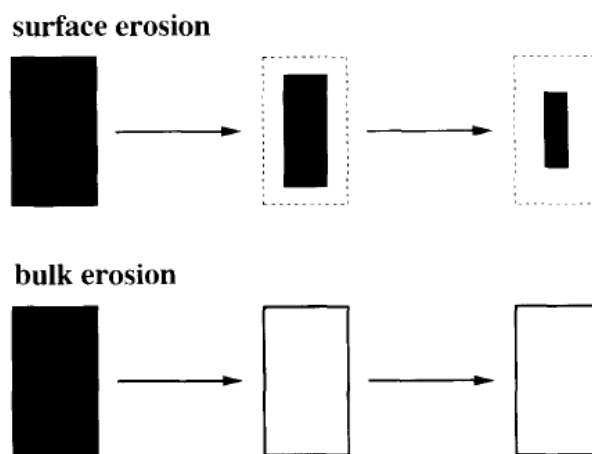


Figure 4.10 (III) Schematic illustration of surface erosion and bulk erosion [54]

A surface erosion mode is the preferred mode in many implant applications, as bulk degradation may lead to “catastrophic” breakdown into small fragments causing localized irritation. Surface erosion also results in a constant release of incorporated drug. PLGA and PLC are anionic polymers that undergo bulk degradation *in vitro*. Embedded drugs are released from the matrix via diffusion initially, followed by degradation of the polymer matrix itself [93]. Thus the first observation of surface erosion of this grade of polymers in the sub-conjunctival space is exciting and opens the door for a more efficient therapeutic route.

4.3 Conclusions

In this chapter, degradation of PLGA5347 and PLC7030 was studied both *in vitro* and *in vivo*. This is the first time, to the author’s knowledge, to test the *in vivo* degradation of poly-lactide-group biodegradable polymers, as films, in the sub-conjunctival space of the rabbit eyes, which demonstrated very different behaviour as compared with the *in vitro* degradation results.

PLGA5347 and PLC7030 both exhibited bulk degradation mechanism *in vitro*, with exponentially decaying molecular weight (M_w) and unchanged film thicknesses (before full disintegration). PLGA5347 started to absorb great amount of water after the first week, and mass loss was initiated on the 3rd week of study. Moreover, the film thickness of PLGA5347 decreased from 3rd week onwards (which is consistent with the mass loss results) until it became immeasurable on the 42nd day. Full degradation was observed for PLGA5347 on the 42nd day. Not as evident, PLC7030 lost 90% of its initial average weight molecular mass at the end of the study (96th day), with minimal water absorption and mass loss (both are less than 2%), as well as almost unchanged dimensions.

In vivo, PLGA5347 was degraded and became non-visible in the rabbit eyes 3 months after the study; whereas PLC7030 persisted throughout the 6 months, with unchanged width and length, but linearly decreasing film thickness. In summary, PLGA5347 degraded homogeneously both *in vitro* and *in vivo*, nevertheless PLC7030 degraded homogeneously *in vitro*, and might degrade heterogeneously *in vivo*. This is quite a novel finding, since no one has reported biodegradable polymers hydrolyze homogeneously *in vitro* but heterogeneously *in vivo*. Due to the different period of degradation for PLGA5347 and PLC7030, tailored period of drug release can be achieved by selecting an appropriate matrix.

Chapter 5

Study of Degradation Behaviour of PLC7030

--The effect of sample shape, thickness and degrading media

In the previous section, interesting results were obtained from the degradation study of 500 μm -microfilms made from PLC7030. It appeared to degrade homogeneously *in vitro* but heterogeneously *in vivo*. This chapter will further investigate the degradation behaviour of PLC7030. The parameters studied are shape of the sample, thickness of sample and degrading media (*in vitro* and *in vivo*) (Table 5.1).

Table 5.1 Parameters of PLC7030 degradation study

Thickness(μm)	Shape	Dimension(mm^2)	Media
500	Rectangle	3×6	PBS, pH7.4
			Rabbit eyes
250	Square	10×10	PBS, pH7.4
	Rectangle	3×6	PBS, pH7.4
			Rabbit eyes
	Disk	$\Phi 2$	PBS, pH7.4
			Rabbit eyes
80	Rectangle	3×6	PBS, pH7.4

5.1 Results and Discussions

5.1.1 Effect of sample shape

Previously, researchers found that degradation rate is affected by the shape and dimension of the samples even for bulk degrading polymers, such as poly (d,l)-lactic acid [94] and poly (lactide-co-glycolide) [95]. Is the degradation of PLC7030 also affected by the shape of samples? Therefore, the effect of sample shape on the degradation of PLC7030 was evaluated in this section. The shapes investigated in this study involved square ($10 \times 10 \text{ mm}^2$), rectangle ($3 \times 6 \text{ mm}^2$) and disk (diameter is 2 mm^2), with thickness of $250 \mu\text{m}$, in PBS buffer, pH7.4, at 37°C for *in vitro* studies and in subconjunctival space of rabbit eyes for *in vivo* studies.

5.1.1.1 *In vitro* degradation

i. Mass loss

PLC7030 (thickness of $250 \mu\text{m}$) square samples started to show notable loss in mass (1.5%) from day 56 onwards, and reached 4.6% on the 84th day of study. Comparatively, the onset time point for the mass loss in rectangular and disk samples was at 28th day, with the same amount of mass loss for square samples on day 56 (more than three times higher mass loss compared to square samples on day 28). Both kept increasing until 4.5% on 84th day for rectangle samples (the results on 84th day coincide with the results for square samples) and 3.5% on the 84th day for disk samples, as shown in Figure 5.1. Though onset time in mass loss for rectangle and disk samples seemed to be earlier than the square samples, due to the great standard deviation values, it can be considered as not much different in mass loss among the three shapes.

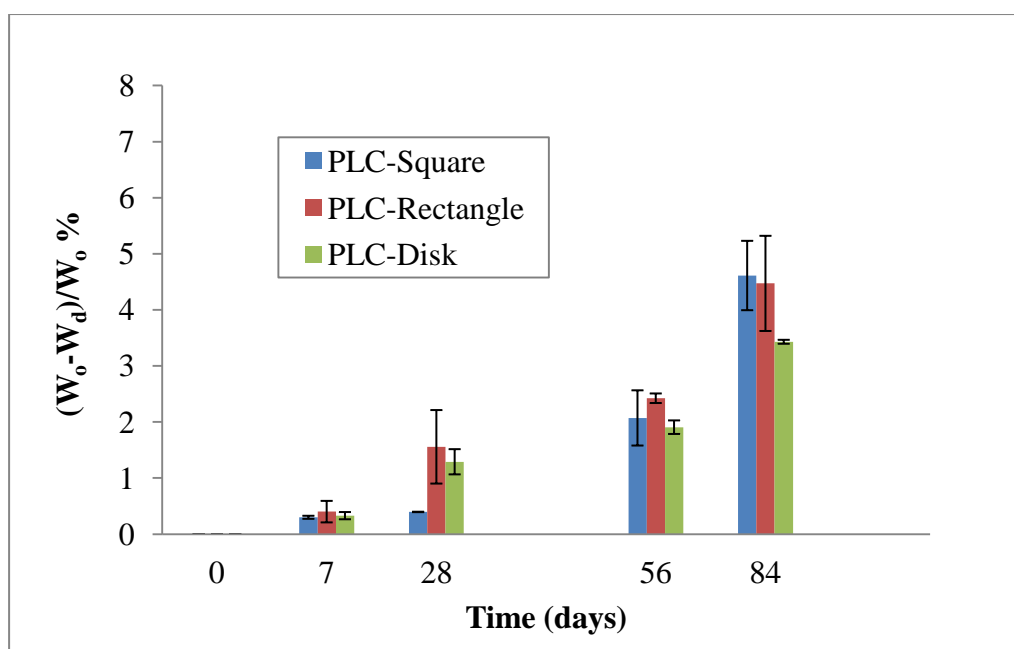


Figure 5.1 Relative mass losses of PLC7030 square, rectangle and disk samples (250 μm), in PBS, pH7.4, and 37°C

ii. Monitoring of M_w and M_n

As expected in bulk degrading polymers, the molecular mass (M_w and M_n) of all samples (three shapes) decreased exponentially with time. This coupled with the fact that fairly small mass loss in the first 30 days provides evidences for the bulk degradation mechanism.

There was no significant difference observed between square and rectangle samples in both M_w and M_n measurements. Though the disk sample seemed to degrade slightly slower, as compared to the square and rectangle samples, the difference is not statistically significant (Figure 5.2). In other words, with a thickness of 250 μm , degradation behaviour of PLC7030 is not affected by the shape of the samples.

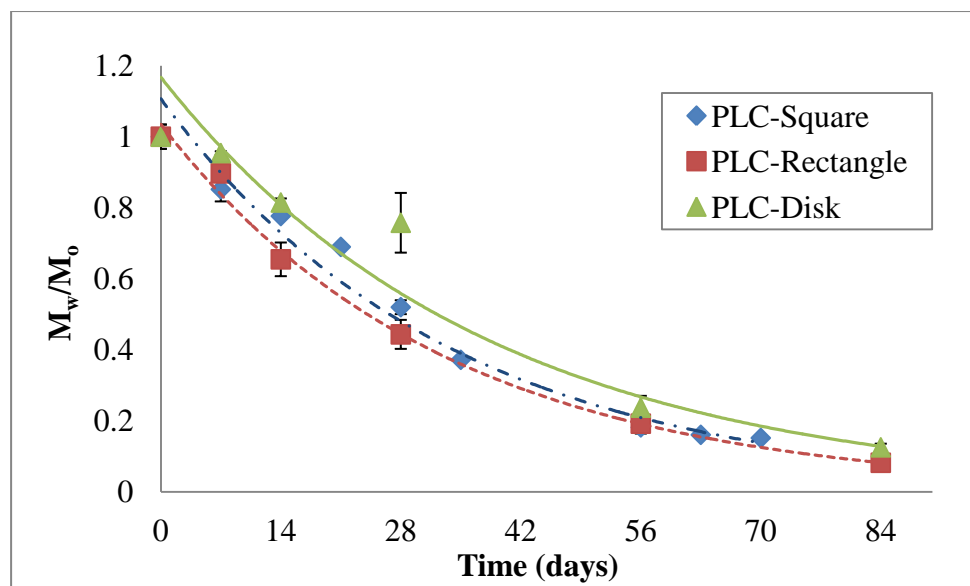


Figure 5.2 Changes of weight average molecular mass of PLC7030 with time for square, rectangle and disk samples (250 μm), pH7.4, 37°C

As discussed in Chapter 2, the rate constant λ for hydrolysis (degradation) can be obtained by exponentially fitting the curve M_n versus time. The constant λ is the rate of ester bonds breakage in the polymer. Higher values of λ reveal faster rates of degradation. By plotting relative M_n (M_n/M_0) versus time for square, rectangle and disk samples, λ can be obtained for each shape (Figure 5.3). The respective values for the three shapes are listed in Table 5.2. Being consistent with results for the change in M_w , λ_{Square} and $\lambda_{\text{Rectangle}}$ shared the same value, whereas λ_{Disk} is lower than λ_{Square} and $\lambda_{\text{Rectangle}}$. That is to say that disk samples tend to degrade slower than square and rectangle samples *in vitro* under the same environment (pH7.4, 37°C).

Additionally, we also calculated the polydispersity index (PDI) by taking the ratio of M_w over M_n , which is a measure of width of the molecular weight distribution for a polymer. The closer the polydispersity approaches a value of one, the narrower is the molecular weight distribution. Else, the higher value of polydispersity index is, the wider the molecular weight distribution. Figure 5.4 demonstrates the change of PDI with time for

square, rectangle and disk samples in the *in vitro* degrading environment. The PDI value for all the three samples gradually increased with time from a value of 2. And there is not a significant difference among the three samples.

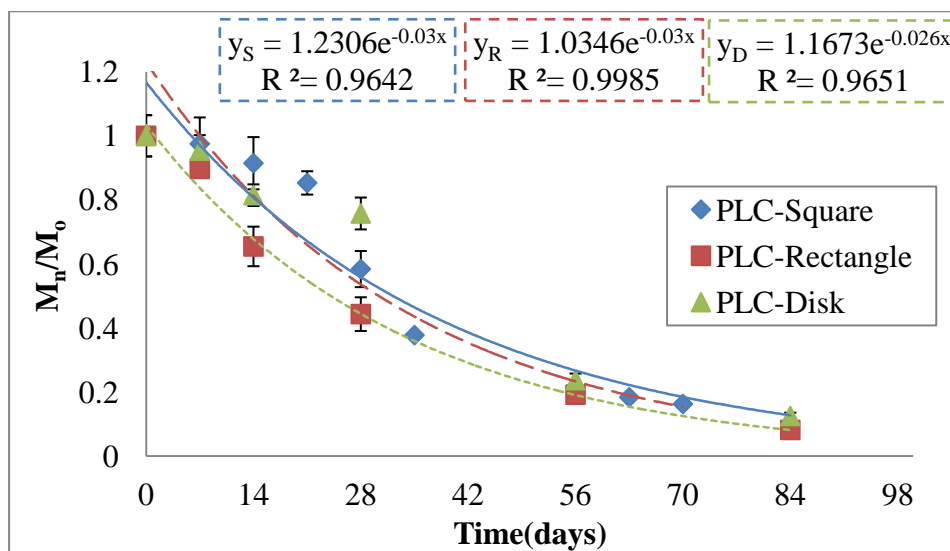


Figure 5.3 Changes of number average molecular mass with time of PLC7030 square, rectangle and disk samples (250 μm), pH7.4, 37°C

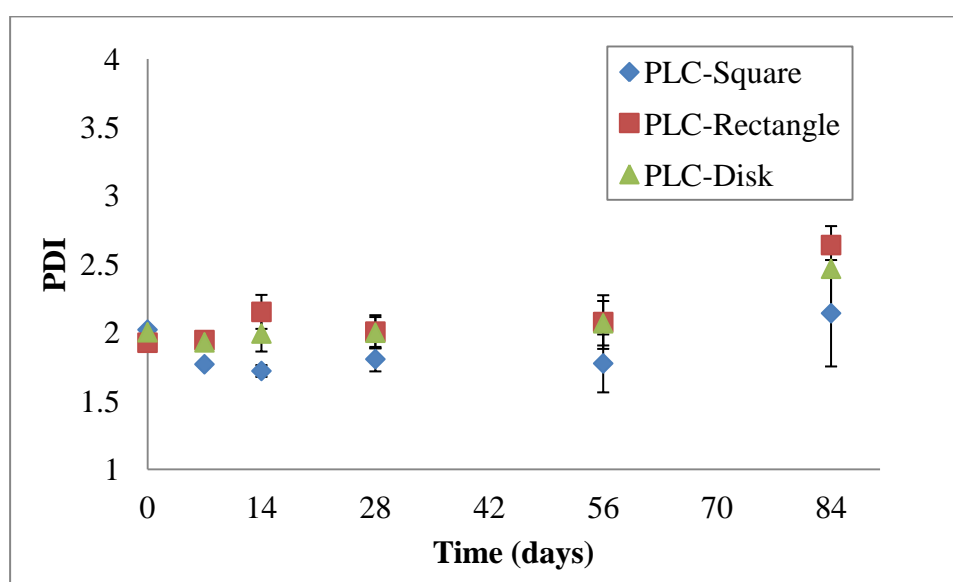


Figure 5.4 Changes of polydispersity index with time of PLC7030 square, rectangle and disk samples (250 μm), pH7.4, 37°C

Table 5.2 List of λ for square, rectangle and disk PLC7030 films in the *in vitro* degradation

Shape	Dimension (mm × mm)	λ (day ⁻¹)
Square	10 × 10	0.03 ± 0.0012
Rectangle	6 × 3	0.03 ± 0.0032
Disk	Φ2	0.026 ± 0.0015

5.1.1.2 Monitoring of *in vivo* degradation

Only rectangle and disk samples were investigated in the *in vivo* degradation study since only rectangle and disk samples were feasible to be inserted in the rabbit's eyes. Moreover, rectangle and square samples degraded in the same manner *in vitro*, thus rectangle samples will represent samples with sharp corners in the *in vivo* study.

i. Change in thickness

The dimension of the samples was captured by slit lamp photography, as shown in Figure 5.5. There was no visual change over 84 days of study for both rectangle and disk samples, however, some of the disks were not traceable after 35 days due to small size of the sample compared to the eye, therefore the standard deviation of thickness change cannot be calculated.

Thicknesses of the rectangle and disk samples were monitored by AS-OCT graphs (Figure 5.6). There was also no difference observed between the thickness of rectangle and disk samples over 84 days with $P=0.09$ from the student t-test (paired two sample for means) (Figure 5.7).

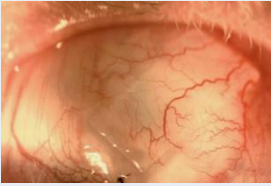

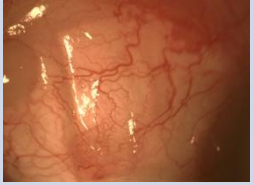
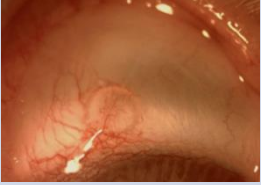


Time (Days)	Slit Lamp	
	Rectangle	Disk
0		
35		
84		

Figure 5.5 Slit lamp photographs of rectangle and disk samples in the rabbit eyes

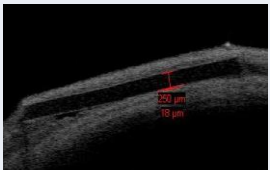
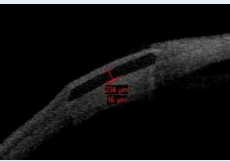
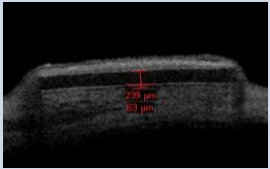
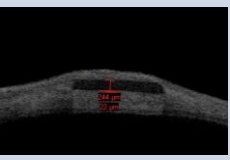
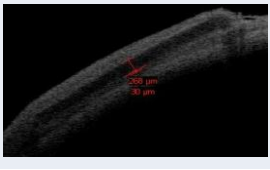

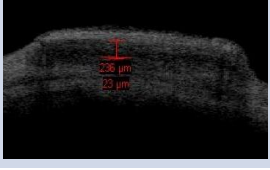
Time (Days)	AS-OCT	
	Rectangle	Disk
0		
28		
63		
84		--

Figure 5.6 Observation and measurement of film thickness (rectangle and disk) by AS-OCT

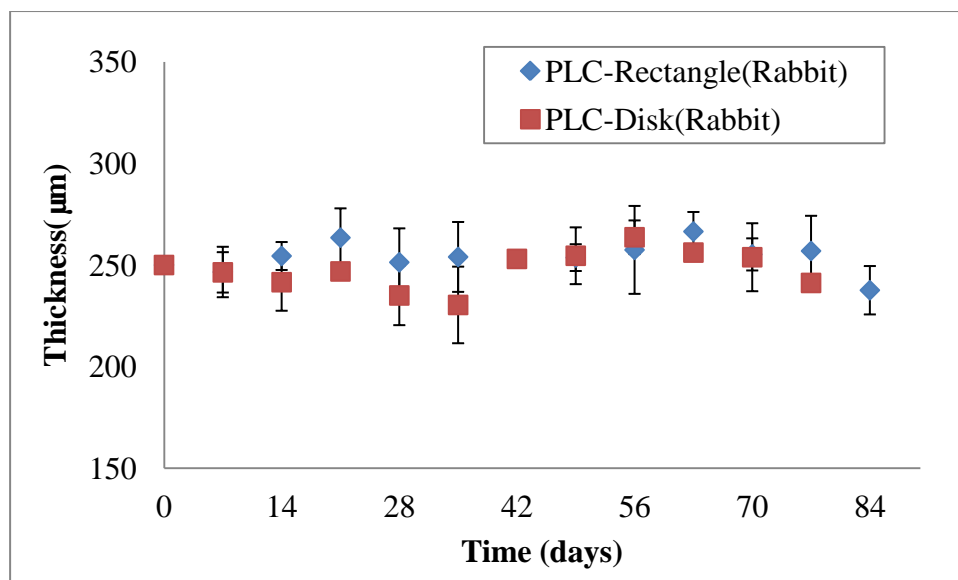


Figure 5.7 Comparison of rectangular and disk film thicknesses *in vivo* (rabbit eyes)

ii. Measurement of M_w and M_n

Both M_w and M_n obtained from GPC measurement showed exponential decay, similar to the observations from bulk degrading polymers. The M_w and M_n at the 84th day for disk samples were missing, as the samples at Day 84 could not be retrieved. Due to those non-traceable samples, the standard deviation for M_w and M_n could not be calculated. As shown in Figure 5.8 there is no distinguishable variation in M_w between rectangle and disk samples, which was verified by statistical analysis, with $P > 0.05$ ($P_{Mw}=0.988$, $P_{Mn}=0.152$).

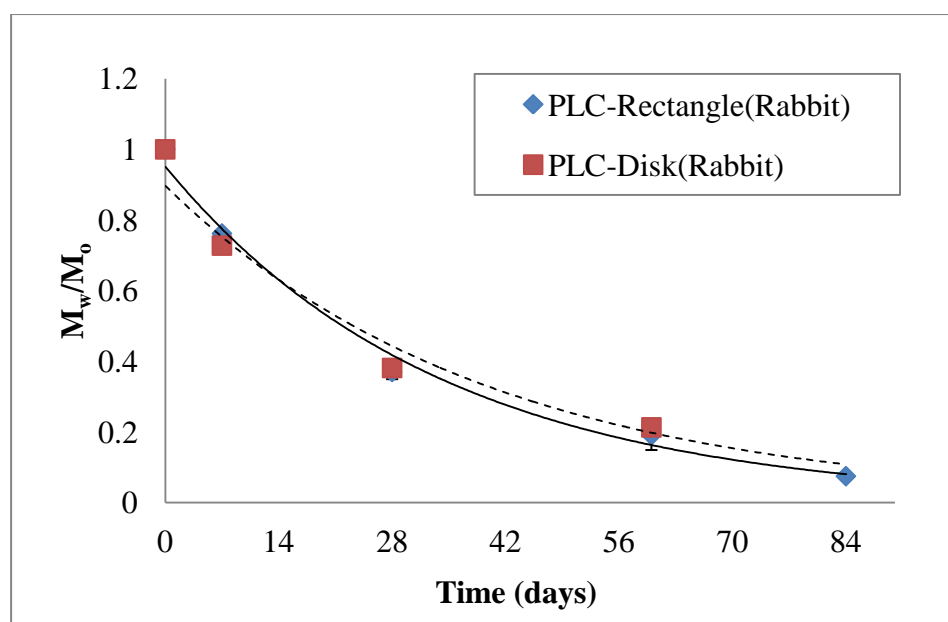


Figure 5.8 Changes of M_w with time of PLC7030 rectangular and disk samples (250 μm), *in vivo*

There was a slight difference of the degradation rate between rectangle and disk samples when measuring M_n . Figure 5.9 reveals a faster degradation rate for rectangular samples as compared to disk samples. In Figure 5.9, one data point is missing for PLC-Disk (rabbit) on Day 84, and the data points on Day 28 for the rectangle and disk samples are almost coincide. The rate constant λ_{Disk} seemed to be lower than $\lambda_{\text{Rectangle}}$ as reflected from M_n , which is comparable to the results obtained *in vitro*. Since some of the disk samples were not traceable after 35 days *in vivo*, the standard deviation cannot be calculated due to limited sample size (Table 5.3).

Figure 5.10 plots of the polydispersity index of the rectangle and disk samples tested *in vivo* versus time. As the PDI of rectangle samples started to increase from Day 56 onwards as compared to the disk samples, which might indicate that the rectangular samples degraded slightly faster than the disk samples. However, the results obtained were indicative, but not exact, due to the irretrievability of the samples from the rabbit

eyes (a disk with 2mm diameter is too tiny for the rabbit eye ball). Therefore, the effect of shape on the degradation of PLC7030 might not be significant either *in vitro* or *in vivo*.

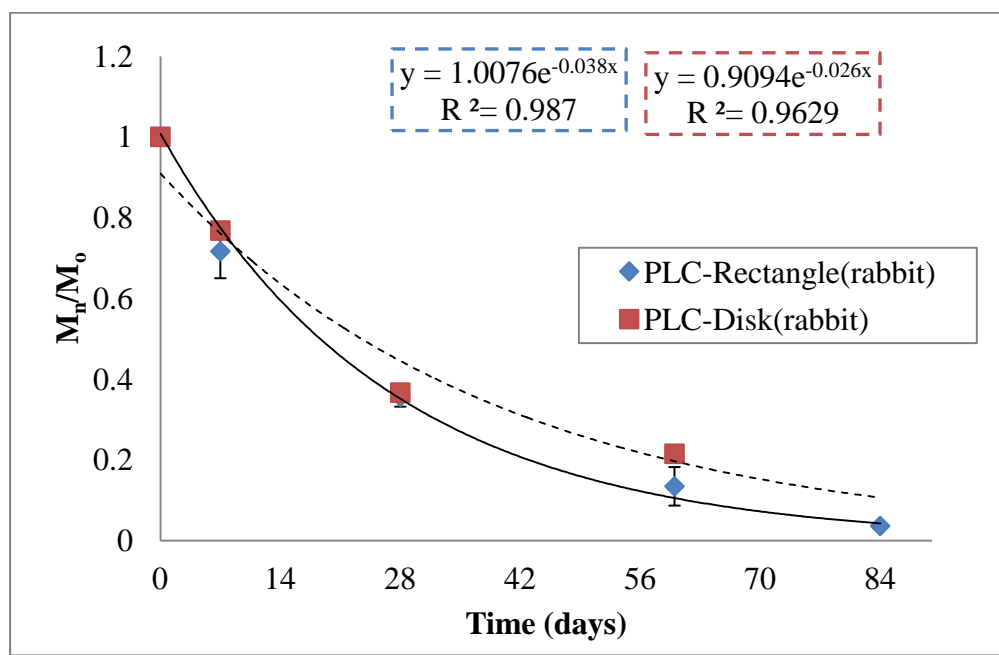


Figure 5.9 Monitoring of M_n of PLC7030 rectangle and disk samples (250 μm), *in vivo*

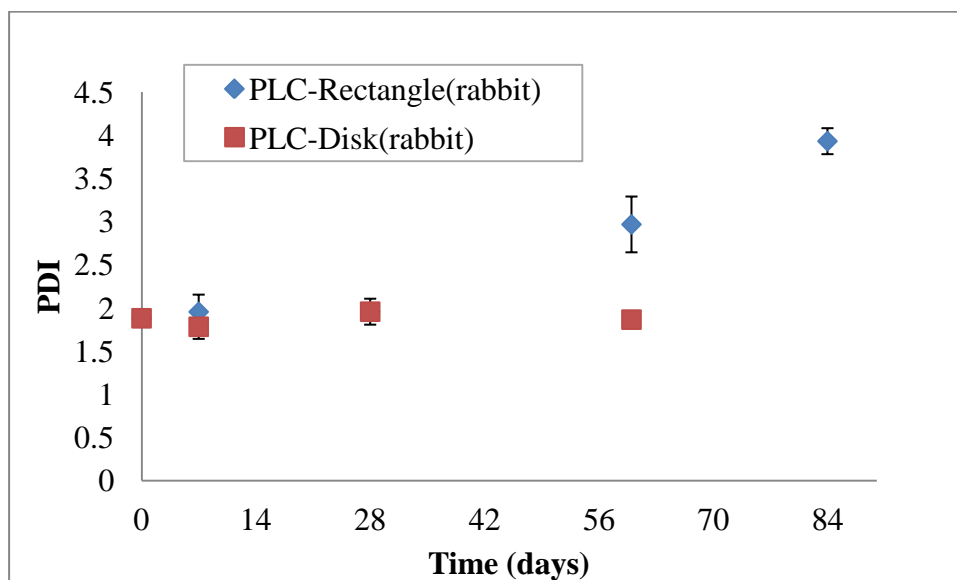


Figure 5.10 Changes of polydispersity index with time of PLC7030 rectangle and disk samples (250 μm), *in vivo*

Table 5.3 List of λ for rectangle and disk PLC7030 films in the *in vivo* degradation

Shape	Dimension (mm \times mm)	λ (day ⁻¹)
Rectangle	6 \times 3	0.038 \pm 0.001
Disk	Φ 2	0.026

5.1.1.3 Summary

The samples with different shapes did not demonstrate distinctive degradation behaviours *in vitro*, but the difference might be more apparent in the *in vivo* condition. The surface-to-volume (S-V) ratios for the square, rectangle and disk samples are 8.4mm⁻¹, 9.0mm⁻¹ and 10.0mm⁻¹ respectively. The onset time for degradation became shorter with increased surface to volume ratio. This is in agreement with literature [94, 95] for similar types of biodegradable polymers. Due to the difference in surface-to-volume ratio of the rectangle and disk samples, they seemed to show differences in degradation rate (λ) both *in vitro* and *in vivo* to some extent as reflected from M_n . And this difference might be more pronounced *in vivo* than *in vitro*. However, due to the irretrievability of some of the disk samples after Day 35, the *in vivo* results obtained might be only indicative.

5.1.2 Effect of film thickness

To resolve the unusual behaviour of PLC films *in vitro* and *in vivo*, as outlined in the previous chapter (500 μ m PLC7030 degraded homogeneously *in vitro* but heterogeneously *in vivo*), the effect of film thickness on degradation behaviour of PLC7030 was further investigated. Since the lactide-group of polymers is normally degraded homogeneously [59], the degradation behaviour should not be affected by film thickness, unless the degradation is auto-catalyzed due to large thickness [96]. However, Burkersroda *et. al.* developed a model, which predicted that the erosion mechanism of a

water-insoluble biodegradable material can undergo either surface erosion or bulk degradation, depending on the device thickness [65]. Therefore, in addition to the 500 μm thickness studied in the previous chapter, the *in vitro* and *in vivo* degradation of 250 μm -thick PLC7030 films and *in vitro* degradation of 80 μm -thick films has been investigated to show how film thickness affects the degradation behaviour of PLC7030.

5.1.2.1 *In vitro* degradation of 500 μm , 250 μm and 80 μm PLC7030 films

i. Mass loss

Mass loss is one of the parameters that measures degradation. For poly lactide-group copolymers, the mass of the sample starts to reduce when a critical molecular weights is reached. The water-soluble degraded products then leach out from the matrix [17].

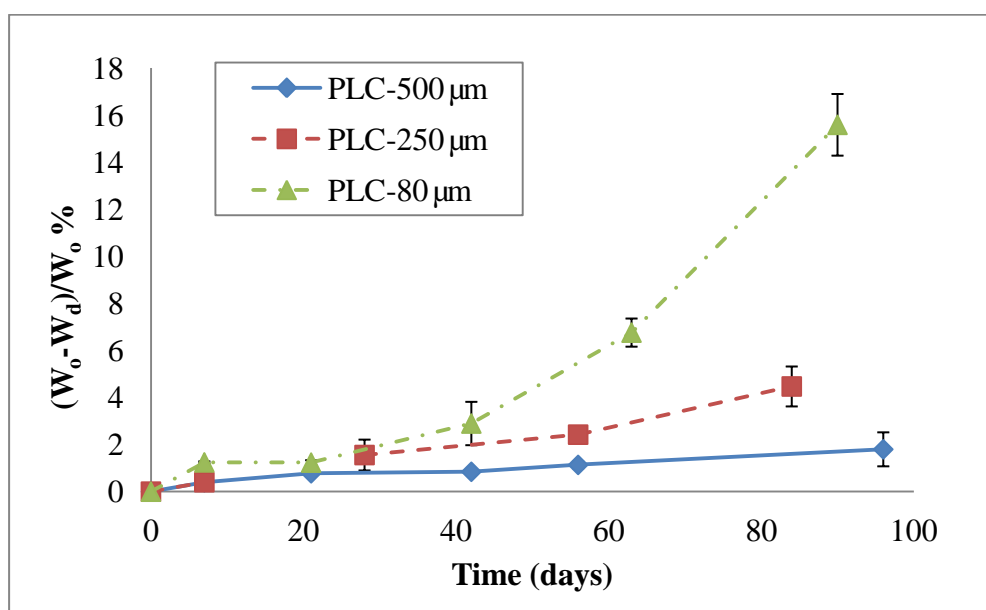


Figure 5.11 Changes in mass loss with time of PLC7030 films, 500, 250 and 80 μm , *in vitro*, pH7.4, 37°C

In the current study, it is interesting to note the increased mass loss with decreased film thickness of PLC7030. As seen from Figure 5.11, all the three samples started to lose similar amounts of mass before Day 21. However, the difference among the three samples became more pronounced after the Day 42. The sample with thickness of 80 μm has lost 16% of its original mass on Day 90, whereas the sample with thickness of 250 μm only lost 4% on Day 84. The mass loss of the sample with thickness of 500 μm was the least with only 1.8% on Day 96. To find out if thinner samples degrade faster than thicker samples, measurement of the molecular mass of samples was conducted.

ii. Measurement of M_w and M_n

The molecular weight M_w of samples with 500, 250 and 80 μm thickness exponentially decreased with time, which reveals the bulk degradation mechanism as seen in Figure 5.12. PLC films with 80 μm thickness appear to degrade slower than films with thickness of 500 μm and 250 μm .

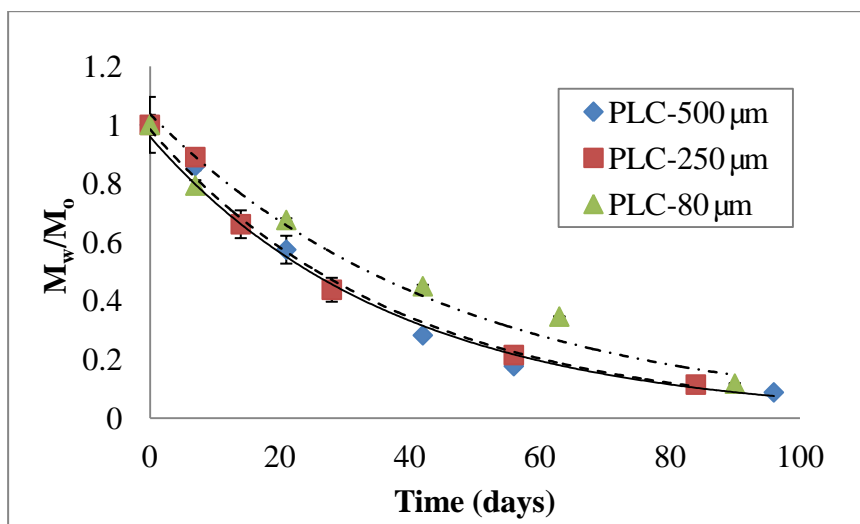


Figure 5.12 Changes of M_w with time for PLC7030 films, 500, 250 and 80 μm , *in vitro*, pH7.4, 37°C

In order to confirm the degradation results, M_n of each sample was measured at pre-determined time points and plotted in Figure 5.13. As discussed earlier, λ values indicate the rate of hydrolysis. As seen from Figure 5.14 thicker films tend to yield a higher value of λ . This contradicts the statement “thinner sample degrades faster than the thicker samples” from the results obtained from mass loss. Why, then, do thinner samples degrade slower, but have more significant loss of mass?

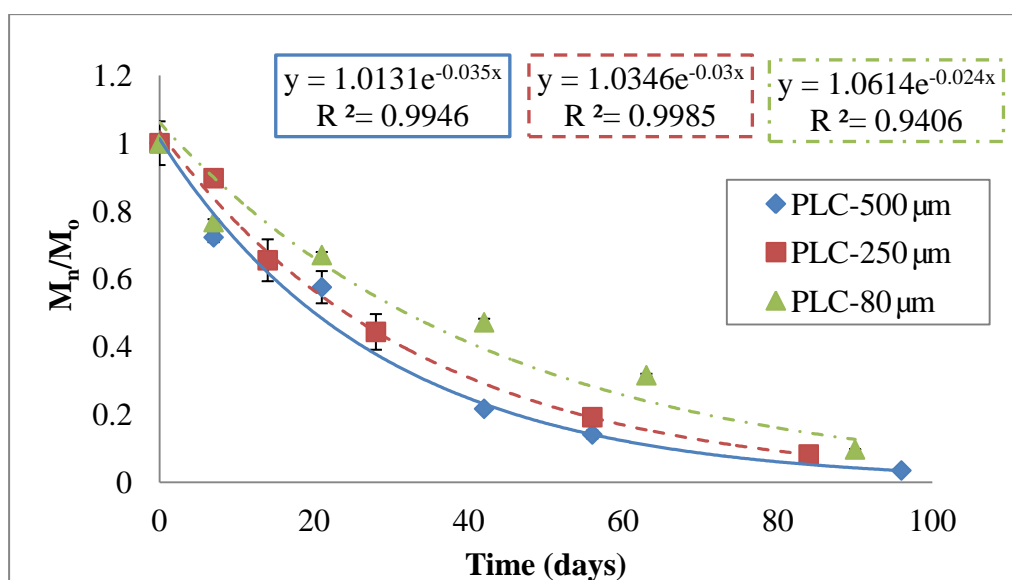


Figure 5.13 Monitoring of M_n for PLC7030 films, 500, 250 and 80 μm , *in vitro*, pH7.4, 37°C

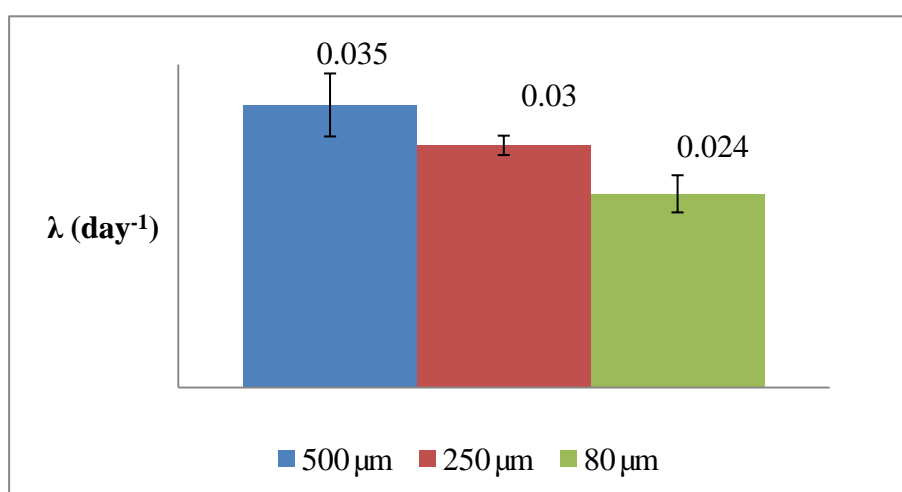


Figure 5.14 List of λ for rectangle PLC7030 films, 500, 250 and 80 μm , *in vitro*, pH7.4, 37°C

According to Göpferich [13], for bulk degrading polymers, the degradation process is auto-catalyzed in the centre of thicker samples, which results in a more acidic centre compared to the surface (pH7.4); as the acidic environment accelerates the degradation process. Therefore, the 500µm-thick films tended to form a polymeric shell of higher molecular weight, which exhibited a higher mechanical stability[13], encapsulating a core of comparatively lower molecular weight. It is believed that when the degradation reaches a critical point [17], the collapsed shell will cause rapid release of degraded products, thus higher mass loss will be expected at the late stage of degradation. For thinner samples, the degradation is uniform. Soluble degraded products were released without any constraints, which will follow the normal pattern of bulk degradation. The auto-catalytic process is not observed in thinner samples, which results in an overall slower degradation rate as compared to thicker samples. That explains why thinner samples degraded slower, but showed higher mass loss.

iii. Thickness

The thickness of 250µm and 500µm samples were also measured by SEM at different time intervals during the degradation studies. *In vitro* observations of film thickness (SEM images) of 250µm and 500µm PLC7030 samples showed that the film thickness (Figure 5.15) did not change over a period of 90 days. The change in thickness for all the samples (500µm, 250µm and 80µm) was also measured by the Elcometer and plotted in Figure 5.16, which did not show significant change throughout the study either. This reflects the bulk degradation mechanism for 250µm and 500µm PLC7030 microfilms degraded *in vitro*.

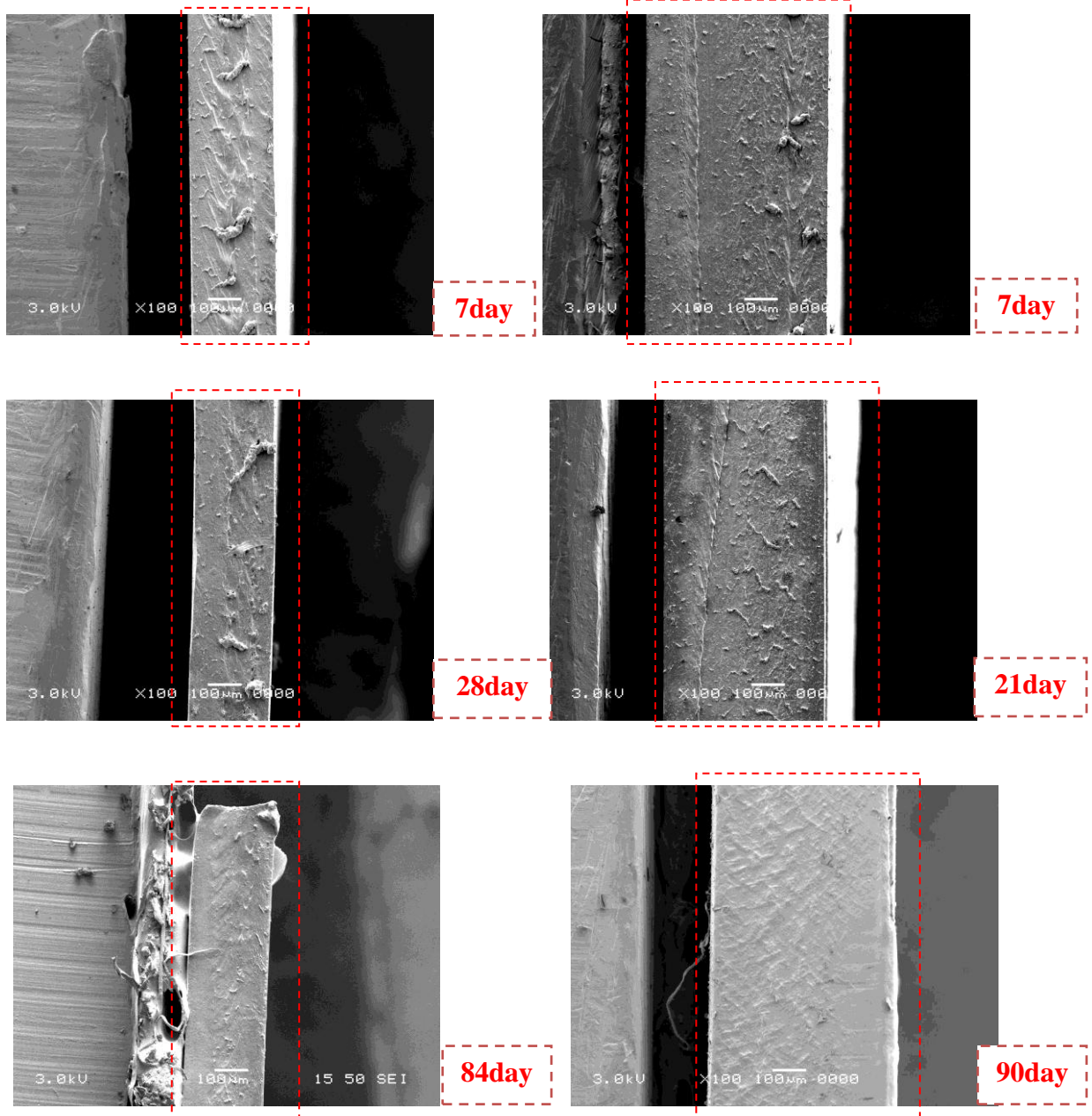


Figure 5.15 SEM images of cross-section 250 μm (left column) and 500 μm (right column) thick PLC7030 films *in vitro*, pH7.4, 37°C

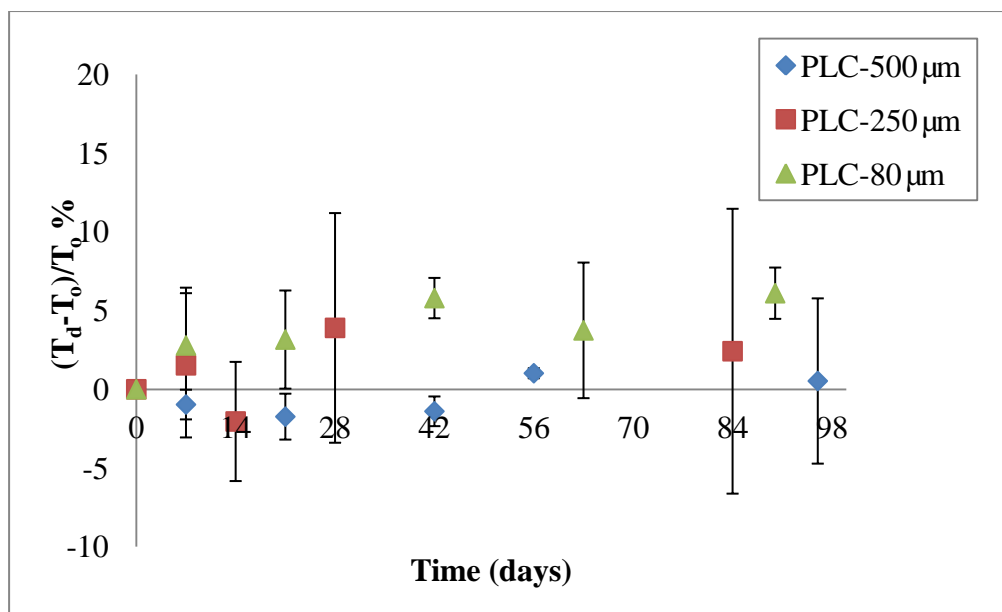


Figure 5.16 Changes in thickness with time for PLC7030 films, 500, 250 and 80 μm, *in vitro*, pH7.4, 37°C

5.1.2.2 *In vivo* degradation study of PLC7030 with thickness 500 μm and 250 μm

We expected to see comparable results as obtained from 500 μm PLC7030 both *in vitro* and *in vivo* (in section 4.2 and section 5.1.2.1), thus the same procedure was conducted. Characterization includes measuring the film thickness by AS-OCT and observing the dimensions of the *in vivo* samples through slit lamp photography.

As seen from the slit lamp photos, the length and width of the 250 μm microfilm did not change over a period of 3 months *in vivo*; and the film thickness did not change visually, as reflected from the AS-OCT graphs in Figure 5.17.

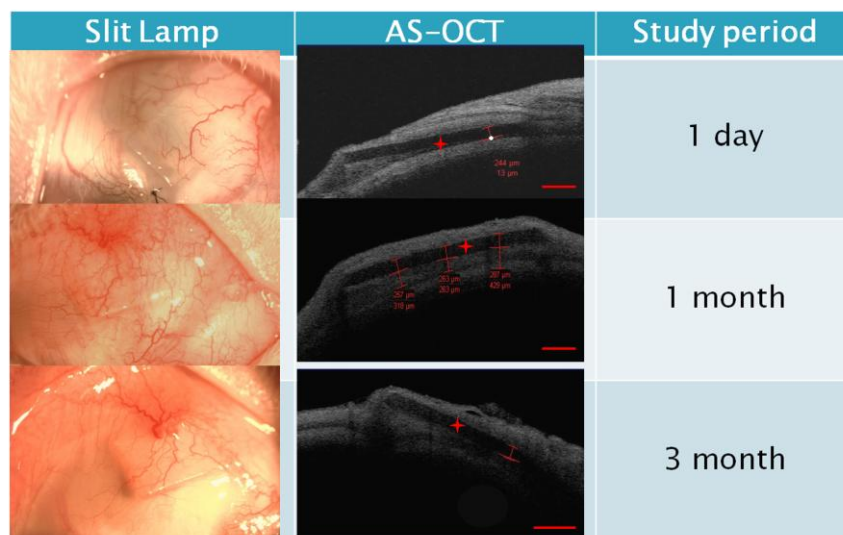


Figure 5.17 Slit lamp and AS-OCT photographs of PLC7030 after subconjunctival implantation in rabbits' eyes at 0, 1 and 3 months (250 μ m, scale bar=500 μ m)

Figure 5.18 plots the change of film thickness over time for both 500 and 250 μ m-thick samples *in vivo*. The film thickness of 250 μ m-thick samples was almost constant over 70 days, and then started to reduce. This result agrees with the result obtained for *in vitro* degradation of 250 μ m-thick PLC7030 (Figure 5.2 and 5.3), which shows bulk/homogeneous degradation. Nevertheless, as discussed in the earlier chapter, film thickness decreased in a linear fashion for PLC7030 with initial thickness of 500 μ m *in vivo*, which demonstrated heterogeneous-degrading phenomenon. These two groups of data are statistically significant ($P < 0.05$). The reason for this difference may be due to the critical thickness which determines the modes of degradation, which will be further discussed in the later section (Section 5.2).

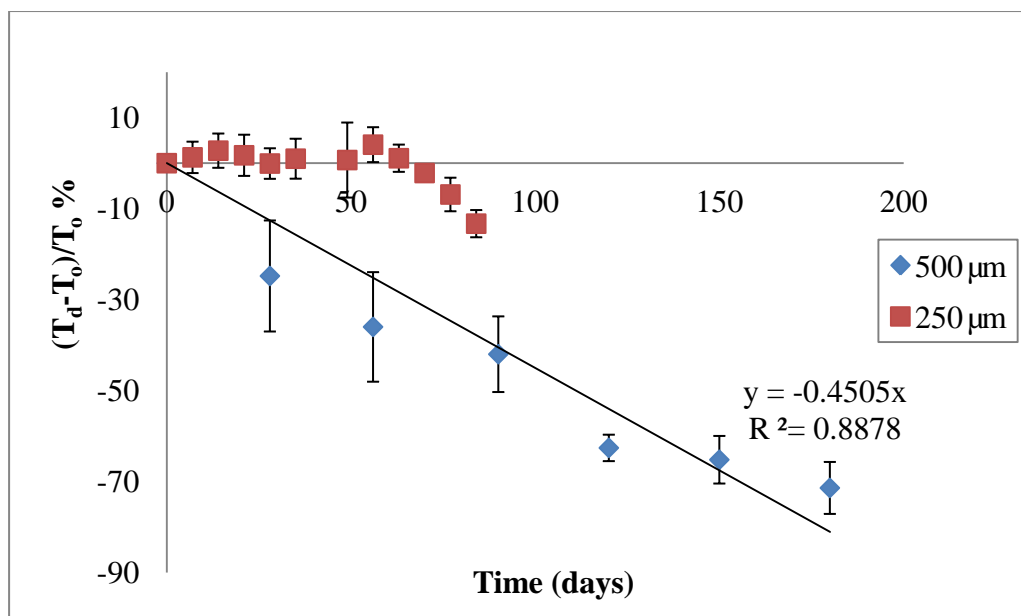


Figure 5.18 Changes in thickness with time for PLC7030 (500 μm and 250 μm) *in vivo*

5.1.2.3 Summary

From this study we note that film thickness affects degradation rate of PLC7030 films, both *in vitro* and *in vivo*. The induction period for mass loss for the three thicknesses of PLC7030 microfilms is approximately 21 days. After 21 days, thinner sample started to lose more mass compared to thicker samples until Day 90 of the study. Thicker films tended to degrade faster despite the lower loss of mass due to the auto-catalytic degradation observed from thicker samples. There was no noticeable change in film thickness for all the thicknesses studied *in vitro* and *in vivo*, except films with thickness 500 μm , which shows reduction in thickness linearly *in vivo*.

5.1.3 Effect of degradation media

Degradation is also affected by the media that the materials are exposed to. The degradation behaviours of samples were investigated in PBS buffer with pH7.4 (*in vitro*) and subconjunctival space of rabbit eyes (*in vivo*). The sample dimensions were specified in the earlier chapter, and the thickness of samples studied in this section is 250 μm only.

5.1.3.1 Rectangle samples (*in vitro* and *in vivo*)

i. Measurement of M_w and M_n

The M_w of rectangular PLC7030 films degrading in PBS buffer with pH7.4 and in rabbit eyes are shown in Figure 5.19. As seen in Figure 5.19, the M_w of PLC7030 (250 μm) decreased both *in vitro* and *in vivo* with time, which demonstrated bulk degradation mechanism with exponentially decaying M_w . In addition, *in vivo* degradation seems to be faster than *in vitro* degradation of PLC7030 and the two groups of data are statistically significant ($P < 0.05$).

Degradation of PLC7030 rectangle samples is observed to be faster *in vivo* than *in vitro*, as seen from the measurement of M_n in Figure 5.20. The degradation rate constant $\lambda_{\text{in vitro}}$ is 0.03 day^{-1} , and $\lambda_{\text{in vivo}}$ is 0.038 day^{-1} , which means the *in vivo* degradation is approximately 25% faster than the *in vitro* degradation process numerically. The two groups of results (M_n) obtained in the experiment are statistically significant, with $P < 0.05$.

The main esterases in the eyes that attribute to hydrolytic degradation were found to be acetylcholinesterase (AChE), butyrylcholine esterase (BuChE) and carboxylesterase. Esters whose chain length exceeds four carbons, will be hydrolyzed primarily by BuChE [97, 98]. Therefore, we believe that the esterases probably did contribute to the hydrolysis of ester

bonds in the polymer backbones for PLC7030, thus increasing the hydrolysis rate (R_h) higher *in vivo* than *in vitro*.

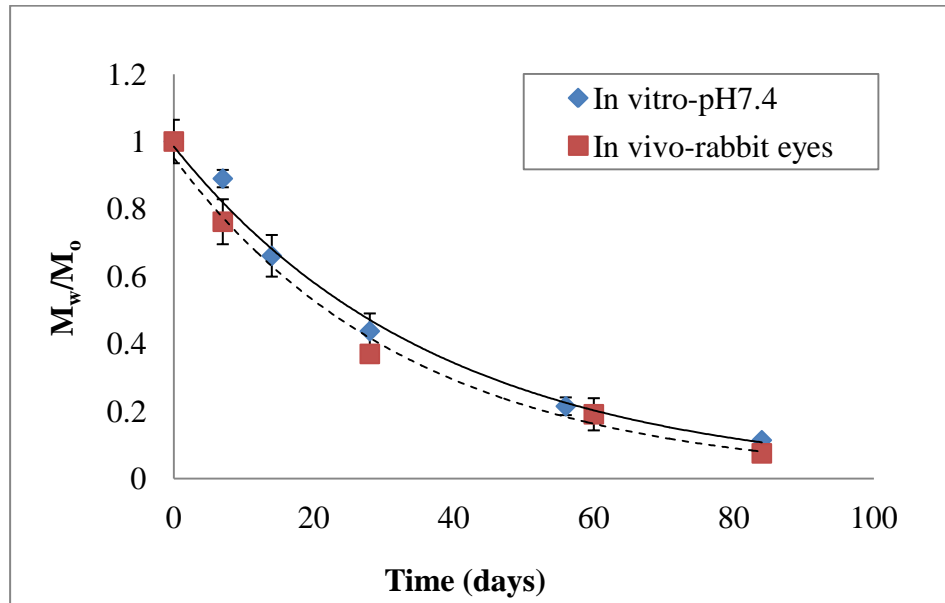


Figure 5.19 Changes of M_w with time of PLC7030 rectangle film in PBS buffer (pH7.4) and in subconjunctival space of rabbit eyes (250 μ m)

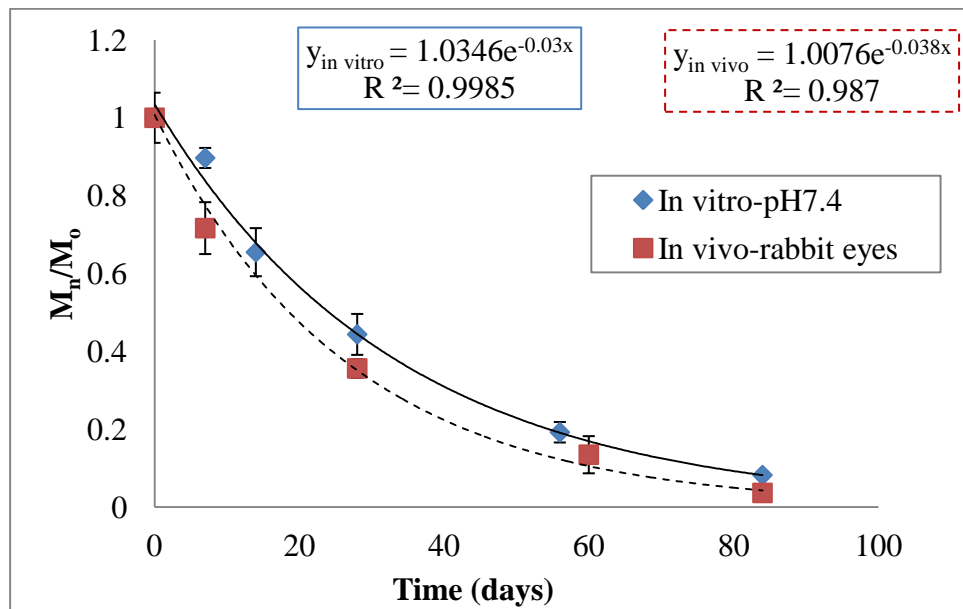


Figure 5.20 Changes of M_n with time of PLC7030 rectangle film in PBS buffer (pH7.4) and in subconjunctival space of rabbit eyes (250 μ m)

ii. Monitoring thickness change (*in vitro* and *in vivo*)

In vitro thickness measurement of PLC7030 microfilms showed that the film thickness did not change over a period of 84 days. It was found that the length and width of the microfilm did not change over a period of 3 months *in vivo*, as seen from the slit lamp photos. The film thickness change was reflected from the AS-OCT graphs shown in Figure 5.17.

Figure 5.27 is a plot of film thickness over time for both *in vitro* and *in vivo* samples. The film thickness was almost constant throughout 84 days *in vitro*. *In vivo*, however, it was constant for the first 70 days, and then decreased slowly in the subsequent 20 days. The two groups of data are statistically different ($P < 0.05$). Both the *in vitro* result and *in vivo* results showed bulk/homogeneous degradation. Nevertheless, *in vivo*, PLC7030 degraded faster than *in vitro*, which was reflected from the earlier drop of film thickness.

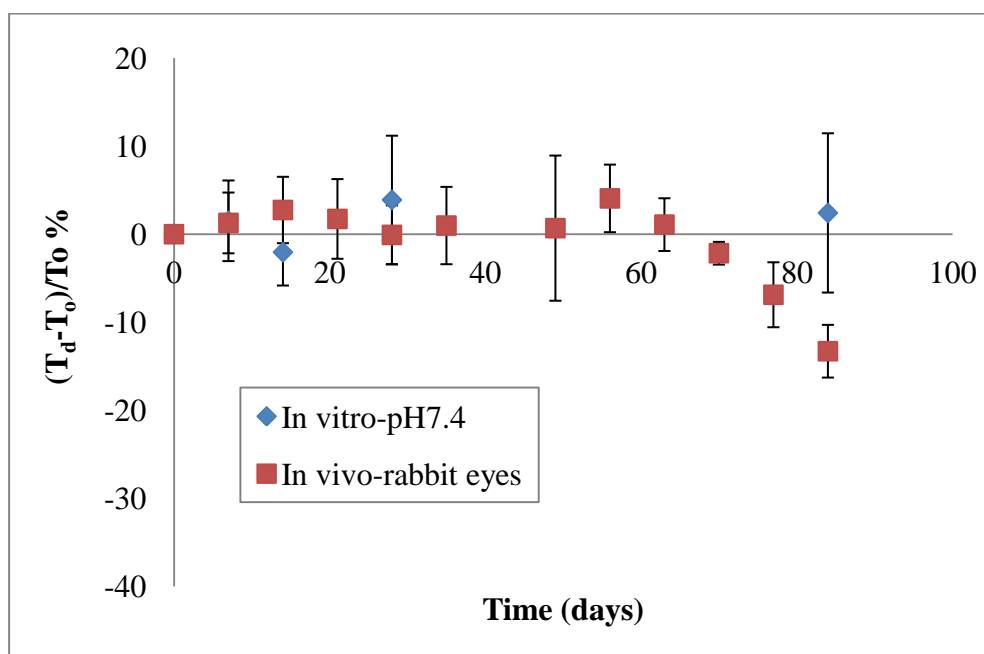


Figure 5.21 Change in thickness with time of PLC7030 rectangle film in PBS buffer (pH7.4) and in subconjunctival space of rabbit eyes (250 μm)

5.1.3.2 Disk samples (*in vitro* and *in vivo*)

i. Monitoring of M_w and M_n

Higher degradation rate was expected in the *in vivo* degradation media comparing to the *in vitro* environment. The M_w and M_n for the disk samples in PBS buffer and rabbit eyes were measured and plotted in Figure 5.22 and Figure 5.23 respectively. Surprisingly, there was not much difference between the two media where the disk samples were exposed, though degradation seems to be slightly faster in the *in vivo* environment. As seen from Figure 5.23, the degradation rate constants are very close, with only less than 5% difference observed between the two conditions. Nevertheless, the *in vivo* data may only be indicative, but not exact, due to limited number of samples tested. Since among the *in vivo* disk samples, at some time points, the sample size might be reduced from three to two, or even to one (the data on Day 60), which was due to the irretrievability of the samples from the rabbit eyes (a disk with 2mm in diameter is too tiny for the rabbit eye ball).

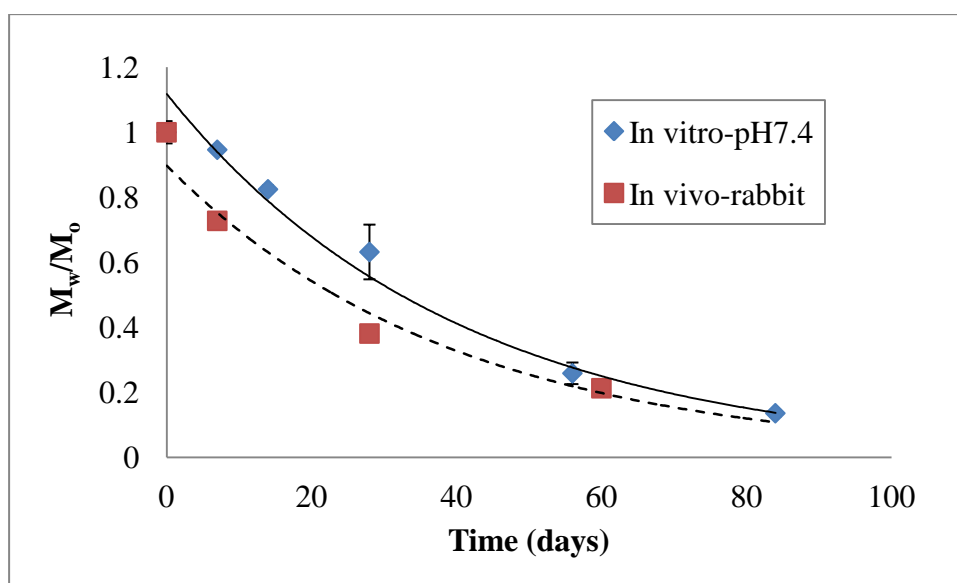


Figure 5.22 Monitoring of M_w of PLC7030 disk sample in PBS buffer (pH7.4) and subconjunctival space of rabbit eyes (250 μ m)

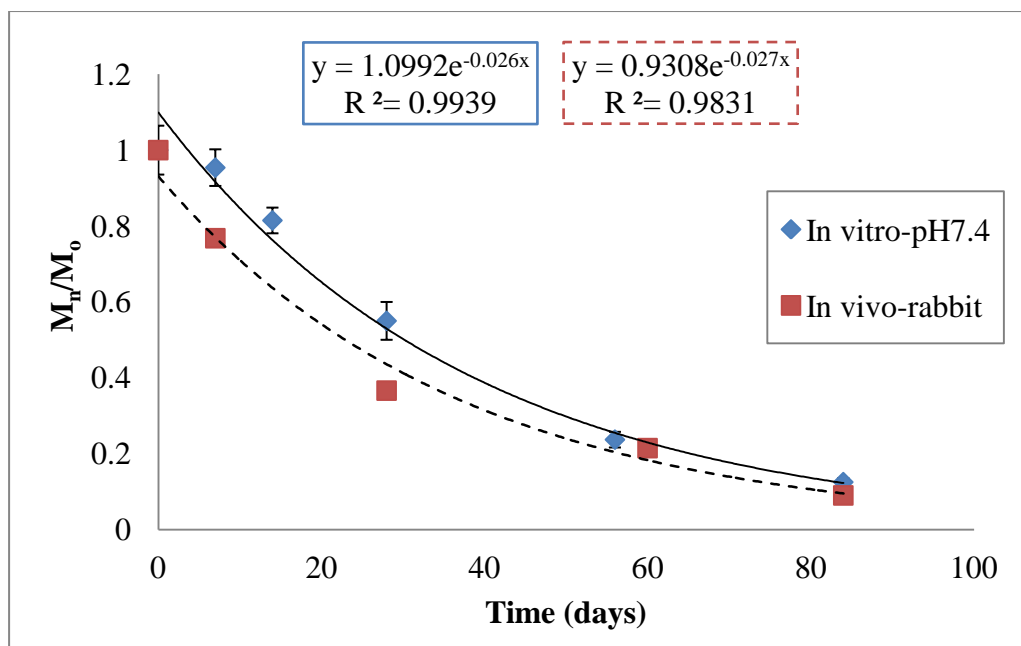


Figure 5.23 Monitoring of Mn of PLC7030 disk sample in PBS buffer (pH7.4) and subconjunctival space of rabbit eyes (250 μ m)

ii. Change in thickness (*in vitro* and *in vivo*)

As shown in Figure 5.24, the change in film thicknesses of samples degrading in the two media fluctuated over time, however, did not demonstrate any trend of either increase or decrease. Therefore, it is concluded that the samples (250 μ m) in the two media degraded homogeneously.

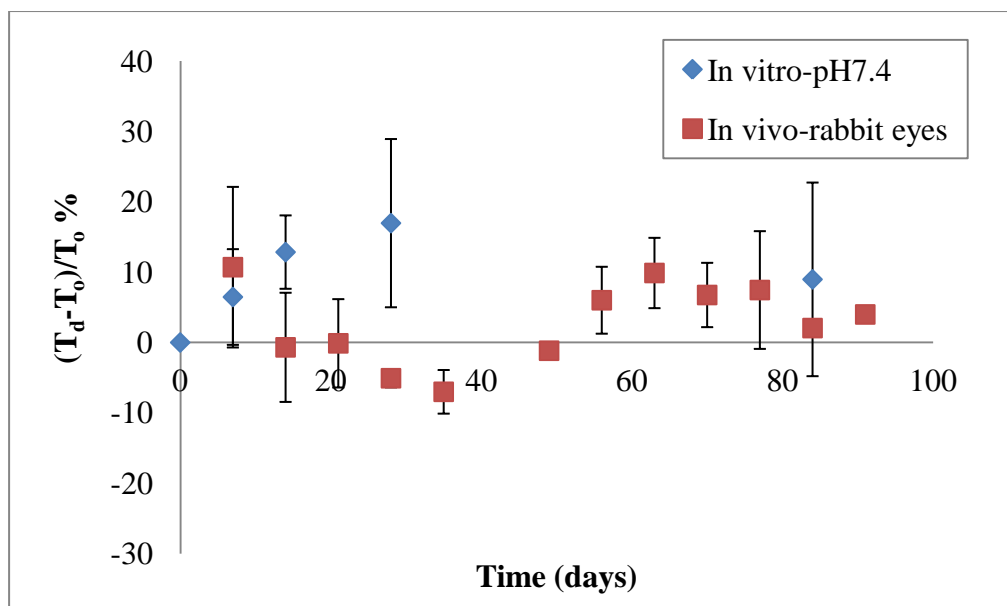


Figure 5.24 Change in thickness with time of PLC7030 disk film in PBS buffer (pH7.4) and in subconjunctival space of rabbit eyes (250 μ m)

5.1.3.3 Summary

Generally, the degradation rate of PLC7030 *in vivo* was faster than that of *in vitro*. The rectangular samples were found to be degrading much faster in the *in vivo* environment compared to in the *in vitro* condition. The difference between the *in vitro* and the *in vivo* degradation rates for disk samples didn't seem to be obvious.

5.2 Mathematical Modelling and Experiments on Degradation

The focus of this section will be to understand the effect of film thickness on the degradation mechanism of PLC7030 through mathematical models. Films with thickness of 500 μ m, degraded homogeneously *in vitro*, but heterogeneously *in vivo*. On the other hand, films with thickness 250 μ m degraded homogeneously both *in vitro* and *in vivo*. All

the calculations are based on PLC7030 films with thickness 250µm, unless otherwise stated.

From the discussion in Chapter 2, it is known that there are two processes dominating the degradation, one is water uptake (R_w), and the other is the rate of hydrolysis of the polymer backbone (R_h). Equation 2.4 expresses a relationship between the two processes. It shows that the degradation is surface eroding if $\varepsilon > 1$, and bulk degradation if $\varepsilon < 1$. And also, when $\varepsilon = 1$, the value of $2^* \langle x \rangle$ is named the critical thickness (L_{critical}). In other words, L_{critical} is the thickness above which surface erosion is the dominant mechanism, while below it, bulk erosion dominates. Therefore, the value for each factor in Equation 2.4 should be calculated to proceed further. Recalling Equation 2.4:

$$\varepsilon = \frac{\langle x \rangle^2 \lambda \pi}{4D_{\text{eff}} \{ \ln \langle x \rangle - \ln [\sqrt[3]{M_n / N_A (N-1) \rho}] \}} \quad \text{Equation 2.4}$$

where $\langle x \rangle$, M_n , ρ are all known parameters for the polymer used (PLC7030) (see Table 5.1). This is assuming all the prepared samples are pore-free. In order to do further calculations, N , λ and D_{eff} have to be obtained.

5.2.1 Calculation of N

N is the average degree of polymerization, which can be calculated by Equation 5.1:

$$\overline{M_n} = \sum_i N_i M_i \quad \text{Equation 5.1[99]}$$

Therefore for copolymer PLC7030, the number average molecular weight can be expressed by Equation 5.2:

$$\overline{M_n} = \sum N_{LA} M_{LA} + \sum N_{CL} M_{CL} = \sum N_i M_i \quad \text{Equation 5.2}$$

The monomer has an empirical formula $(C_6H_{10}O_2)_{0.3} + (C_3H_4O_2)_{0.7}$, ($M_i=84.6\text{Da}$), thus obtain

$$N = \frac{d\overline{M}_n}{dM_i} = \frac{90000\text{Da}/2}{84.6\text{Da}} = 532 \quad \text{Equation 5.3}$$

5.2.2 Calculation of λ

The value λ is the rate constant for hydrolysis, i.e. rate of ester bonds breakage in the polymer, which can be obtained from the graph of M_n versus time for the respective samples. Figure 5.16 shows the exponentially decayed M_n with time, and the two groups of data are statistically significant ($P < 0.05$).

By fitting the experimental data exponentially, the λ values can be obtained:

$$\lambda_{\text{in vitro}} = 0.03 \pm 0.003 \text{ day}^{-1} = 0.03 \text{ day}^{-1} / (24 \text{ hour} * \text{ day}^{-1}) / (3600 \text{ sec} / \text{hour}^{-1}) \approx (3.5 \pm 0.35) \times 10^{-7} \text{ sec}^{-1}$$

$$\lambda_{\text{in vivo}} = 0.038 \pm 0.0015 \text{ day}^{-1} = 0.038 \text{ day}^{-1} / (24 \text{ hour} * \text{ day}^{-1}) / (3600 \text{ sec} / \text{hour}^{-1}) \approx (4.4 \pm 0.2) \times 10^{-7} \text{ sec}^{-1}$$

The calculated λ values are in accordance with the results obtained by other researchers [59, 100].

5.2.3 Diffusion coefficient of water D_{eff} .

The value of D_{eff} of water into PLC7030 can be calculated by measuring water uptake over time. The sorption curves for PLC7030 ($250\mu\text{m}$) in PBS (*in vitro*) and in Gel (*in vivo*) are plotted in Figure 5.25. As discussed in Chapter 2, for Fickian diffusion (of water into polymer), a linear relationship between M_t/M_∞ versus \sqrt{t} , is described in the early stage with the mathematical expression:

$$\frac{M_t}{M_\infty} = \frac{2}{l} \left(\frac{D_{\text{eff}} t}{\pi} \right)^{1/2} \quad \text{Equation 2.6 (recall)}$$

Therefore, diffusion coefficient D_{eff} can be obtained from Equation 2.7, where k is the gradient of the linear portion:

$$D_{\text{eff}} = \frac{k^2 l^2 \pi}{4} \quad \text{Equation 2.7 (recall)}$$

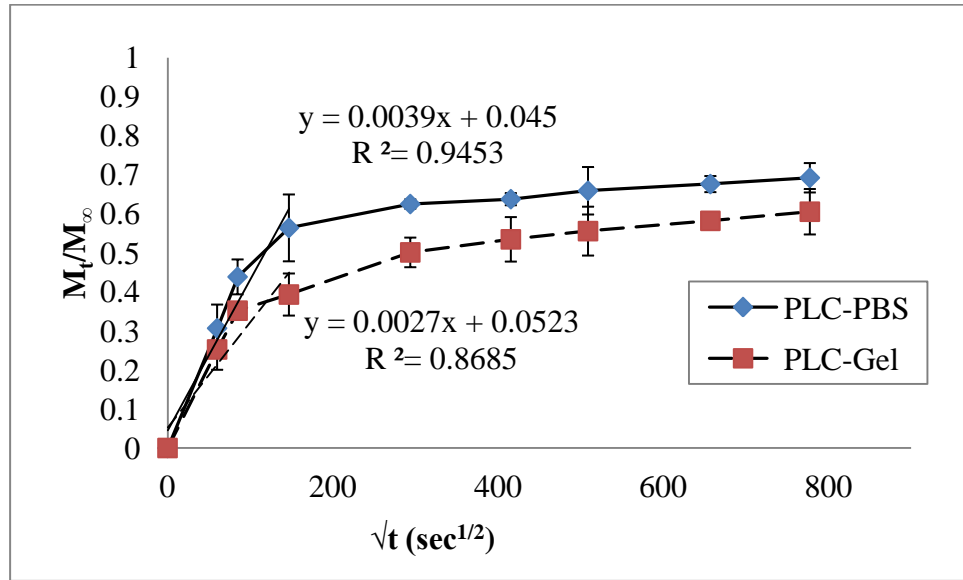


Figure 5.25 Water sorption curves for PLC7030 (250 μm) samples in PBS and Gel (70% PBS)

The value k can be obtained from Figure 5.25, by taking linear fitting of the early stage in the water sorption curve of PLC7030. It was noticed that the k values for PLC in PBS and in Gel are not the same, which basically demonstrates D_{eff} differs *in vitro* and *in vivo*. Then substituting k values into Equation 2.7, D_{eff} was obtained for both in PBS and in Gel. The values for each necessary parameter to calculate the modes of degradation for PLC are listed in Table 5.4.

Table 5.4 List of calculated parameters for 250 μm *in vitro* and *in vivo* PLC7030 samples

	250 μm in PBS (<i>in vitro</i>)	250 μm in Gel (<i>in vivo</i>)
Known parameters		
$\langle x \rangle$ (cm)	0.0125	0.0125
M_n (Da)	90,000	90,000
ρ (g/cm ³)	1.3	1.3
N_A (mol ⁻¹)	6.02×10^{23}	6.02×10^{23}
Calculated parameters		
λ (sec ⁻¹)	$(3.5 \pm 0.35) \times 10^{-7}$	$(4.4 \pm 0.2) \times 10^{-7}$
N	532	532
D_{eff} (cm ² /s)	7.47×10^{-9}	3.58×10^{-9}
ε	$4.66 \times 10^{-4} < 1$	$1.23 \times 10^{-3} < 1$

As shown in Table 5.4, the value of D_{eff} for PLC7030 in PBS buffer is higher than in Gel with 70%PBS. It is believed that the diffusion coefficient of a diffusant through a polymer matrix is strongly dependent on the diffusant concentration and temperature [101]. Yoon *et al.* did a series of experiments on measuring the diffusion coefficient of water in biodegradable polymers, such as PLLA, PCL and PGA with lower molecular weight than the PLC7030. The water pressures used in Yoon *et al.*'s studies were about ten times higher than those used in this current study. Their D_{eff} values for various biodegradable polymers were found to have increased with elevated water pressure and temperature [102]. Therefore, it is valid that the D_{eff} values obtained here are approximately one magnitude lower than the value calculated in the literature.

The measurement of D_{eff} using the gel is to approximate tissue water content. It is only an approximate value, since the only similarity of the gel condition and the rabbit eyes is the water content. In the rabbit eyes, especially in the subconjunctival space, there is no

“water bathing” of the films as happens with the *in vitro* PBS and gel conditions; instead, water needs to be transported across the epithelium of the conjunctiva to reach the film at a certain rate [103]. It was reported by Candia *et al.* that the unidirectional water fluxes across the conjunctival epithelium is approximately 240-360 $\mu\text{l}/\text{hour}/\text{cm}^2$ (based on the value obtained from Li *et al.*) [104, 105], which is equivalent of 1-1.5ml of water directly supplied to the PLC film (3mm×6mm) per day only. Additionally, the value calculated by Candia *et al.* was on isolated cultured conjunctival tissue, which did not take into account the discrepancy of the opposite trans-cellular water transport [104]. Moreover, from the earlier research done [106], a layer of collagen surrounding the implanted PLC7030 film was noticed in the histological graphs even in the first month upon implantation, which potentially retarded the water penetration further. Therefore, the *in vivo* D_{eff} is expected to be much lower than the value calculated from the simulated gel condition.

With all the necessary parameters, the indicator for modes of degradation (ϵ) was calculated. The values of ϵ for both *in vitro* and *in vivo* degradation were less than 1, which indicated bulk degradation for PLC7030 with thickness 250 μm both *in vitro* and *in vivo*.

5.2.4 Analysis on degradation behaviour of PLC7030 with thickness 500 μm

Degradation behaviours of PLC7030 with thickness 250 μm both *in vitro* and *in vivo* were predicted to be bulk erosion from the model. Then can this model predict and explain why 500 μm PLC7030 degraded homogeneously *in vitro* but heterogeneously *in vivo*?

Burkersroda *et al.*'s model predicted that the mechanism of degradation is dominated by either λ/D_{eff} or l (film thickness) [65]. With increased rate of degradation, decreased diffusion coefficient of water and increased film thickness, the bulk degradation mechanism may transform to surface erosion even for the same polymer. The known

parameters and N are still the same as PLC7030-250µm. Therefore, by assuming $\epsilon=1$, the relationship between λ/D_{eff} and the rest of parameters can be established as in Equation 5.4 below:

$$1 = \frac{\langle x \rangle^2 \pi}{4 \{ \ln \langle x \rangle - \ln \left[\sqrt[3]{M_n/N_A (N-1)\rho} \right] \}} \left(\frac{\lambda}{D_{\text{eff}}} \right) \quad \text{Equation 5.4}$$

For PLC with thickness 500µm, $\frac{\langle x \rangle^2 \pi}{4 \{ \ln \langle x \rangle - \ln \left[\sqrt[3]{M_n/N_A (N-1)\rho} \right] \}}$ is a constant, which is equal to $1.517 \times 10^{-4} \text{cm}^2$. Therefore $\frac{\lambda}{D_{\text{eff}}}$ can be calculated, which is $6.59 \times 10^3 \text{cm}^{-2}$. And this is a critical value of $\frac{\lambda}{D_{\text{eff}}}$, above which, the degradation is surface erosion.

The *in vitro* degradation rate constant λ of PLC (500µm) was acquired from the results above in section 5.1.2.1, which is $0.035 \text{ (day}^{-1}\text{)}$, and then converted to $4.051 \times 10^{-7} \text{ (sec}^{-1}\text{)}$. Assuming the value of D_{eff} for PLC7030 is irrespective of film thickness, and then the *in vitro* D_{eff} is $7.47 \times 10^{-9} \text{cm}^2/\text{s}$. The *in vitro* $\frac{\lambda}{D_{\text{eff}}}$ value for PLC film with thickness 500µm is 54.2cm^{-2} , which is 100 times lower than the critical value ($6.59 \times 10^3 \text{cm}^{-2}$). Therefore, the bulk degradation mechanism *in vitro* for 500µm PLC7030 is confirmed.

Due to the fact observed in section 4.1.2, where the film thickness decreased with time in a linear manner, the degrading mechanism is most likely dominated by surface erosion for the 500µm PLC films *in vivo*. Another way of looking at this is that $\frac{\lambda}{D_{\text{eff}}}$ has to be two orders of magnitude more than *in vitro* $\frac{\lambda}{D_{\text{eff}}}$ value for the 500µm sample to exhibit surface erosion.

However, there was no measurement of individual λ or D_{eff} measurement *in vivo* from current work. Nevertheless, due to the fact that thicker films tend to degrade faster *in*

vitro, (section 5.1.2.1), the λ of 500 μm PLC film is expected to be greater *in vivo* as compared to the *in vitro* environment ($\lambda_{\text{in vitro}} = 4.051 \times 10^{-7} \text{ sec}^{-1}$).

Additionally, as discussed in the previous section (section 5.2.3), due to variety of constraints in the rabbit eyes, the *in-vivo* diffusion coefficient D_{eff} is expected to be much lower than the value calculated from gel condition ($3.58 \times 10^{-9} \text{ cm}^2/\text{s}$). Thus the *in vivo* $\frac{\lambda}{D_{\text{eff}}}$ value of PLC-500 μm is higher than the critical value of $\frac{\lambda}{D_{\text{eff}}}$ ($6.59 \times 10^3 \text{ cm}^{-2}$), and $D_{\text{eff_in vivo}}$ for PLC-500 μm should be in the magnitude of $10^{-11} \text{ cm}^2/\text{s}$, and the critical value of $D_{\text{eff_in vivo}}$ for PLC-500 μm can be calculated as:

$$D_{\text{eff_in vivo}} \leq \lambda_{\text{in vitro}} / \left(\frac{\lambda}{D_{\text{eff}}} \right)_{\text{critical}} = \frac{4.051 \times 10^{-7} \text{ sec}^{-1}}{6.59 \times 10^3 \text{ cm}^{-2}} = 6.15 \times 10^{-11} \text{ cm}^2/\text{s}$$

The validity of $D_{\text{eff_in vivo}}$ was verified for the PLC-250 μm *in-vitro* and *in-vivo* degradation. The D_{eff} values (PBS-*in vitro*, $7.47 \times 10^{-9} \text{ cm}^2/\text{s}$ and gel-*in vivo*, $3.58 \times 10^{-9} \text{ cm}^2/\text{s}$) was thus replaced by $D_{\text{eff_in vivo}} = 6.15 \times 10^{-11} \text{ cm}^2/\text{s}$ in Table 4.4, and $\epsilon_{\text{in_vitro}}$ and $\epsilon_{\text{in_vivo}}$ were calculated to be 0.057 and 0.072, both < 1 , which confirms the bulk degradation mechanism for PLC-250 μm *in vitro* and *in vivo* even if $D_{\text{eff_in vivo}}$ is as low as in the magnitude of 10^{-11} .

5.2.5 Prediction of critical thickness of PLC7030

By obtaining the range of D_{eff} and λ values, the effect of D_{eff} and λ on critical thickness (L_{critical}) of PLC7030 can be graphically represented by the 3D plot, as Figure 5.26. The value of L_{critical} varies from micron to centimetre, which all depends on D_{eff} and λ . It is noticed that when D_{eff} is getting larger, the effect of λ becomes more obvious, whereas the effect of D_{eff} becomes less influential if λ is getting bigger. Additionally from the previous calculation, the critical thickness is greatly dependent on $\frac{\lambda}{D_{\text{eff}}}$.

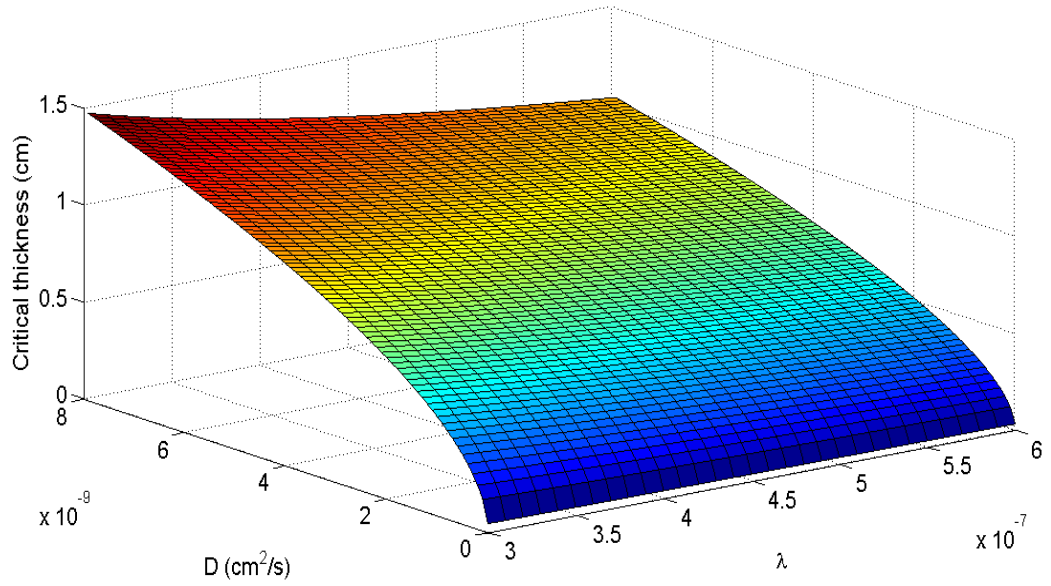


Figure 5.26 Dependence of critical thickness (L_{critical}) on the diffusion coefficient of water (D_{eff}) and degradation rate constant (λ) for PLC7030

Based on the 3-D graph and the values of λ obtained from degradation of PLC7030 with thickness $250\mu\text{m}$ both *in vitro* and *in vivo*, the critical thicknesses can be determined with varied D_{eff} (Figure 5.27, X-axis is in log scale). The D_{eff} obtained from the *in vitro* sorption test are $7.47 \times 10^{-9} \text{ cm}^2/\text{s}$ in PBS and $3.58 \times 10^{-9} \text{ cm}^2/\text{s}$ in gel. Therefore, these two values are substituted in the curve, which gives

$$L_{\text{critical_PBS}} = 1.33\text{cm}$$

$$L_{\text{critical_Gel}} = 0.81\text{cm}$$

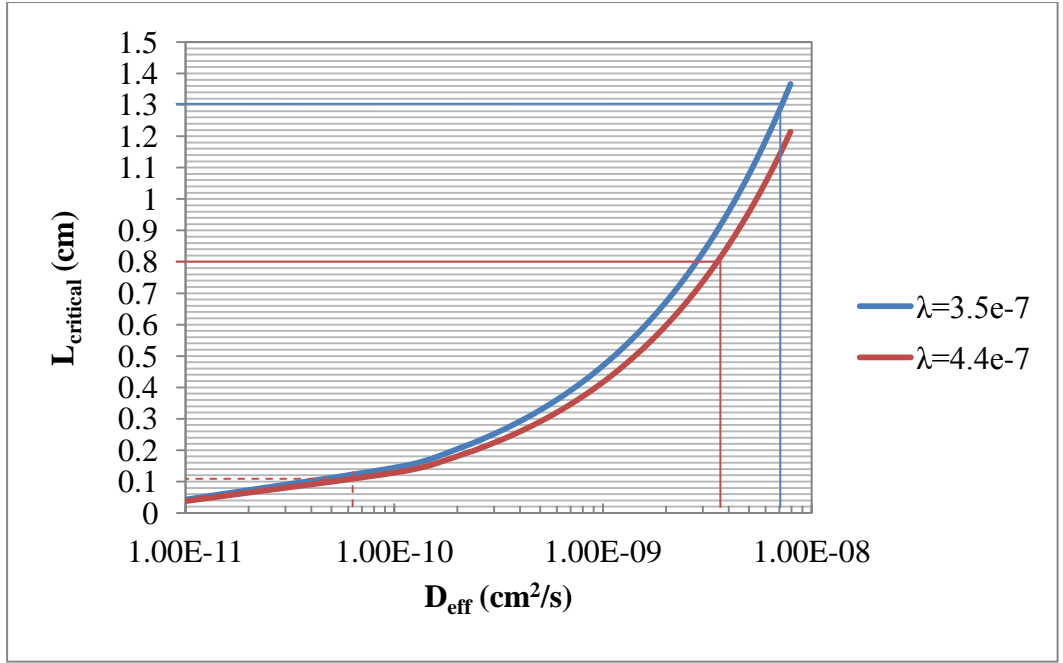


Figure 5.27 Determination of $L_{critical}$ with different D_{eff} and λ values for PLC7030

As discussed earlier on the actual value of D_{eff} in the subconjunctival space of rabbit eyes, due to the discrepancy in the actual *in vivo* condition, D_{eff} would be expected to be much lower than that of being immersed in the gel. Hence, by taking the simulated $D_{eff_in\ vivo}$ value into calculation of $L_{critical}$, totally different result will be acquired. $D_{eff_in\ vivo}$ calculated from 500 μ m *in vivo* simulation is $6.15 \times 10^{-11} \text{ cm}^2/\text{s}$, substituted in the curve where $\lambda_{in\ vivo} = 4.4 \times 10^{-7} \text{ s}^{-1}$, then $L_{critical_in\ vivo}$ becomes 0.10cm. This value is ten times lower than that calculated from the *in vitro* degradation study of PLC7030 (250 μ m), and revealed the significance of diffusivity of water in a polymer matrix on determining the critical thickness of degradation.

5.3 Conclusions

This chapter focused on studying the effects of different parameters on degradation of PLC7030 films. Parameters investigated include shape, thickness and degradation media. Though the parameters studied here are not the usual major parameters, such as molecular weight, crystallinity, temperature etc., and do not seem to have much effect on the degradation behaviour. However, all the three parameters were found to have an impact on the degradation performance, possibly affecting the drug release profiles, especially in actual clinical applications.

Firstly, the samples with different shapes did not demonstrate distinctive degradation behaviours *in vitro*, but the difference might be more apparent in the *in vivo* condition. Experimental results revealed that the square and rectangle samples (250 μm) seemed to degrade slightly faster compared to the disk samples, but the difference was not significant. And this difference might be more pronounced *in vivo* than *in vitro*. However, due to the irretrievability of some of the disk samples after Day 35, the *in vivo* results obtained might be only indicative.

Secondly, though bulk degradation is said to be homogeneous, the thickness of sample was found to have an impact on the degradation rate of PLC7030. Thinner films demonstrated slower degradation rate but higher mass loss than the thicker films *in vitro*.

Thirdly, the degradation behaviour of PLC7030 *in vitro* and in the subconjunctival space of rabbit eyes differed, and the disparity became larger when the film thickness increased from 250 μm to 500 μm . Since PLC-250 μm demonstrated homogeneous degradation *in vitro* and *in vivo*, whereas PLC-500 μm seemed to degrade homogeneously *in vitro*, but heterogeneously *in vivo*.

The last section interpreted the degradation behaviour of PLC7030 by applying the mathematical model developed previously in the literature. The work and discussion was primarily concentrated on analyzing the effect of three parameters on the degradation mechanism based on the value calculated from the experiments, namely the diffusivity of water through the polymer (D_{eff}), the degradation rate constant (λ) and the thickness of sample. Finally, the critical thickness of PLC7030 was calculated as in the *in vitro* and *in vivo* environments, and *in vitro* condition tends to yield a higher value of critical thickness due to comparatively slower degradation (lower λ) and faster diffusion of water into the polymer matrix (higher D_{eff}).

Therefore, the degradation of PLC7030 is affected by film thickness and degrading media, and it seems to be affected also slightly by the shape of the samples. Mathematical model reveals that the modes of degradation can change from heterogeneous to homogeneous degradation, depending on the film thickness, as well as the ratio of degradation rate constant over diffusivity of water through the polymer matrix ($\frac{\lambda}{D_{\text{eff}}}$).

Chapter 6

Study of Drug Release from PLC7030 Films

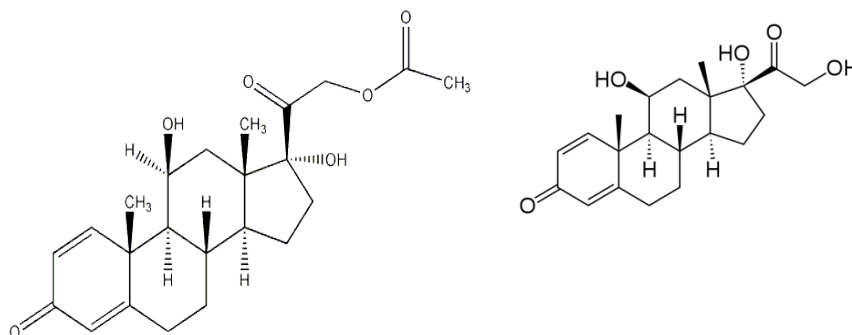
The degradation behaviours of PLC7030, investigated in the previous chapters, revealed that blank PLC7030 can degrade longer than 90 days *in vitro* and *in vivo* homogeneously. Therefore, PLC7030 is chosen to be the drug carrier material (instead of PLGA5347) for the subsequent drug release studies, due to the required duration of drug release in clinical application (typically 3 months).

Preliminary work on drug release involved study of degradation of the drug loaded films and release of prednisolone acetate release *in vitro* from PLC7030 film with thickness 250µm over 30 days. Three drug loadings (weight percentage) were used in the study, namely 5%, 10% and 20%. Subsequently, the drug release study was prolonged to 90 days, and the effect of film thickness (500µm and 80µm) on drug release was investigated. The best-suited drug loaded film (with correct thickness and amount of daily drug release) was selected to be tested *in vivo*. Then *in vitro* and *in vivo* drug release behaviours were compared and evaluated. Last but not least, the experimental drug release result will be fitted individually into a developed mathematical model. Effect of each parameter in the model will be discussed.

Both prednisolone acetate and prednisolone are inflammatory drugs, which are the active components in the PRED FORTE® eye drop, applied after glaucoma filtration surgery. The physical properties of prednisolone acetate and prednisolone are summarized in Table 6.1.

Table 6.1 Physical properties of prednisolone acetate and prednisolone

Characteristics	Prednisolone acetate(PA)	Prednisolone(P)
Nature of drug	Hydrophobic	Hydrophobic
Aqueous solubility	0.017mg/ml[107]	0.238mg/ml[107]
Molecular weight	402.48 g/mol	360.44 g/mol

Structure

6.1 Results and Discussion

The work involved study of degradation of the drug loaded films (90days) and release of prednisolone acetate *in vitro* from PLC7030 film with thickness 250 μ m. The effect of drug loading on release behaviour was evaluated for PA-loaded (5%, 10% and 20%) PLC films with thickness 250 μ m for 35 days, and then the study was extended to 144 days for 500 μ m-thick PA-loaded PLC films (5%, 10% and 20%). Subsequently, the *in vitro* drug release was conducted on PA-loaded PLC films (5%, 10% and 20%) with different thicknesses, namely 500 μ m, 250 μ m, 80 μ m and 40 μ m. The effect of film thickness was then investigated for 90 days and longer (when the film is exhaust of drug or when the film is no longer intact) for each drug loading. The cumulative release and rate of release (both exact amount and fraction of release) were calculated and compared.

6.1.1 *In vitro* degradation study of drug loaded films (250 μm)

Degradation behaviour of non drug-loaded PLC films was evaluated in the previous chapter. It is also important to investigate whether the drug loaded into the polymer has an effect on the degradation behaviour. Degradation of PLC microfilms with and without drug was tested *in vitro*. The degradation was evaluated by water absorption, change in M_w and change in M_n .

6.1.1.1 Water absorption and mass loss

Figure 6.1 shows water absorption gradually increases with time for blank PLC films, and PA-loaded PLC films with 5%, 10% and 20% loading percentages. In the first 14 days, the amount of water absorption for all the samples was not distinguishable. Differences among the four samples started to be more observable from 21 days onwards. It is indicated that with increased drug loading percentages, water absorption increased as well.

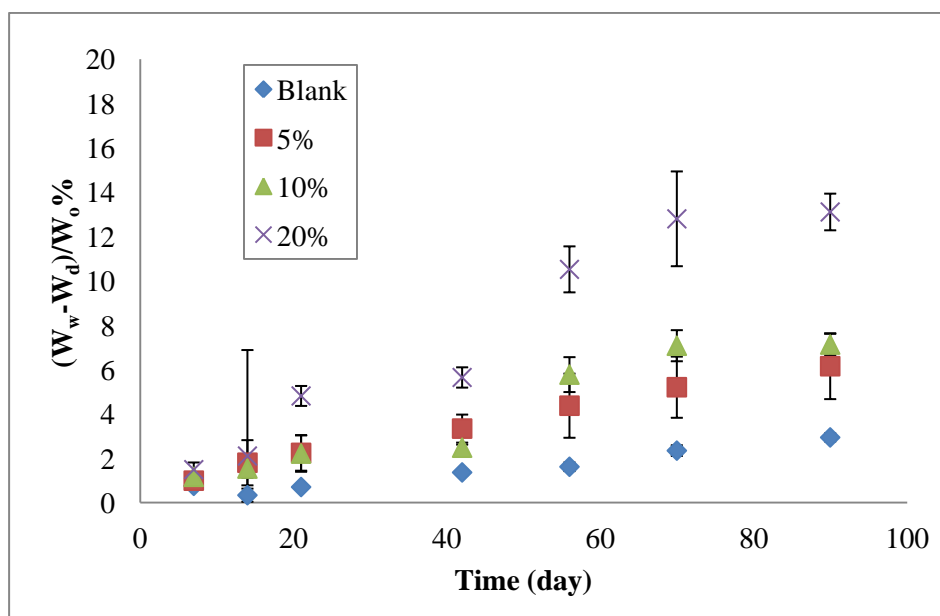


Figure 6.1 Water absorption of PLC7030 films (250 μm), with 0%, 5%, 10% and 20% PA (PBS pH7.4, 37°C)

For drug loaded samples, the mass loss is due to both the release of drug as well as the loss of oligomers and monomers due to degradation. As shown from Figure 6.2, the mass loss from drug-loaded samples is always higher than the blank samples, due to releasing of drugs, and the higher drug loading, the higher mass loss generally. Comparing the drug loaded samples with the blank samples, the onset point for degradation seems to be earlier (Day 42 for drug loaded PLC samples, whereas Day 56 for blank PLC samples). The observation for early significant mass loss of drug loaded samples could be due to the pores generated in the polymer matrix with drug released out. The pores basically provided an easier route for the degraded products (oligomers and monomers) diffusing out of the matrix.

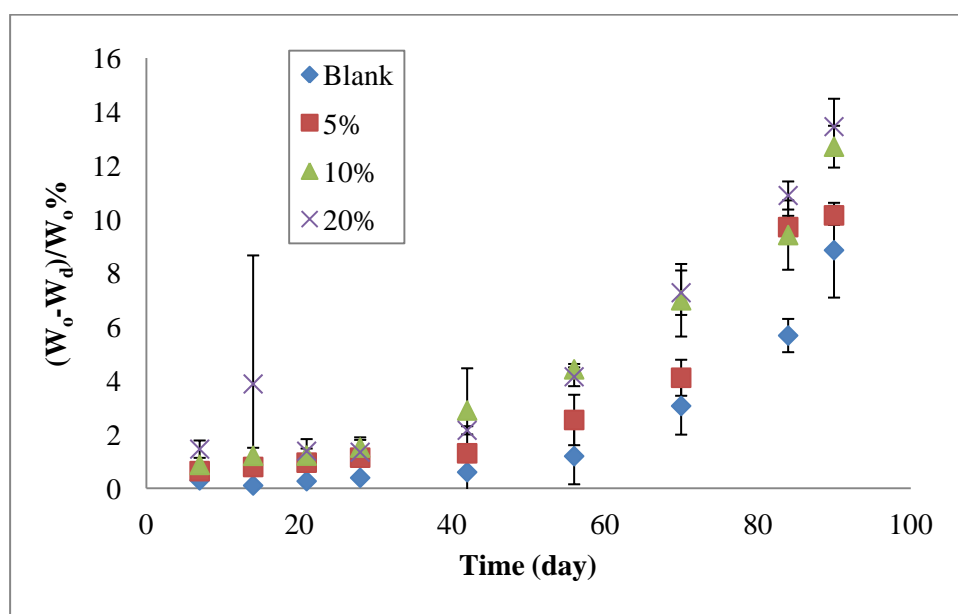


Figure 6.2 Mass loss from PLC7030 films (250 μ m), with 0%, 5%, 10% and 20% PA (PBS pH7.4, 37°C)

The SEM images verified that higher the drug loading, the more pores generated (Figure 6.4). Prior to immersion into the buffer, higher drug loading showed a rougher surface, with drug particles embedded in the polymer visually. On Day 30, pores and pits can be

seen from the surface of each drug loaded sample, which demonstrated the loss of drugs on the surface. On Day 63, number of pores was found to be more, and the size of the pores was larger.

As demonstrated in Figure 6.3, in a two-dimensional system, there is a critical value for the active agent in the matrix, where all the drug particles are in contact with each other, which is 45%; however in a three-dimensional matrix, the critical loading value is 15% [70]. This implies that, in 20% PA-loaded PLC films, the drug particles may be inter-connected; thus once the drugs are released, the inter-connected pores formed would host more water in the matrix. There was no appreciable difference between 5% loading and 10% loading observed in the experimental results. This may be also due to being below the critical value (15%) needed for interconnectedness.

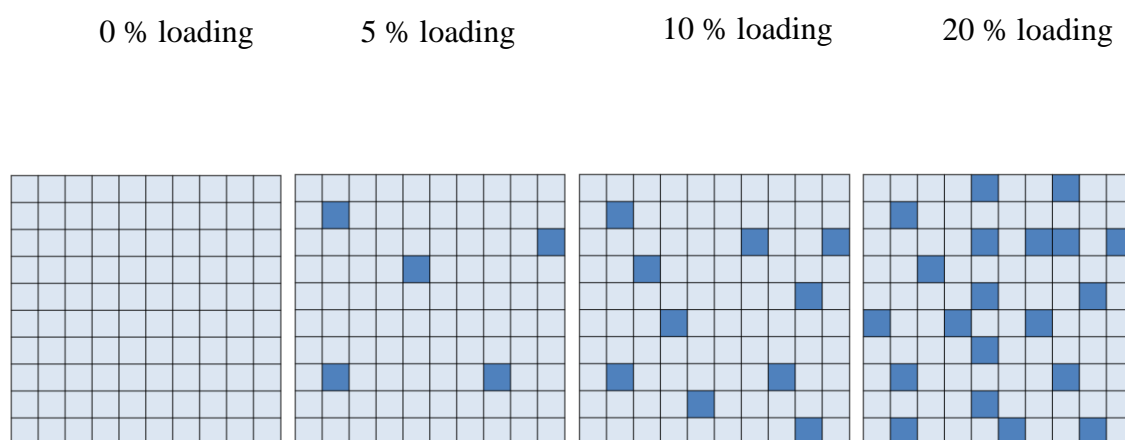


Figure 6.3 A two-dimensional representation of random distributed drug particles in polymer matrix (filled squares) (Idea adopted from Ctierke and Hsu)[108]

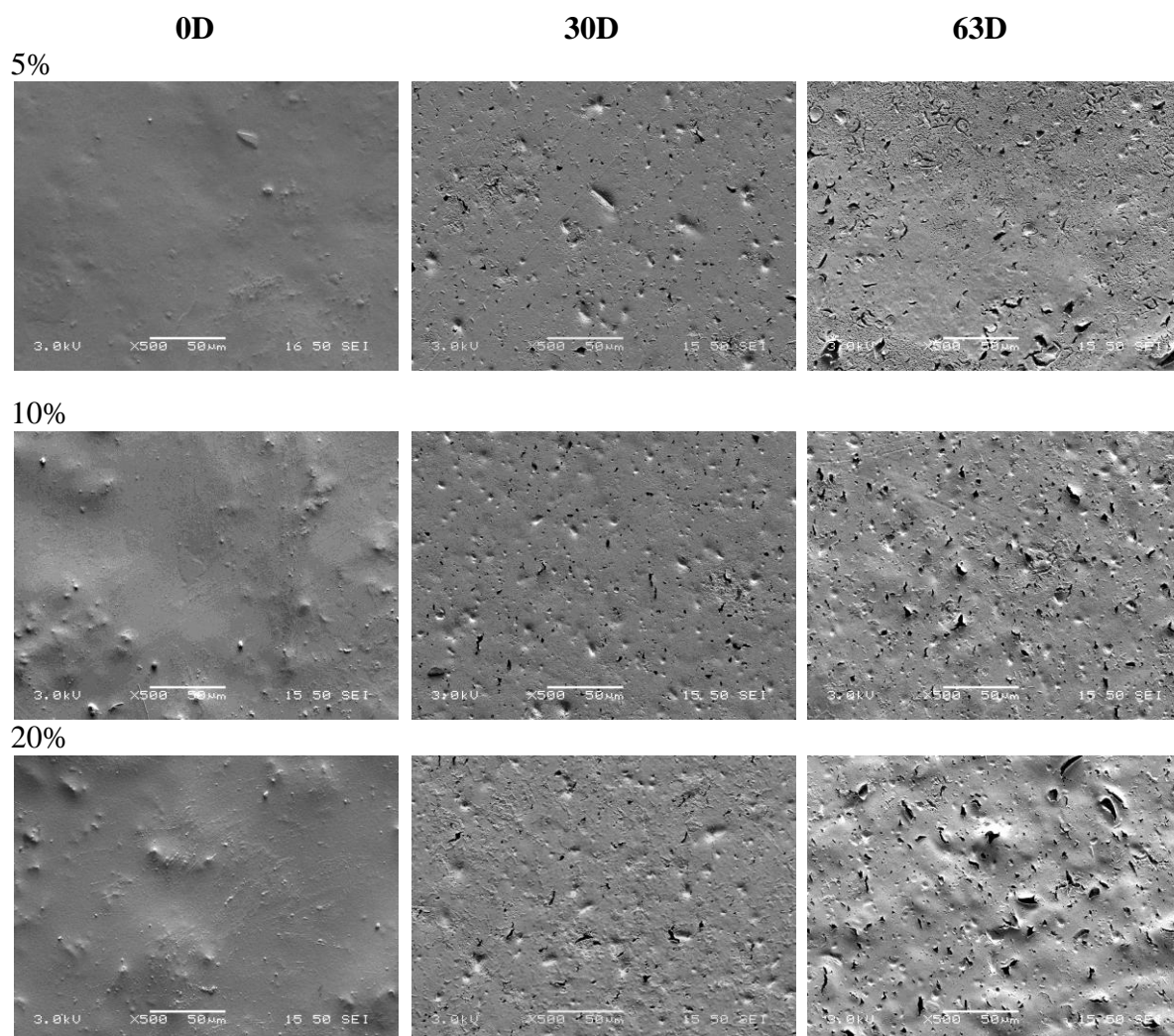


Figure 6.4 SEM images of 250 μm 5%, 10% and 20% prednisolone acetate-loaded PLC7030 films in PBS buffer at 0 day, 30 day and 63 day (PBS pH7.4, 37°C)

6.1.1.2 M_w and M_n

M_w and M_n of PLC microfilms with and without drug were obtained *in vitro* from GPC. It was found that degradation is not affected by amount of drug loaded in the film despite higher water absorption and mass loss observed from higher loadings ($P=0.998$ from ANOVA test). PLC7030 degraded slowly (about 20% drop in M_w and M_n) in the first 21 days, following by a drastic decrease thereafter. The exponentially decayed M_w and M_n revealed a homogeneous degradation mechanism.

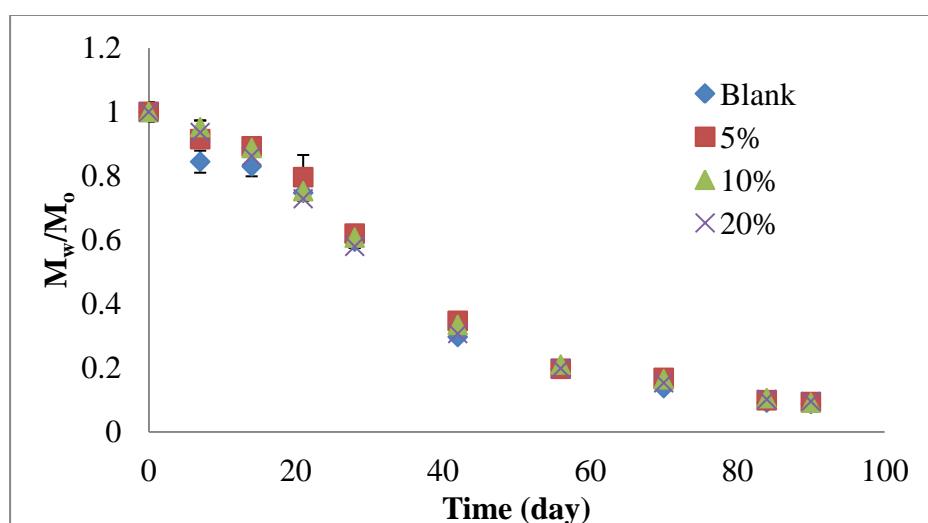


Figure 6.5 Monitoring of M_w of PLC7030 films (250 μm), with 0, 5%, 10% and 20% PA (PBS pH7.4, 37°C)

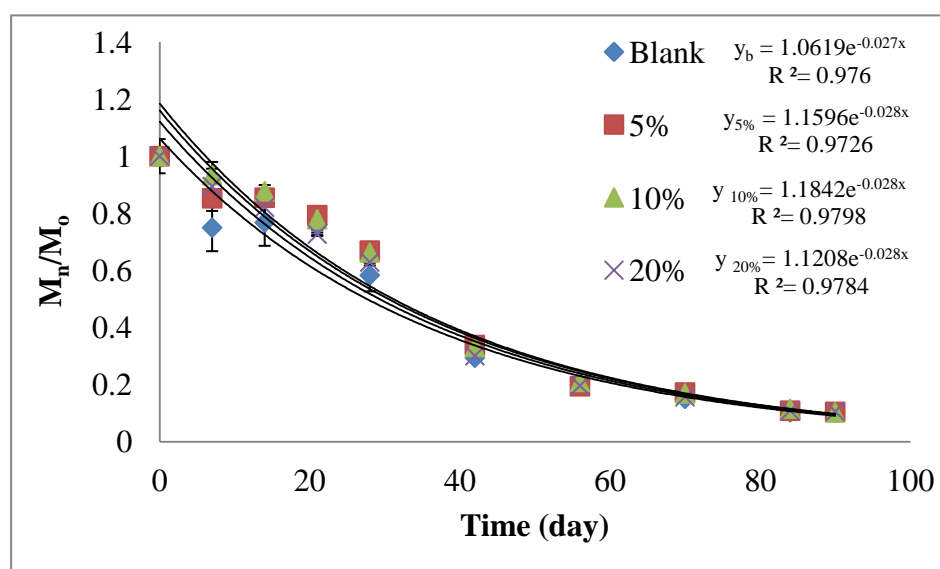


Figure 6.6 Monitoring of M_n of PLC7030 films (250 μm), with 0, 5%, 10% and 20% PA (PBS pH7.4, 37°C)

6.1.2 *In vitro* drug release - Effect of drug loading

6.1.2.1 Preliminary *in vitro* drug release (250 μm)

The solubility of PA in PLC7030 was found to be quite low, which was verified by MDSC. As seen from Figure 6.7, pure PA existed as white powder with a melting peak at 225-240°C. Upon loading to PLC7030 (20% loading), this peak was still observable, but with a broader peak range as measured by MDSC. The drug is partially (~7% dissolved) dispersed inside the polymer matrix, instead of being dissolved.

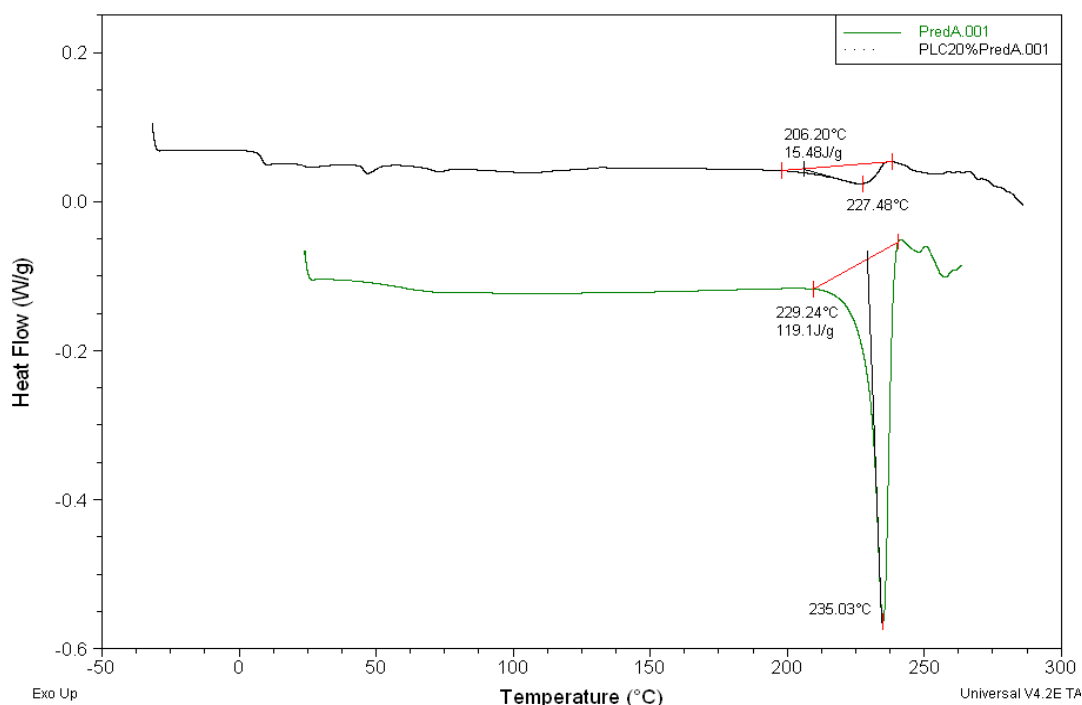


Figure 6.7 MDSC curves of pure prednisolone acetate drug powder and PLC7030 film loaded with 20% prednisolone acetate

Before testing the drug release, the actual drug loading percentages of the PA-loaded films were determined. Polymer dissolved in the solution has no effect on the detection of concentration of PA. The actual loadings of the drug, as indicated in Figure 6.8, were adopted in the subsequent drug release calculation.

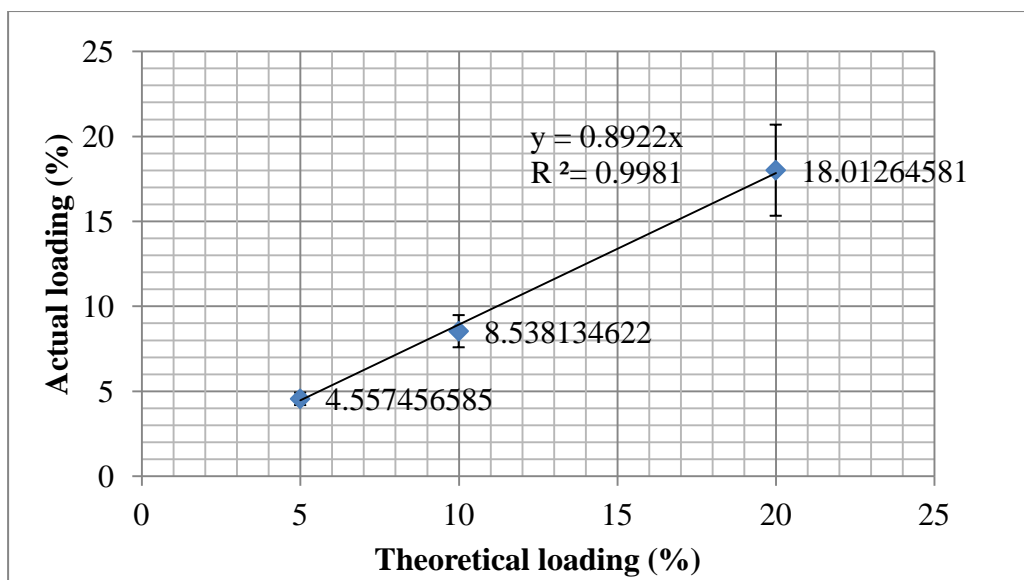


Figure 6.8 Comparison of theoretical loading and actual loading of PA-loaded PLC7030

i. Cumulative release and rate of release (weight)

Preliminary drug release study on PLC7030 films (250 μ m) with 5%, 10% and 20% PA loaded was conducted for 35 days. The *in vitro* cumulative drug released (weight) is shown in Figure 6.9, which revealed well-controlled and sustained releases of PA from the 5%, 10% and 20% PA-loaded microfilms. Figure 6.10 demonstrates the daily amount of drug released from the 5%, 10% and 20% PA-loaded microfilms. Due to the hydrophobicity nature of PA, the burst observed from the three loadings was minimal. The 5% loaded microfilm demonstrated a more steady release from day two, with a constant release rate at 0.005mg/day. Although 10% and 20% loading showed a comparatively uncontrolled pattern in the first 3 days, a steady release was subsequently observed, with a constant release rate of 0.008mg/day (10% loading) and 0.01mg/day (20% loading). A very constant release from 5%, 10% and 20% loaded microfilm was observed from 7 days onwards.

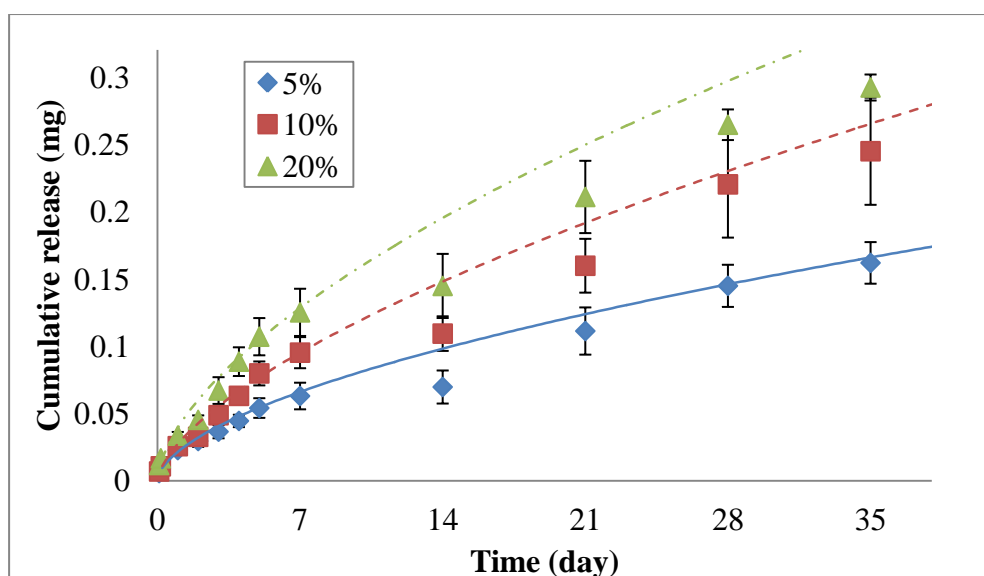


Figure 6.9 Cumulative release (weight) of PA from 5%, 10% and 20% loaded PLC films (250 μ m, PBS pH7.4, 37°C)

With increased drug loading, the amount of drug released was observed to be higher. Generally, for a monolithic dispersion system, there are two processes for drug releasing from the polymer matrix into the buffer. One is dissolution of the drug particles in the polymeric matrix, and the subsequent step is diffusion of the dissolved drug from the polymer matrix to the surface. As Higuchi model suggests, in the monolithic dispersion system, the dissolved drugs in the surface layer of the polymer matrix diffuse into the buffer first. The next layer will start to deplete if the surface layer is exhausted (Figure 6.11).

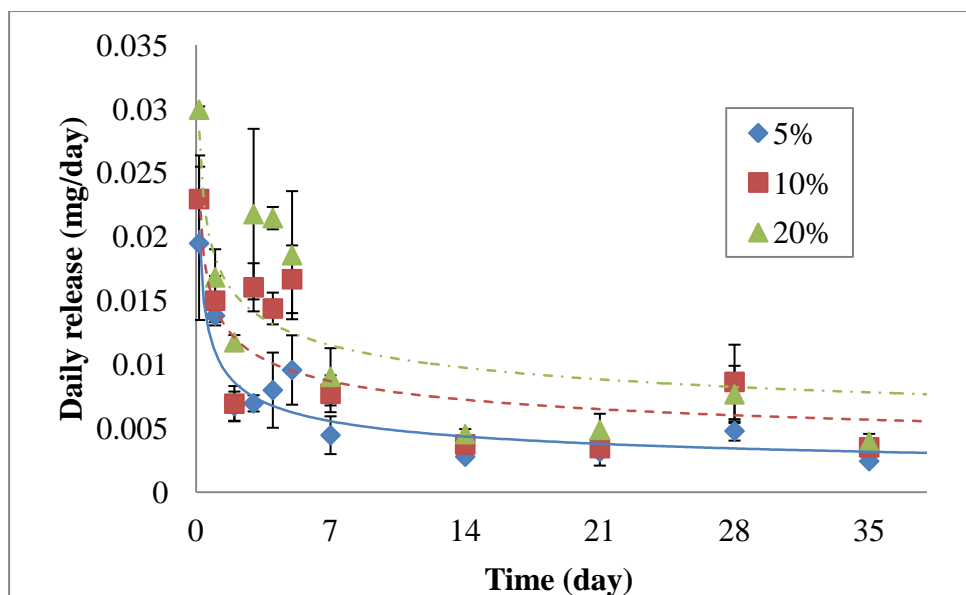


Figure 6.10 Rate of release (weight) of PA from 5%, 10% and 20% loaded PLC films (250 μm , PBS pH7.4, 37°C)

Higher loading results in comparatively more non-dissolved drug on the surface of the film. These drug particles initially on the surface would diffuse and dissolve into the surrounding aqueous medium. That explains the higher burst for higher loadings.

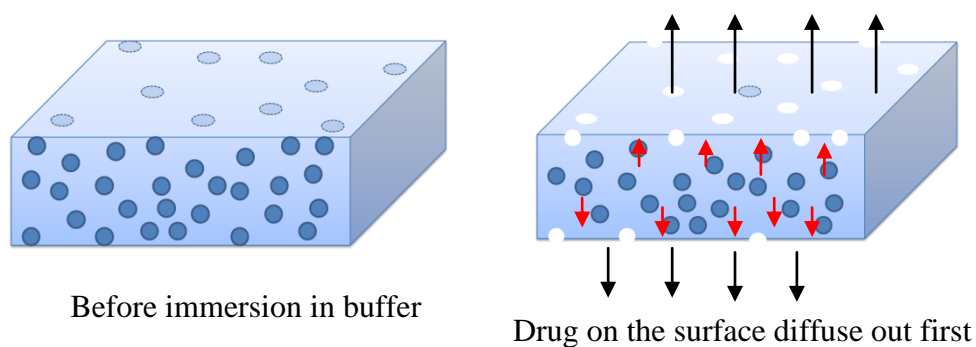


Figure 6.11 Schematic demonstration of drug release from PA-loaded PLC7030 films in the first 30 days

ii. Cumulative release and rate of release (fraction)

The cumulative percentage of drug released is shown in Figure 6.12. The *in vitro* study revealed a steady, sustained release of PA from the 5%, 10% and 20% PA-loaded microfilms. In 35 days, about 9.5%, 7.5% and 4% of the initial loaded drug on 5%, 10% and 20% loaded microfilms were released respectively.

As discussed earlier, due to limited solubility of PA in PLC, the microfilm can be categorized as a complex monolithic dispersion system. In this system, the drug particles (the particles not on the surfaces) need to dissolve in the polymer matrix before diffusing out of the film. With the drug leaves the polymeric matrix, cavities are formed on the surface, which may host more water, and provide easier pathways for the remaining drugs. This is verified by water absorption results (Figure 6.1) and SEM images (Figure 6.4). Thus the release is expected to be higher than pure diffusion-controlled release (combination of Fickian and Case II diffusion). As seen from Figure 6.11, the powers of the each fitted equation are slightly higher than 1/2. Though degradation may further increase the release, it is not a critical factor in the first 35 days.

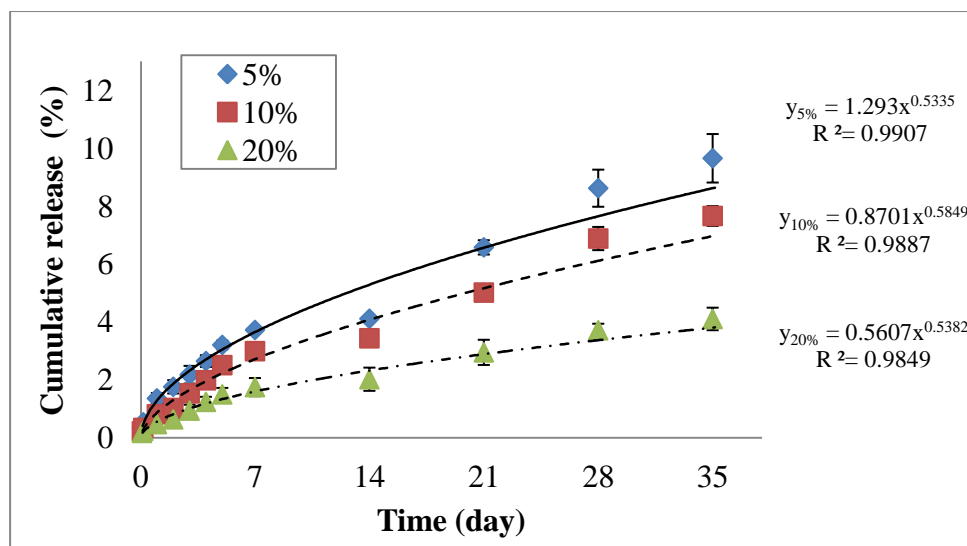


Figure 6.12 Cumulative release (%) of PA from 5%, 10% and 20% loaded PLC films (250 μm , PBS pH7.4, 37°C)

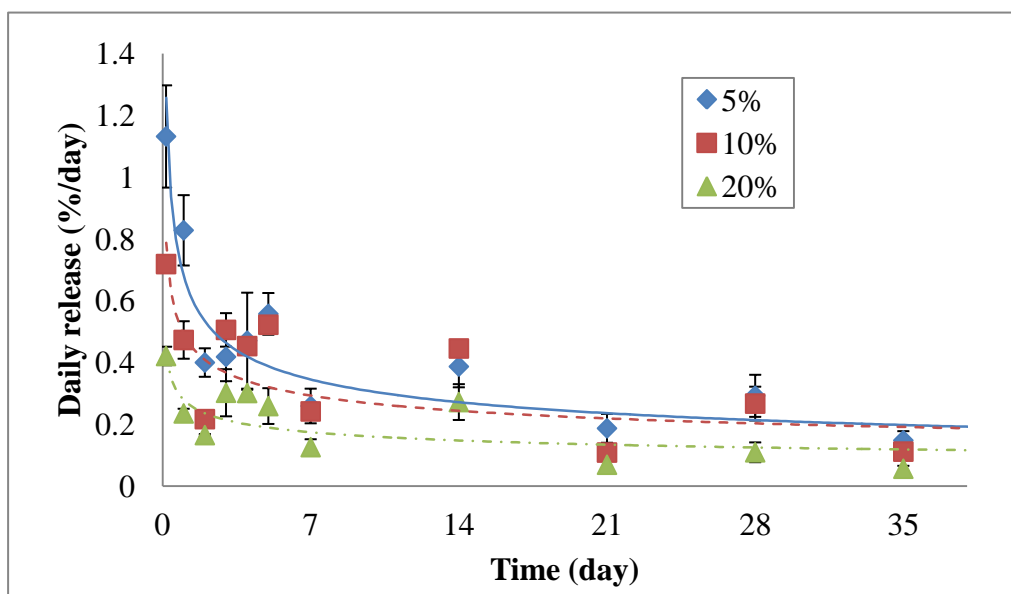


Figure 6.13 Rate of release (weight percentage) of PA from 5%, 10% and 20% loaded PLC films (250 μm , PBS pH7.4, 37°C)

The percentage of drug released daily for each loading is plotted in Figure 6.13. The fitted curves for each loading suggested a diffusion-controlled release mechanism over a period of 35 days, with nearly a constant amount of drug released after 7 days. Despite of the

first seven days, approximately 0.3% was released per day for 5% loading, 0.28% was released per day for 10% loading and 0.18% released per day for 20% loading.

It was observed that with increased drug loading, the percentage released (cumulative and rate of release) became lower, which obeys the Higuchi model. Since the study was only conducted for 35 days, it was believed that the effect of degradation has not much effect on the drug release behaviour.

6.1.2.2 In vitro drug release from 500 μ m-thick PA-loaded PLC7030 film

Preliminary results revealed the effect of drug loading on PA-loaded PLC films (250 μ m) in 35 days of release study, where degradation was not playing an important role. Therefore, this section will focus on the later stage of the releasing process, where the effect of degradation becomes significant.

Drug release experiments were done on 500 μ m-thick PA-loaded PLC7030 film (5%, 10% and 20% loading). The reasons for choosing 500 μ m as the film thickness instead of other choices is firstly due to the same sample preparation method (solution casting) as 250 μ m films; secondly is to correlate the degradation behaviour studied in the previous chapter with the drug release performance; thirdly, thicker films are capable to load more amount of drugs for the same loading percentage as compared to the thinner films.

i. Cumulative release

Figure 6.14 demonstrates prednisolone acetate release from 500 μ m thick PLC7030 films with various initial loadings. The release profiles match the theoretical agent release from a polymer slab by diffusion and erosion perfectly, as proposed by Heller and Baker [109]. It can be concluded that the drug loading has a significant effect on the drug release profile. And the release profile can be divided into two stages: (1) Diffusion controlled

release up to 56 days. (2) Accelerated degradation-induced release from 56 days to the end of study (144 days).

- Stage 1: Diffusion controlled release up to 56 days

PLC7030 films underwent random scission by hydrolysis homogeneously from beginning of study, which can be verified by the continuous decrease of M_w (Figure 6.5). However, the movement of the drug from the degrading matrix is very rapid initially due to the short diffusive path (near surface), so the diffusion of the drug dominated the release in this stage. The diffusion controlled release was discussed in the previous section (6.1.2.1 preliminary *in vitro* drug release from 250 μm thick PLC films). Higher drug loading resulted in higher amount of drug released. The difference observed from fractional cumulative release is not as apparent though, lower loading gave a higher fractional drug release. Approximately only 3%-4% of the loaded drug was released for all the three loadings.

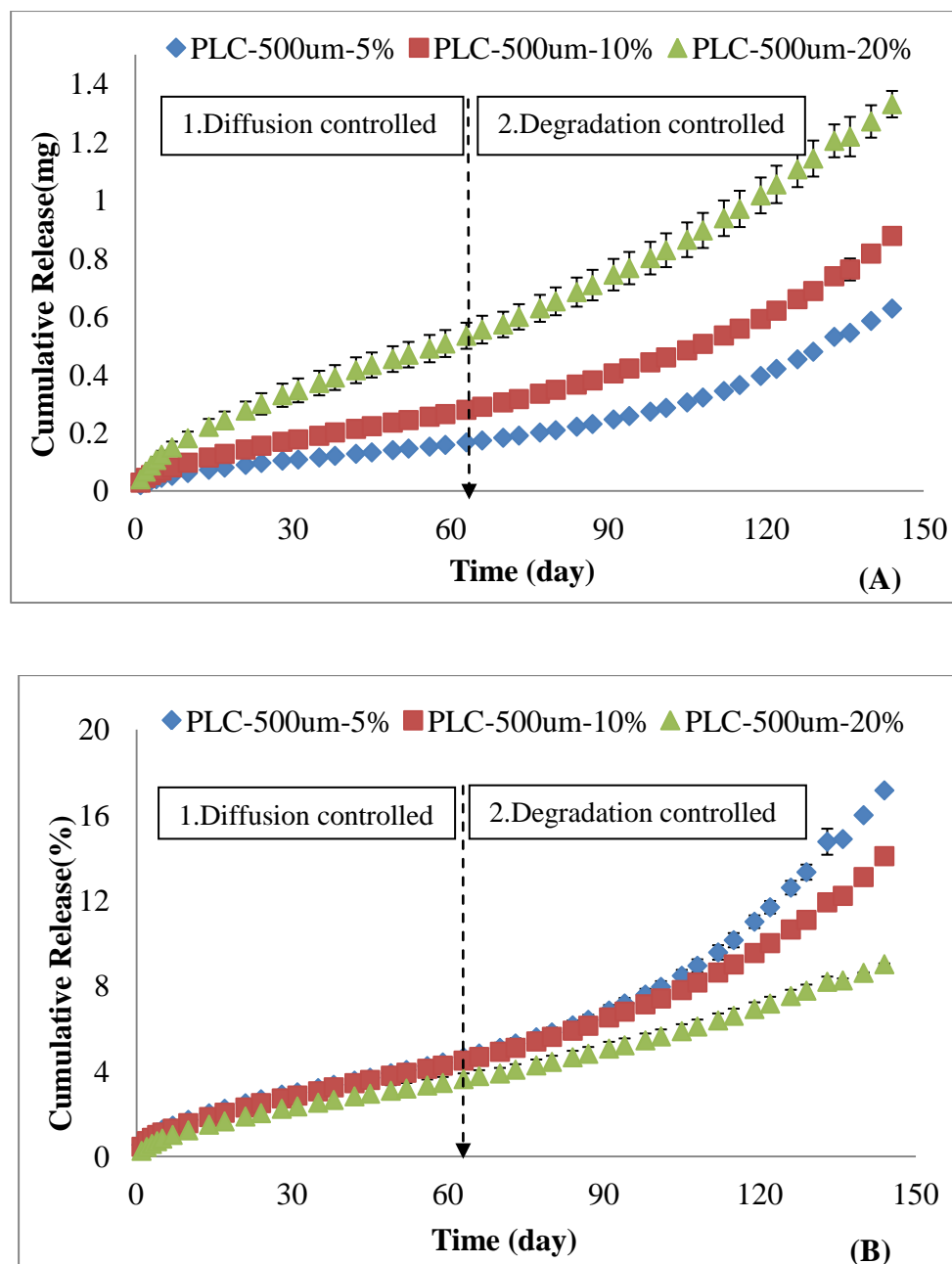


Figure 6.14 Cumulative release of PA from 5%, 10% and 20% loaded PLC7030 films (500 μm , PBS pH7.4, 37°C) , (A) is the cumulative weight, (B) is the cumulative weight fraction

- Stage 2: Degradation controlled release (from 56 days onwards)

This stage is noted as faster release of prednisolone acetate as compared with Stage 1. At the start of this stage, the molar masses (both M_w and M_n) were about 80% of their initial

values. The subsequent substantial degradation of PLC7030 caused leaching of oligomers and monomers from the matrix, as indicated from the mass loss graph (Figure 6.2), with significant mass commencing from day 56. When degradation of the matrix polymer became more intensive, the drug release profile changed from diffusion controlled to degradation controlled.

Difference in amount and fraction of drug released among various loadings was noticed from Stage 1. With degradation started to play a major role, the difference mentioned above was observed to be more and more pronounced. In Stage 2, leaching of degraded oligomers caused micro-pores on the surface, and eventually the inter-connected channels would be formed. The pores and inter-connected channels filled with water, provided an easier pathway for the drug release, and drug release is fast through due to degradation (Figure 6.15).

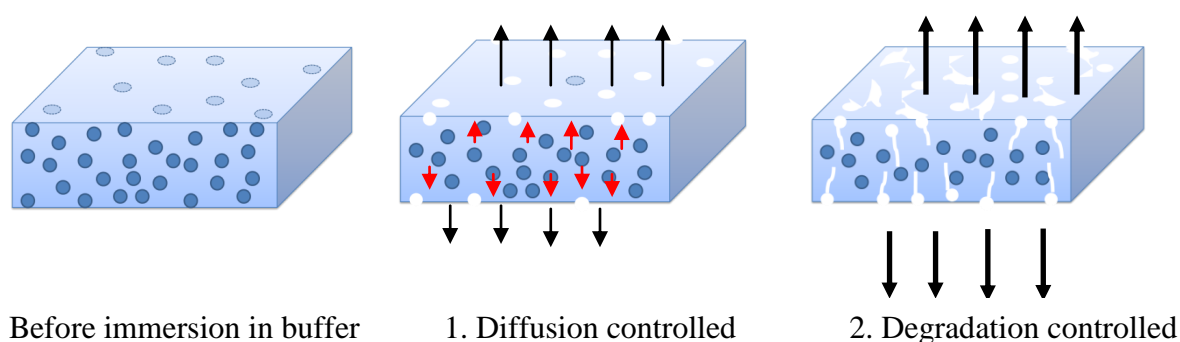
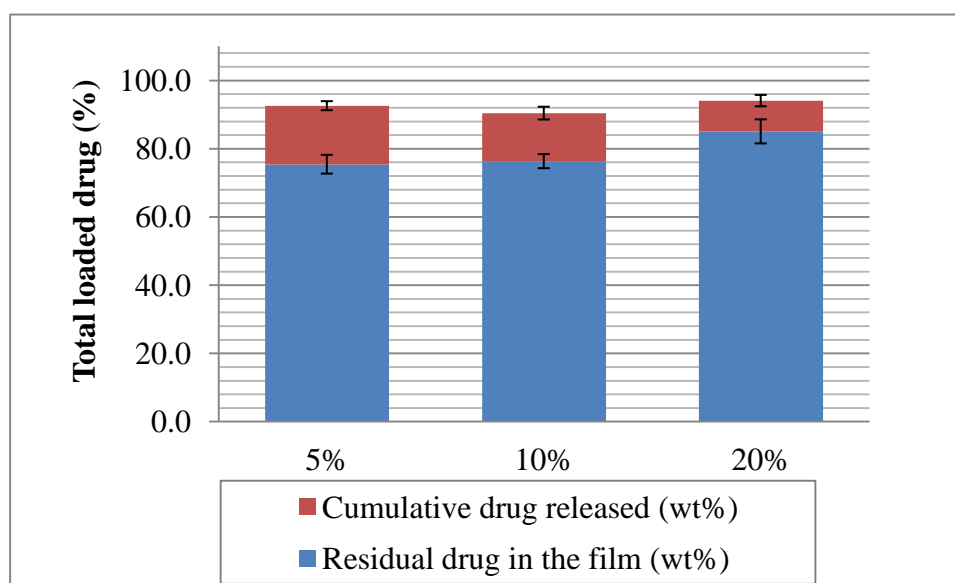


Figure 6.15 Schematic demonstration of drug release from PA-loaded PLC7030 films

At the end of study (144days), there was 17%, 14% and 9% drug released from 5%, 10% and 20% PA-loaded PLC film with thickness 500 μ m respectively. Noticeably, on 144 day, the PLC film was quite brittle and needed to be handled with extra care. However, there were less than 20% of the loaded drugs released from each sample by day 144. In order to

verify and confirm the fraction of drug released is correct, the residual drug in the films retrieved on 144th day of study was tested. As indicated in Figure 6.16, there were roughly 75%, 76% and 85% of drugs remaining in the film. The summation of cumulative released drug and residual drug is close to but slightly less than 100%, which may be due to transferring and sample handling during the drug release study.



	5%	10%	20%
Cumulative drug release (wt%)	17.16±1.33	14.08±1.88	9.02±1.68
Residual drug in the film (wt %)	75.43±2.75	76.33±2.07	85.05±3.53

Figure 6.16 Cumulative drug released and residual drug in the remaining films

ii. Rate of release

As discussed above, there are two stages involved in the release of PA from PLC7030 films, namely diffusion control and degradation control. With degradation progressed, the rate of release became faster, nevertheless, still maintained at a constant level for all the

loadings. Figure 6.17(A) shows the daily amounts of release were 0.002mg/day, 0.003mg/day and 0.006mg/day for 5%, 10% and 20% loaded PLC films in the diffusion controlled region. Gradually it was then increased to 0.004mg/day, 0.006mg/day and 0.01mg/day for 5%, 10% and 20% loaded PLC films in the degradation controlled regime.

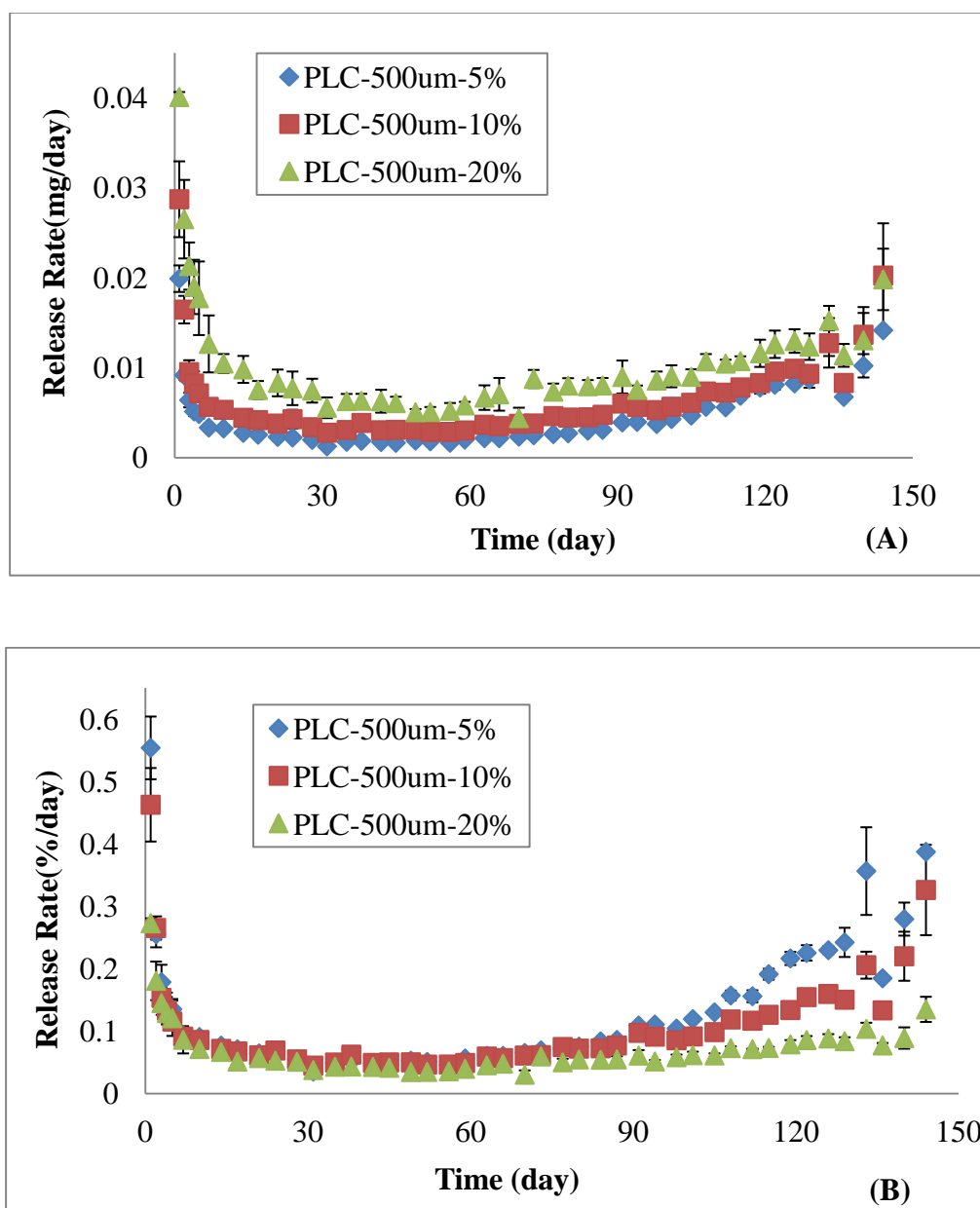


Figure 6.17 Rate of release of PA from 5%, 10% and 20% loaded PLC7030 films (500 μ m, PBS pH7.4, 37°C) , (A) is the weight per day, (B) is the weight fraction per day

Figure 6.17(B) shows that the fractional rate of releases was quite stagnant from the 7th day onwards until the 60th day, which was maintained at 0.5%-0.6% per day for all the three loadings. From Day 60 to Day 144, the difference among the three loadings became more obvious, with higher fractional rate of release goes to lower loadings.

6.1.2.3 *Summary*

There were two stages observed in the prednisolone-acetate loaded PLC release profiles, namely diffusion control and degradation control, without observing notable burst initially even for 20%-loaded films. Drug release is affected by initial drug loading. Higher loading generally released more amount of drug cumulatively and on daily basis, but the fractional drug release is lower, which is to say, higher drug loading is capable to release higher amount of drug daily for a comparatively longer period.

6.1.3. *In vitro* drug release - Effect of film thickness

The drug release profile is influenced by drug loading, as studied in the previous section. Will film thickness affect the release profile?. This chapter will concentrate on how film thickness influences the drug release performance.

The 5%, 10% and 20% PA-loaded PLC7030 films with thickness 40 μ m, 80 μ m, 250 μ m and 500 μ m were prepared. The actual drug loadings were tested and the results are listed in Table 6.2 below. The drug released from each thickness was compared for individual drug loading respectively.

Table 6.2 Actual loading of PA-loaded PLC7030 films with different thicknesses

Theoretical Loading (%)	Actual Loading (%)			
	500 μm	250 μm	80 μm	40 μm
5	5.60 \pm 0.04	4.56 \pm 0.53	4.62 \pm 0.13	5.40 \pm 0.06
10	10.85 \pm 0.62	8.54 \pm 0.92	8.56 \pm 0.33	10.21 \pm 0.08
20	24.85 \pm 1.70	18.01 \pm 2.27	20.24 \pm 1.34	20.22 \pm 0.63

6.1.3.1 Diffusion controlled stage

As discussed earlier, diffusion controlled stage is from Day 0 to approximately Day 56. The cumulative release (weight) for samples with thickness 40 μm , 80 μm , 250 μm and 500 μm were plotted individually for each drug loading, as shown in Figure 6.18 (A-5%, B-10% and C-20%). The cumulative amount of drug released was found to be independent of film thickness in the diffusion controlled stage, which is in accordance the prediction by the Higuchi model (Equation 2.18), as thickness is not a parameter in Equation 2.18.

$$M_t = A(2DC_{ss}C_o t)^{1/2} \quad \text{Recall Equation 2.18}$$

Therefore, rate of release in terms of weight is also not affected by the film thickness in this stage (Figure 6.19). Since in the Higuchi model, taking first derivative of M_t over time, thickness is not a parameter in the equation:

$$\frac{dM_t}{dt} = \frac{d}{dt} [A(2DC_{ss}C_o t)^{1/2}] = \frac{1}{2} A(2DC_{ss}C_o)^{1/2} t^{-1/2} \quad \text{Equation 6.1}$$

The daily release amounts from 5%, 10% and 20% loaded PLC films are 0.0025mg/day, 0.004mg/day and 0.007mg/day respectively, irrespective of film thickness.

However, the fractional release (both cumulative and rate of release) is affected by the film thickness. Again, applying the Higuchi model, the fractional cumulative release and release rate can be expressed by Equation 2.21 and Equation 2.22, and was found to be inversely proportional to film thickness.

$$\frac{M_t}{M_o} = \left[\frac{(8DC_{ss}t)^{1/2}}{l} \right] C_o^{-1/2} \quad \text{Recall Equation 2.21}$$

$$\frac{d}{dt} \left(\frac{M_t}{M_o} \right) = \frac{(2DC_{ss})^{1/2}}{l(C_o t)^{1/2}} \quad \text{Recall Equation 2.22}$$

Figure 6.20 demonstrates the fractional cumulative release of PA from PLC matrix (5%, 10% and 20% loadings). As predicted from the Higuchi model, thinner samples released much higher percentage of drugs for all the three drug loadings. If fitting the cumulative release (%) by power equation $y=kt^n$, the values of n is generally larger than 0.5 in all the cases, which indicates a combination of Fickian diffusion and Case II diffusion, named anomalous diffusion [70]. The higher extrapolated n value is mainly due to pores generated on the sample surface and cavities gradually formed inside the matrix. Since the solubility of PA in PLC is quite low, even with 5% loading, the system can be taken as a complex monolithic dispersion system, with the dispersed drug particles connected to each other. The fluid from the surrounding media then filled the cavities, which increased the system's overall permeability of the matrix. In addition, there is an overall trend for value of n, where n increased with decreased film thickness due to increased surface-to-volume ratio [18]. For samples with thickness 250 μm and 500 μm , n is very close to but slightly higher than 0.5. Nevertheless, samples with thickness 40 μm and 80 μm showed much higher value than 0.5.

The rate of release also followed the same trend as the fractional cumulative release, as thinner films released a higher percentage of PA daily (Figure 6.21). Noticeably, the

40 μm -thick PA loaded PLC films did not demonstrate well-controlled percentage of drug released daily even in the first 14 days for all the three loadings.

6.1.3.2 Degradation controlled stage

Even though diffusion is still playing a role in the release mechanism, the second stage is no longer dominated by diffusion. Instead, it is controlled by degradation of the polymer matrix. Thus the Higuchi model is not applicable to predict the release profile.

Noticeably, the samples with thickness of 40 μm released drug faster than the rest, so that it has been released 70-80% of the loaded drug in the first stage. When degradation speeded up the release, the samples were exhausted of drugs in the early time (84th day) of degradation controlled stage, as indicated from Figure 6.20 and Figure 6.21. Therefore, 40 μm -thick PA loaded PLC samples will not be discussed in this stage. Additionally, the preliminary drug release study on samples with thickness of 250 μm was only conducted for 35 days, which is also not subjected to the following discussion. The main comparison was based on samples with thickness of 80 μm (thinner sample) and 500 μm (thicker sample).

The actual amount of drug released from all the thickness was almost the same in the first stage, as discussed previously. However, the amount of drug released from thinner samples (80 μm) seems to be higher than thicker samples (500 μm) in the degradation-controlled stage, as seen from Figure 6.18). The effect of film thickness on the degradation performance was discussed in the previous chapter, and results showed that thinner films had greater mass loss (Figure 5.11) but slower degradation rate (Figure 5.13) than the thicker samples. This difference was more obvious with 20% PA-loaded samples. The average daily amount of release from 80 μm -thick and 500 μm -thick samples

increased to 0.55-0.6mg/day (5% loading), 0.68-0.75mg/day (10% loading) and 0.01-0.012mg/day (20% loading) respectively.

The larger amount of release from thinner samples may be due to significant mass loss. When the oligomers and monomers degraded from random chain scission diffused out of the bulk, a more porous matrix would be generated. Therefore, the drug particles were given more free volume for the diffusion inside the bulk. Together with the normal diffusion process, the leaching oligomers and monomers would also bring the drugs along to the surrounding media.

As shown in Figure 6.20, samples with 80 μ m thickness released 55-70% of the loaded drug at the end of the study (Day 114), whereas sample with 500 μ m thickness only released 7-10% at the end of the 120th day. Degradation study of PLC7030 showed that on the 96th day, the M_w of the matrix has dropped almost 90% (approximately 15kDa), and 500 μ m-thickness samples were found brittle and fragile on the 120th day. Therefore, PA is expected to be released from the 500 μ m-thickness samples faster and faster. However, due to the bulk degradation mechanism of PLC7030, when the critical M_w for the onset of mass loss of PLC7030 has reached [17], the drug release would be increased drastically, which is highly above the toxic level, thus lead to undesirable side effects.

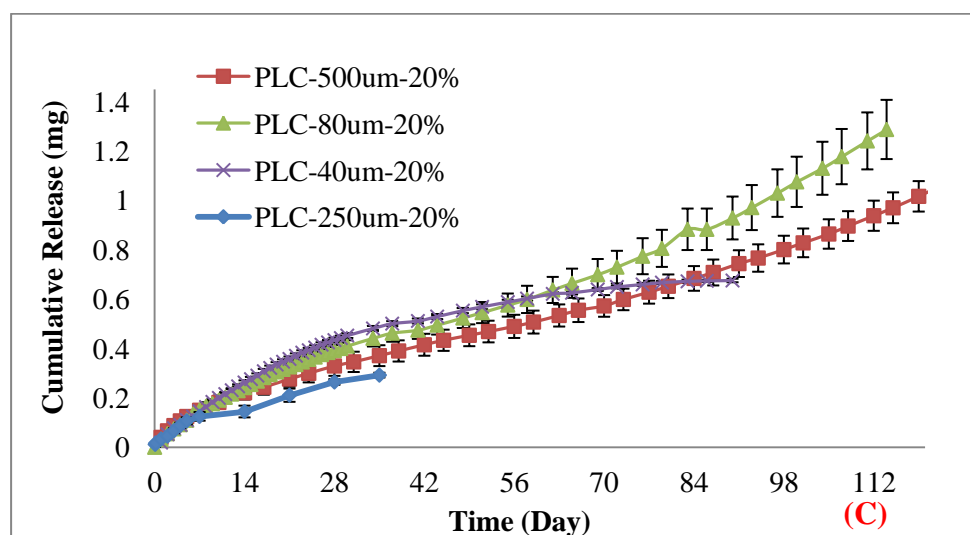
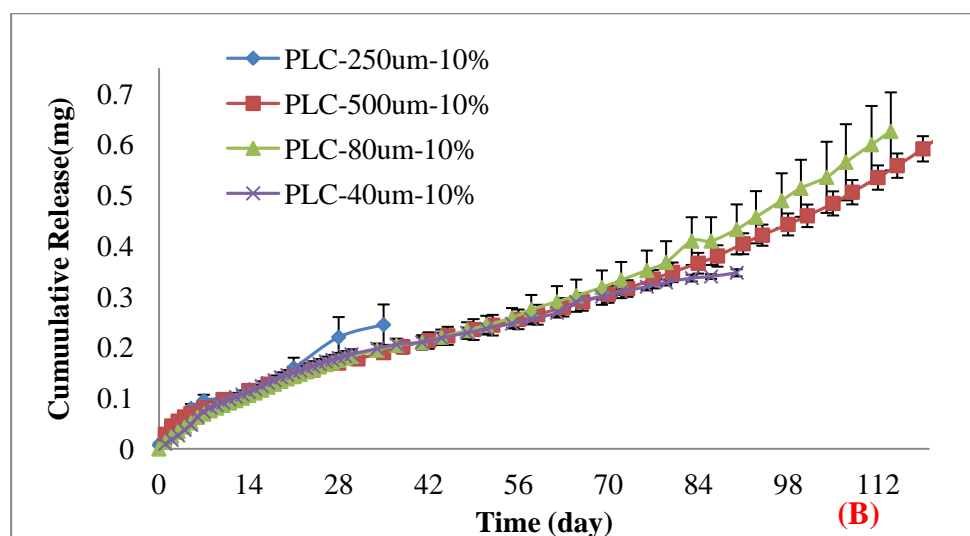
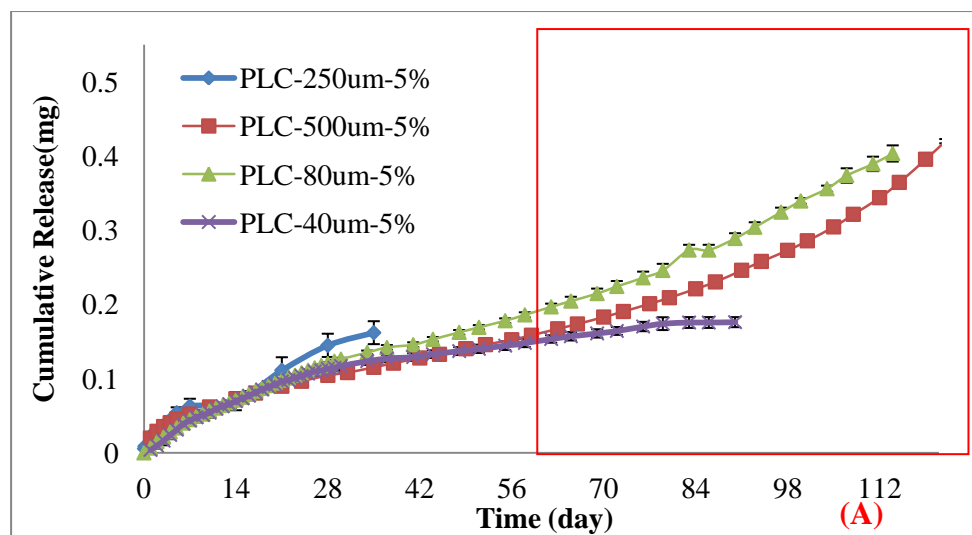


Figure 6.18 Cumulative releases (weight) of PA-loaded PLC7030 films with thickness 40 μm , 80 μm , 250 μm and 500 μm (PBS pH7.4, 37°C), (A) 5%, (B) 10% and (C) 20%

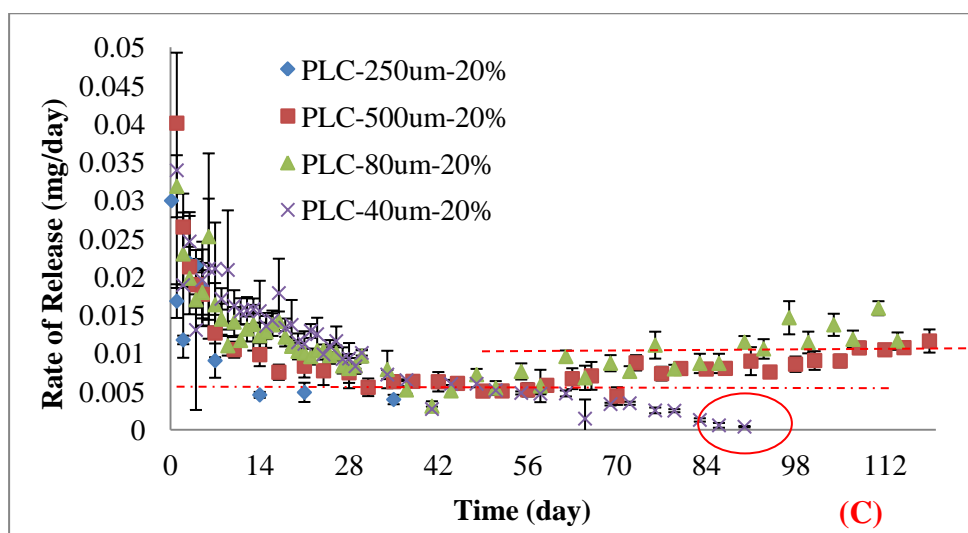
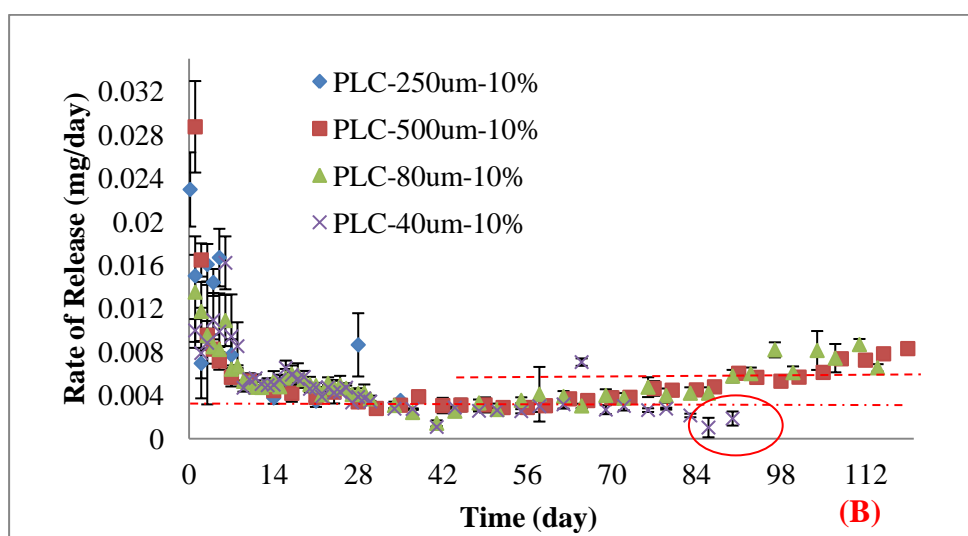
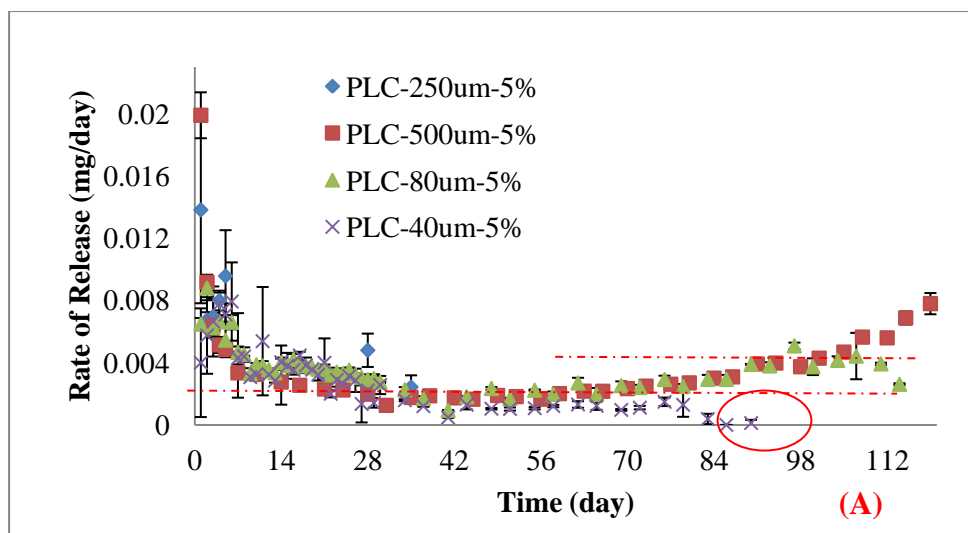


Figure 6.19 Release rates (weight) of PA-loaded PLC7030 films with thickness 40 μm , 80 μm , 250 μm and 500 μm (PBS pH7.4, 37°C), (A) 5%, (B) 10% and (C) 20%

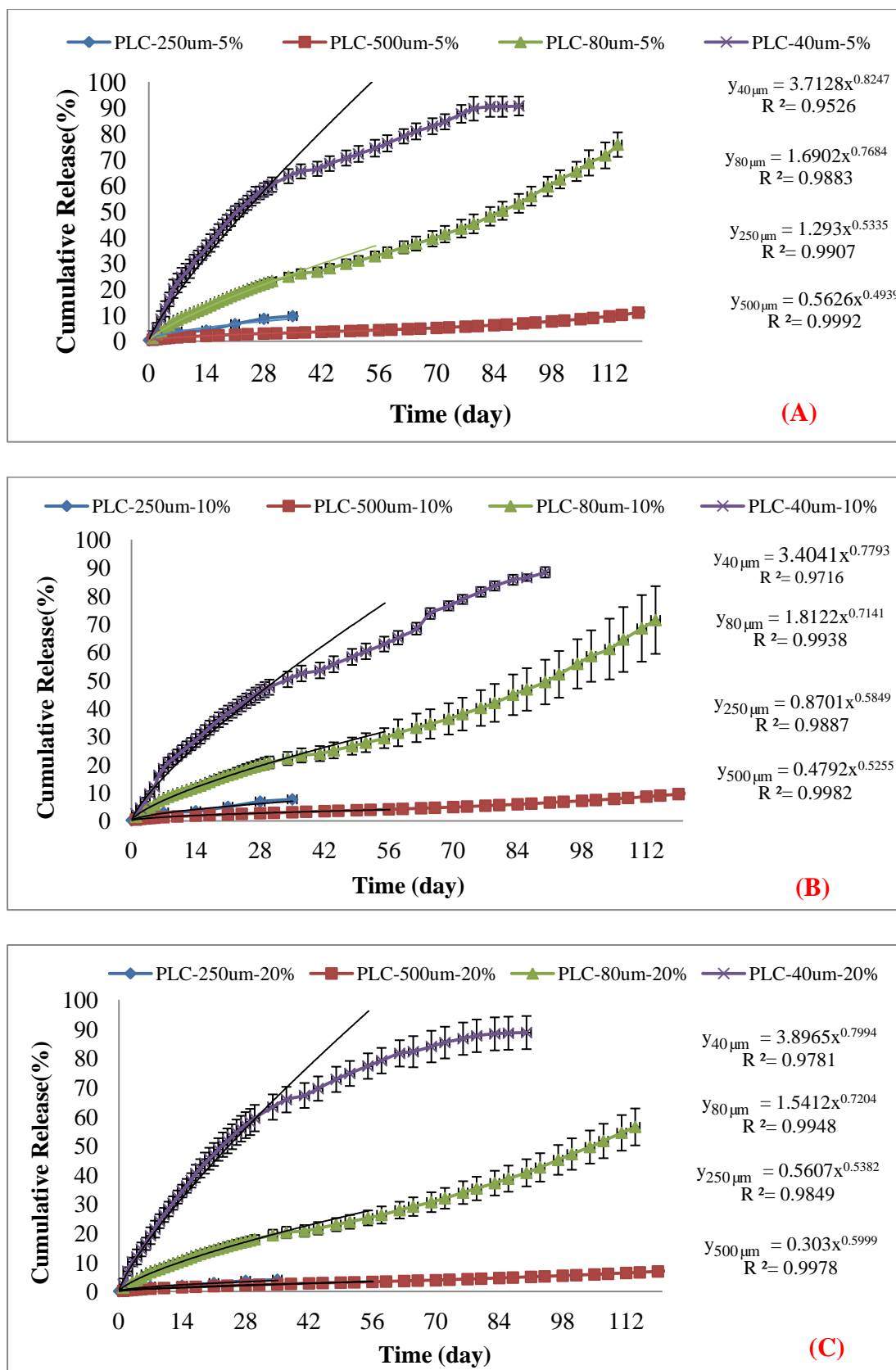


Figure 6.20 Cumulative releases (%) of PA-loaded PLC7030 films with thickness 40 μm , 80 μm , 250 μm and 500 μm (PBS pH7.4, 37°C), (A) 5%, (B) 10% and (C) 20%

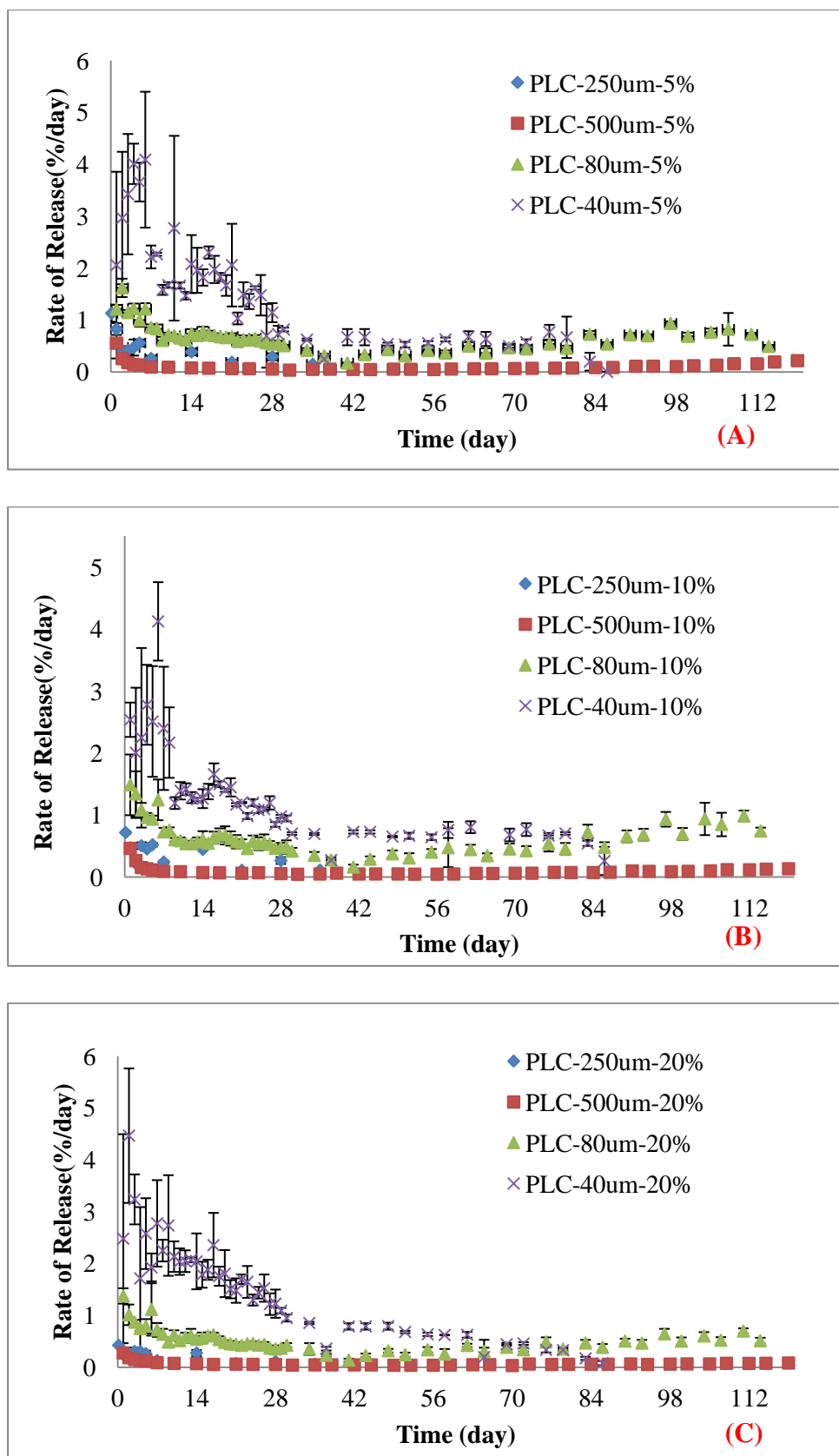


Figure 6.21 Release rates (%) of PA-loaded PLC7030 films with thickness 40 μ m, 80 μ m, 250 μ m and 500 μ m (PBS pH7.4, 37°C), (A) 5%, (B) 10% and (C) 20%

6.1.4 *In vitro* and *in vivo* drug release – 20%-loaded PLC7030 film (80 μm)

PRED FORTE® (prednisolone acetate ophthalmic suspension, USP) 1% is an ophthalmic suspension of PA that is commercially available and widely used. One drop (40 μL) of PRED FORTE® 1% approximately contains 0.04mg of PA. PRED FORTE® 1% is typically applied (1 drop every 4 hours every day) after glaucoma filtration surgeries to reduce inflammation and prevent scarring for at least three months [110]. This equates to 0.24mg of PA topically applied to the eye per day. Assuming 5% bioavailability [7, 111] of the drug optimistically, then only 0.012mg of the drug can actually reach the targeted site. The amount of drug required is quite close to the amount released daily from 20% PA-loaded PLC films *in vitro* (Since practically, 80 μm PLC films were easy to be inserted and more comfortable to be worn in the rabbit eyes as tested). Additionally, the amount of drug released is independent of film thickness. From the *in vitro* study, 20% loaded 80 μm PLC films are capable to achieve controlled release over a period of 114 days, with minimal burst initially and approximately 55% of the loaded drug was released on Day 114, therefore, 20% PA-loaded microfilm with thickness 80 μm were selected to be tested in the rabbit eyes for *in vivo* drug release evaluation over a period of 84 days.

The *in vivo* drug release profile is consistent with the *in vitro* result, which also consists of two stages (diffusion controlled and degradation controlled). Generally speaking, the *in vivo* release of PA from 20% PA-loaded PLC7030 with thickness 80 μm is faster and higher than the *in vitro* release results. As seen from Figure 6.22 (B), on the 84th day, there was about 59% of PA released from the *in vivo* samples, whereas the *in vitro* samples only released 37% of the loaded drug. The daily amount of PA released *in vivo* was found to be around two folds of that released *in vitro* despite of the *in vitro* results obtained in the first seven days (Figure 6.22(A)).

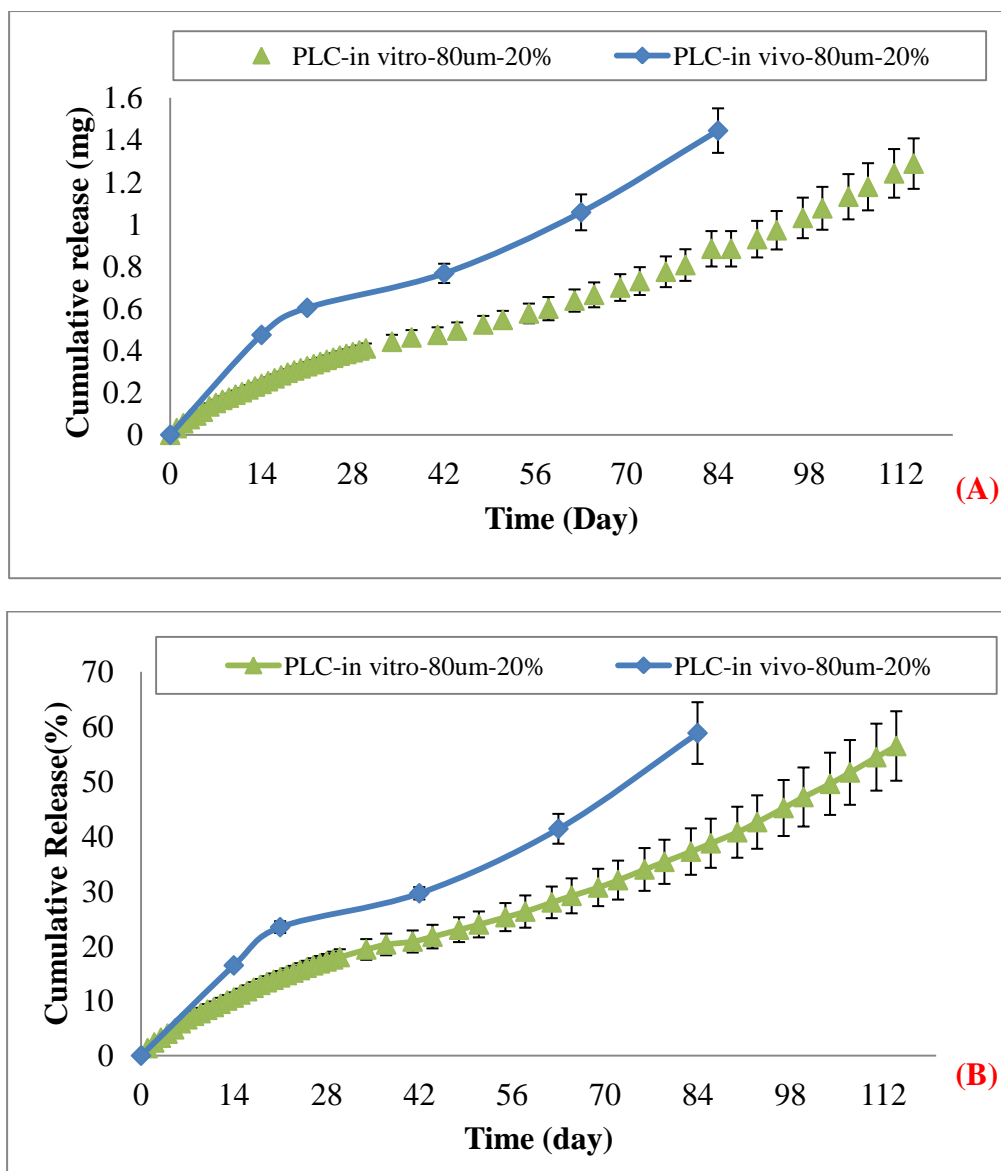


Figure 6.22 Cumulative releases of 20% PA-loaded PLC7030 films with thickness 80 μm, *in vitro* and *in vivo* (A) weight and (B) weight percentage

Due to the complex dynamic environment in the rabbit eyes (e.g. drug clearance), the driving force for diffusion of drug through the polymer matrix is expected to be higher. Thus a higher release was observed in the first stage *in vivo*. Moreover, the degradation of PLC7030 (with dimension $3 \times 6 \times 0.25 \text{ mm}^2$) was noticed to be almost 27% faster in the subconjunctival space of rabbit eyes as compared to in the *in vitro* PBS environment (Section 5.1.3.1). Consequently, the onset point for degradation-controlled stage was

brought earlier than the *in vitro* release profile, which was noted to be around 42 days (the onset point for the second stage *in vitro* was 56 day).

The amount released per day (*in vivo*) was enough to be potent for at least 84 days (potency was verified in rabbit's glaucoma model by ophthalmologists) [112], but this is out of the scope of discussion of the thesis.

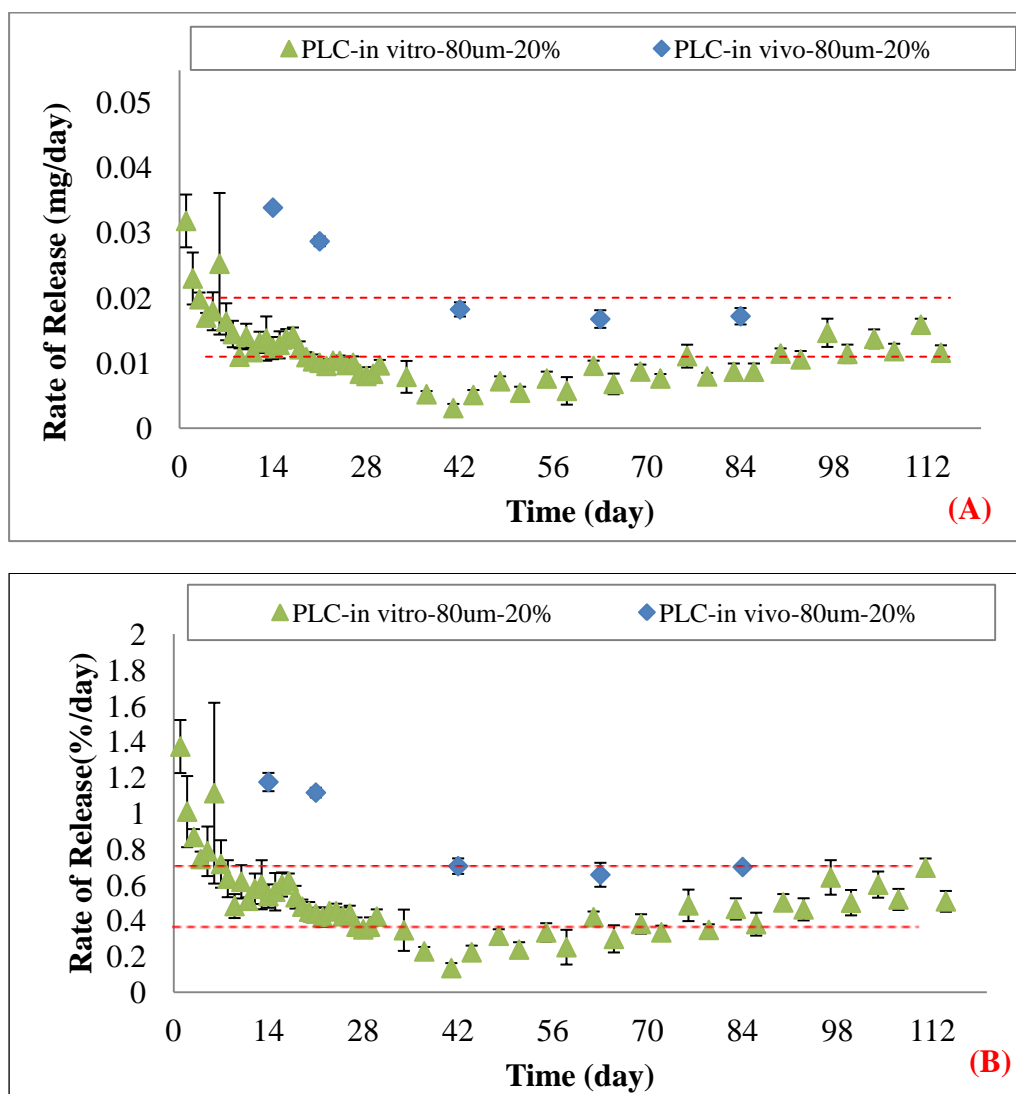


Figure 6.23 Cumulative releases of 20% PA-loaded PLC7030 films with thickness 80 μ m, *in vitro* and *in vivo*

6.2 Mathematical Modeling of Drug Release

Mathematical models for drug release from bulk degrading polymer usually employ the well-established Higuchi model for diffusion-controlled non-degradable systems. As discussed in Chapter 2, the model developed by Lao *et al.* gave a quite good prediction of the tri-phase release of a hydrophobic drug-paclitaxel from PLGA [76, 77], which consists of burst release, release due to degradation relaxation of polymer matrix and diffusion of drug from the polymer matrix.

Prednisolone acetate (PA) release from PLC7030 has been discussed in the previous sections, this Chapter (section 6.1). Due to the hydrophobic nature of PA, burst release was not observed from the release profiles, even for loading as high as 20%. If the PA release from PLC7030 can be modelled, then a quantitative physical interpretation for the release phases is possible. Rothstein *et al.* [113] suggested three requirements to supplant the need to explore the release mechanisms when designing of a new control release devices.

The requirements are (1) the model must be applicable to a wide range of active agents, (2) the release of such active agents must be described from readily acquirable parameters to allow predicting the release profile as well as daily dose, (3) the model must be good enough to catch the releasing behaviours, which have been documented for that system.

Since PLC7030 with thickness 80 μm degraded homogeneously *in vitro* and *in vivo*, this is similar as PLGA used in Lao *et al.*'s model. Additionally, like paclitaxel, PA is also a very hydrophobic drug. Therefore, the mathematical model to fit the experimental results was adopted from Lao *et al.* [77]; the validity of this model was also confirmed, according to the requirements of modelling.

The difference between the model in this thesis and the Lao's model is that we have removed the “burst” effect term in the modified model. Thus the original modelling equation (Equation 2.26) was modified as follows:

$$\frac{M_t}{M_\infty} = \varphi_d \left\{ 1 - \sum_{n=0}^{\infty} \frac{8}{(2n+1)^2 \pi^2} \exp \left[\frac{-D (2n+1)^2 \pi^2 (t)}{4l^2} \right] \right\} + \varphi_r [e^{k_r(t-t_d)} - 1] \quad \text{Equation 2.26}$$

Where $\varphi_r + \varphi_d = 1$.

Another difference is the absence of the parameter t_r , and t_d represents end of diffusion-controlled stage and starting of degradation-controlled stage. As in the experimental results of PA release from PLC, the first stage was diffusion control, following by degradation controlled.

The degradation relaxation constant k_r strongly depends on the rate of polymer degradation, which is the rate of oligomers and monomers production. Thus, the value k_r was taken to be the rate constant obtained from the polymer degradation as a preliminary approximation. The degradation rate constants for 0%, 5%, 10% and 20% PA-loaded PLC7030 films with thickness 250 μm were obtained and listed in Table 6.3. The degradation rate constants are found almost independent of the drug loading. The degradation behaviour of PLC7030 was evaluated in Chapter 5, which found the degradation rate constant decreased with decreased thickness. The degradation rate constants (k_r) for PA-loaded PLC7030 films with thickness 250 μm and non-drug loaded PLC7030 film with thickness 80 μm , 500 μm are listed in Table 6.3 below. The k_r value for blank 80 μm was taken as a reference value to start modelling.

Table 6.3 List of first order degradation rate constant for PA-loaded PLC7030

Samples	5% 250 μm	10% 250 μm	20% 250 μm	0% 250 μm	0% 80 μm	0% 500 μm
k_r (day^{-1})	0.028	0.028	0.028	0.027	0.024	0.035
R_2	0.972	0.980	0.978	0.976	0.941	0.995

6.2.1 Effect of drug loading

Prednisolone acetate is a very hydrophobic drug, with limited solubility in PLC7030 and water. Worth noting that the local amount of water surrounding the drug is not high, thus the drug dissolution process was difficult, which explains why the initial burst release was not observed in the experiment.

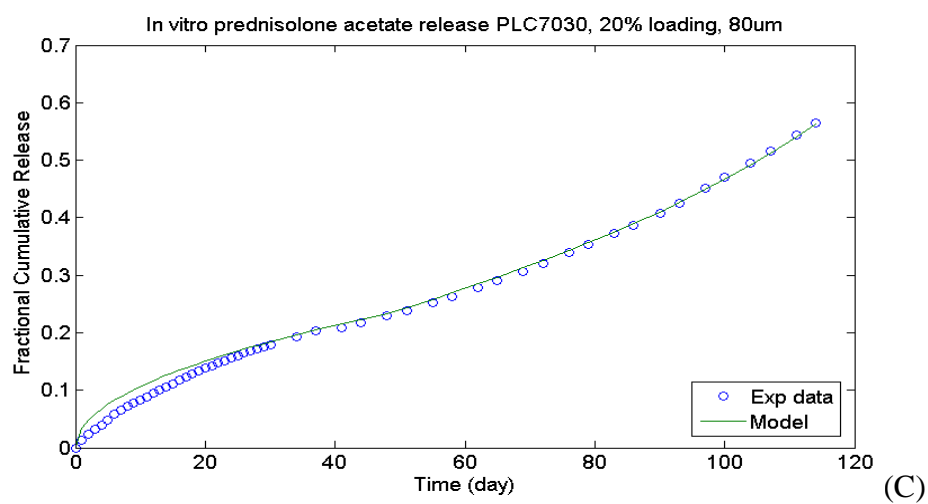
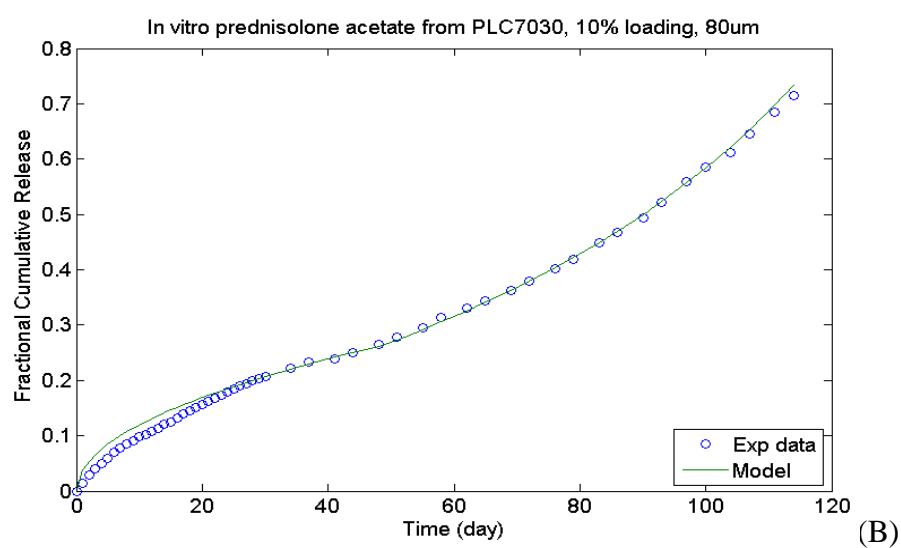
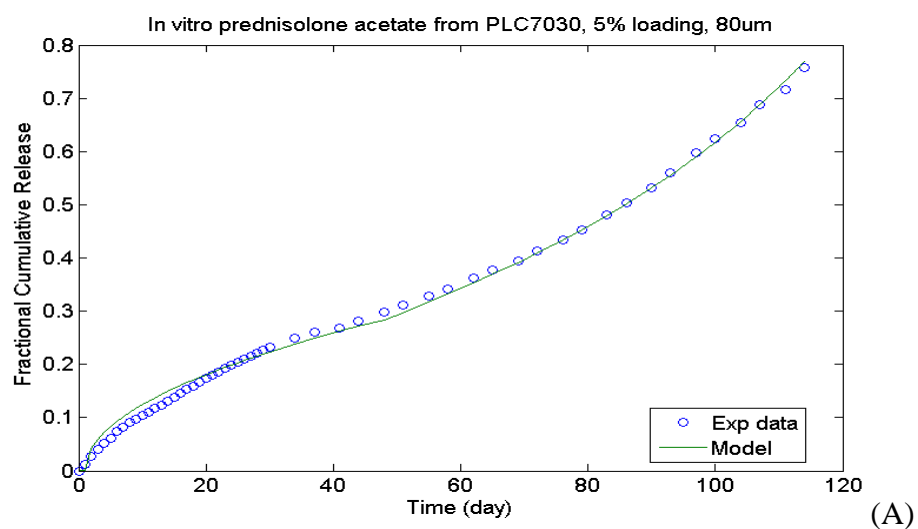
MATLAB software was used to determine the model parameters of prednisolone acetate release from PLC7030 films. The model parameters are summarized in Table 6.4 along with the values obtained from 80 μm thick film loaded with 5%, 10% and 20% prednisolone acetate. The simulated graphs for each loading are shown in Figure 6.24.

Initially, the release was mainly controlled by diffusion of prednisolone acetate from PLC7030. The model determined the diffusion coefficient of PA through PLC7030 matrix, reported for the first time, was found to be in the magnitude of $10^{-8} \text{ cm}^2/\text{s}$. The diffusion of prednisolone acetate from PLC7030 proceeded relatively fast, until release reached the degradation-controlled stage. The fast diffusion agrees with the literature, which indicated that PLC7030 is permeable to lipophilic drugs [114]. The diffusivity value was noticed to decrease with increased drug loading percentages, which is similar as the literature for similar drug system [77].

The fractional release from diffusion (ϕ_d) was more than 90% from the simulated results, whereas ϕ_r was approximately less 10%. This corresponds to the mass loss results

obtained from the degradation study of PLC7030 (with and without drugs). Since the on the 56th day, the degrading matrix only lost less than 5% of mass; and even on the 90th day, only around 10-12% mass loss was observed.

With the relaxation of degraded polymer chains as well as drug dissolution, micro-pores were created in the polymer matrix. The ϕ_r values obtained from different loadings did not demonstrate any significant difference. Nevertheless k_r and t_d decreased slightly with elevated drug loading percentages.



Each experimental data point is an average of 3 repeated experiments (n=3)

Figure 6.24 Experimental and model data fitting of prednisolone acetate release from PLC7030 films (80 μm thick) with (A) 5%, (B) 10% and (C) 20% loadings

Table 6.4 Model parameters for PA from PLC7030 80 μ m thick films

Parameters	Description	Unit	5%	10%	20%
<i>Known parameters</i>					
l	Half thickness	cm	40×10^{-4}	40×10^{-4}	40×10^{-4}
k_r	Degradation constant	day ⁻¹	0.024	0.024	0.024
<i>Unknown parameters</i>					
			<i>Fitted Value</i>		
k_r	Degradation constant	day ⁻¹	0.0265	0.0260	0.0238
D_{eff}	Diffusion coefficient	cm ² /day	2.410×10^{-8}	2.108×10^{-8}	1.647×10^{-8}
ϕ_r	Fraction of relaxation	--	0.076	0.077	0.055
ϕ_d	Fraction of diffusion	--	0.924	0.923	0.945
t_d	Start of degradation	day	52.000	50.000	49.000
R^2	Correlation coefficient	--	0.996	0.997	0.999

6.2.2 Comparison of *in vitro* and *in vivo* release

The experimental results obtained in last Chapter showed that in general *in vivo* drug release is higher and faster than that *in vitro*. This was mainly due to two reasons: one is accelerated degradation, as tested in Chapter 5, and the other one is that clearance rate of drugs in the animal is greater than under the (static) *in vitro* condition. Ohtori, A. and K. Tojo studied elimination of dexamethasone salt (DMSB), after intravitreal injection was higher in the vitreous body than *in vitro* [115]. Similar *in vitro* and *in vivo* drug dissolution comparison was also reported by other researchers [116, 117].

MATLAB software was the tool to determine the model parameters of prednisolone acetate release from PLC7030 films. The model parameters are summarized in Table 6.5 along with the values obtained from *in vitro* and *in vivo* drug release from the 20% PA loaded 80 μm thick film. The experimental data and the simulated data from the model for the *in vivo* release are shown in Figure 6.25.

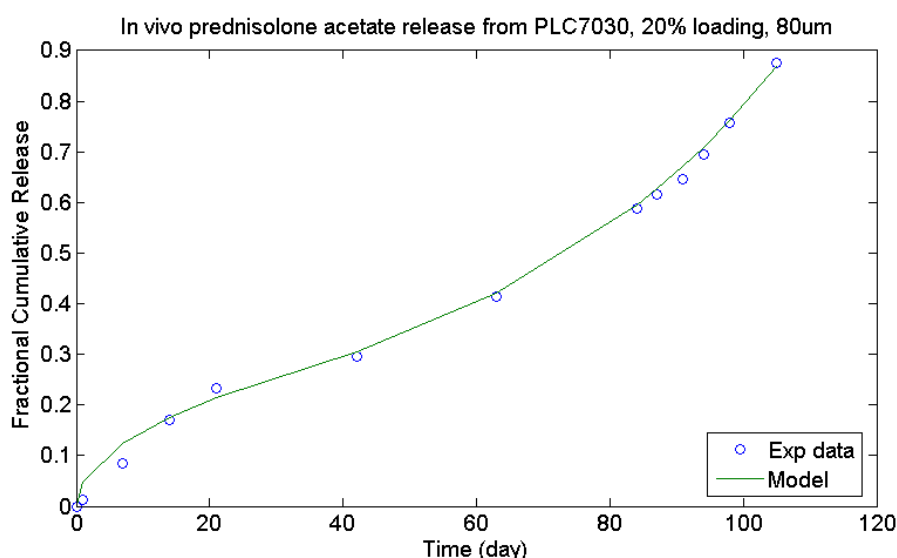


Figure 6.25 Experimental and model data fitting of *in vivo* prednisolone acetate release from PLC7030 films (80 μm thick) 20% loadings

The model value of diffusion coefficient of PA *in vivo* is almost double of that *in vitro*, which demonstrates faster diffusional release in the subconjunctival space of rabbit. This matches perfectly well with the experimental results and those reported in the literature. Secondly, both the degradation rate constant (k_r) and fraction of relaxation release (ϕ_r) are greater *in vivo* than *in vitro*, due to the faster *in vivo* degradation noticed in the experiment (Chapter 5). Noticeably, the degradation rate constants calculated from the model match the values obtained from degradation study previously.

Table 6.5 Model parameters for PA release from PLC-80 μm films, *in vitro* and *in vivo*

Parameters	Description	Unit	20%- <i>In vitro</i>	20%- <i>In vivo</i>
<i>Known parameters</i>				
l	Half thickness	cm	40×10^{-4}	40×10^{-4}
k_r	Degradation rate	day^{-1}	0.026	>0.026
<i>Unknown parameters</i>				
			<i>Fitted Value</i>	
k_r	Degradation rate	day^{-1}	0.0238	0.0310
D_{eff}	Diffusion coefficient	cm^2/day	1.6468×10^{-8}	3.285×10^{-8}
ϕ_r	Fraction of relaxation	--	0.0550	0.0800
ϕ_d	Fraction of diffusion	--	0.9450	0.9200
t_d	Start of relaxation	day	49.0000	48.0000
R^2	Correlation coefficient	--	0.9984	0.9974

6.2.3 Summary

The modified model for bi-phase release profile (diffusion controlled and degradation controlled) can predict the release of prednisolone acetate from PLC7030 films quite well (with $R^2 > 0.99$), with similar k_r values obtained from experiment. The diffusion coefficient of the PA in PLC7030 was simulated to be in the magnitude of $10^{-8} \text{ cm}^2/\text{s}$. The D_{eff} obtained *in vivo* is two folds of that modelled from that *in vitro*. The fraction of degradational release is less than 8%, whereas the fraction of diffusional release is more than 90%. The onset of degradational release was modelled to be around 50 days, regardless of the *in vitro* and *in vivo* conditions.

6.3 Conclusion

Prednisolone acetate was loaded into PLC7030 films at 5%, 10% and 20% (weight percentage). There were two stages observed in the drug release profiles, which are diffusion-controlled stage and degradation-controlled stage. Surprisingly, initial burst was not seen for all the loadings, which may be due to the hydrophobic nature of PA. In the diffusion controlled stage, the Higuchi model governed the release behaviour, with slightly higher than 0.5 for the power exponent values. In the degradation-controlled stage, the release profile was no longer governed by the Higuchi model, instead, an exponent increase in the cumulative release profile was noted

The effect of drug loading on release performance was also evaluated. The amount of drug released (both cumulative and rate of release) increased with drug loading, whereas the fractional drug release (both cumulative and rate of release) decreased with drug loading.

Thickness was also found to affect the drug release performance. The fractional releases (cumulative and rate of release) increased almost inversely proportional to the film thickness throughout the study period, as expected. Noticeably, due to the fast release from 40 μm films, the loaded drug was exhausted in the matrix before degradation played a significant role.

The drug release of 20% PA-loaded PLC7030 films (80 μm) was also conducted *in vivo* (in the subconjunctival space of rabbit eyes after glaucoma filtration surgery). The amount and percentage of drug released are both higher than those obtained *in vitro*, with almost double the release rate being seen *in vivo*.

Lastly, the release profiles were expressed mathematically by modifying an existing model. The modified model predicted the experimental results quite well.

Chapter 7 Conclusion and Future Recommendations

7.1 Final Conclusions

For this project, the working hypothesis was that biodegradable microfilms with predicted degradation behaviour can control the release of corticosteroid sustainably in the anterior segment of the eye for postoperative treatment with equal or better therapeutical effects than the eye drop. Was the hypothesis confirmed?

7.1.1 Characterization and selection of candidate material

To address the hypothesis, the first phase of the study was to develop and characterize biodegradable microfilms made from two different biomaterials (PLGA5347 and PLC7030) for their potential application as vehicles for intraocular drug delivery, especially on surgical insertion into the subconjunctival space, as well as the *in vitro* and *in vivo* degradation behaviours of both polymers.

Microfilms made from PLGA5347 and PLC7030 were developed, and then the degradation behaviour of the two biomaterials was studied both *in vitro* and *in vivo*. This is the first time, to the author's knowledge, to test the *in vivo* degradation of poly-lactide-group biodegradable polymers, as films, in the sub-conjunctival space of the rabbit eyes, which demonstrated very different behaviour as compared with the *in vitro* degradation results.

In the *in vitro* environment, full degradation was observed for PLGA5347 on the 42nd day with great amount of water absorption and mass loss. Not as evident, PLC7030 lost 90% of its initial average weight molecular mass at the end of the study (96th day), with minimal water absorption and mass loss (both are less than 2%), as well as almost unchanged dimensions.

In vivo, PLGA5347 was fully invisible in the rabbit eyes 3 months after the study; whereas PLC7030 persisted throughout the 6 months, with unchanged width and length, but linearly decreasing film thickness. In summary, PLGA5347 degraded homogeneously both *in vitro* and *in vivo*, nevertheless PLC7030 degraded homogeneously *in vitro*, and might degrade heterogeneously *in vivo*. This is quite a novel finding, since no one has reported biodegradable polymers hydrolyze homogeneously *in vitro* but heterogeneously *in vivo*. Due to the different period of degradation for the two characterized polymers, PLC7030 was chosen to be the suitable drug-loading material for subsequent degradation and drug release studies.

7.1.2 Degradation study of PLC7030

The second phase of the study was to further investigate the degradation behaviour of the selected biomaterial from the above study. The focus of the study was on the effect of shape and thickness of the sample as well as the degrading media (*in vitro* and *in vivo*) on the degradation kinetics. It was found that all the three parameters have an impact on the degradation performance, possibly affecting the drug release profiles, especially in actual clinical applications.

Firstly, the shape of samples was found to affect the degradation of PLC7030. Experimental results revealed that the samples (250µm) with sharp edges (square and rectangle) seemed to degrade faster compared to round samples (disk). And this difference appeared to be more pronounced *in vivo* than *in vitro*.

Secondly, though bulk degradation is said to be homogeneous irrespective of thickness, the thickness of sample had been found to have an impact on the degradation rate of PLC7030. Thinner films demonstrated slower degradation rate but higher mass loss than the thicker films *in vitro*.

Thirdly, the degradation behaviour of PLC7030 *in vitro* and in the subconjunctival space of rabbit eyes differed, and the disparity became larger when the film thickness increased from 250 μm to 500 μm . Since PLC-250 μm demonstrated homogeneous degradation *in vitro* and *in vivo*, whereas PLC-500 μm seemed to degrade homogeneously *in vitro*, but heterogeneously *in vivo*.

The degradation behaviour of PLC7030 was also interpreted by applying the mathematical model developed previously in the literature. The work and discussion was primarily concentrated on analyzing the effect of three parameters on the degradation mechanism based on the value calculated from the experiments, namely the diffusivity of water through the polymer (D_{eff}), the degradation rate constant (λ) and the thickness of sample. Finally, the critical thickness of PLC7030 was calculated as in the *in vitro* and *in vivo* environments, and *in vitro* condition tends to yield a higher value of critical thickness due to comparatively slower degradation (lower λ) and faster diffusion of water into the polymer matrix (higher D_{eff}).

7.1.3 Drug release study from PLC7030

The third phase of the study was to develop the drug loaded microfilms with selected materials from above studies and exploit the drug release potential of a single layer polymeric microfilm. The release mechanism was aimed to be examined as an effect of drug loading percentages, film thickness, as well as the *in vitro/in vivo* media. The experimental release results were also aimed to correlate with mathematical drug release models.

The corticosteroid-prednisolone acetate was loaded into PLC7030 films at 5%, 10% and 20% (weight percentage). There were two stages observed in the drug release profiles, which are diffusion-controlled stage and degradation-controlled stage. Initial burst was not seen for all the loadings, which may be due to the hydrophobic nature of PA. The

release in the diffusion controlled stage was governed by the Higuchi model, with slightly higher than 0.5 for the power n . In the degradation-controlled stage, the release profile was noted to be an exponential increase in the cumulative release profile.

The effect of drug loadings on release performance was evaluated. The amount of drug released (both cumulative and rate of release) increased with drug loading, whereas the fractional drug release (both cumulative and rate of release) decreased with drug loading.

Thickness was also found to affect the drug release performance. Despite of the independent on film thickness in the diffusion controlled stage on amount of PA released, the fractional releases (cumulative and rate of release) increased almost inversely proportional to the film thickness throughout the study period. Noticeably, the thinner the sample, the faster release it is, which was possibly exhausted of drug in the first stage of release (diffusion controlled).

The equivalent amount of PA required from the PRED FORTE® eye drop was calculated to be 0.012mg/day. While the *in vitro* drug release from 20% PA-loaded PLC7030 microfilms (80 μ m) demonstrated daily amount released of 0.01mg/day. Therefore, the drug release of 20% PA-loaded PLC7030 films was also conducted in the subconjunctival space of rabbit eyes after glaucoma filtration surgery. The amount and percentage of drug released are both higher than those obtained *in vitro*, with almost doubled amount released daily. And the efficacy was found to be sustained over a period of 90 days.

Lastly, the release profiles were expressed mathematically by modifying an existing model. Both *in vitro* and *in vivo* experimental results matched well as the data predicted from the mathematical model.

7.2 Future Recommendations

The author would like to recommend a few future works related and based on current work.

7.2.1 *In vitro* degradation study of PLC7030

Current *in vitro* and *in vivo* degradation study of PLC7030 includes monitoring of water absorption, mass loss, change in M_w and M_n , change in film thickness, and morphology. However, a more comprehensive study which involves other properties during degradation such as change in crystallinity, mechanical properties (Young's Modulus, etc.), etc. will make the study more complete.

Moreover, the current *in vitro* degradation study of PLC7030 was conducted in PBS for 90 days. However, this is not a good interpretation of the *in vivo* degradation environment mainly due to the presence of esterases in the eye. The author would like to recommend in the future *in vitro* degradation study, instead of using PBS, a cultured medium with esterase extracted from the eye can be used.

7.2.2 Various types of drug loaded for drug release study

The drug prednisolone acetate studied in this work is a hydrophobic drug, which performed quite well. Therefore, the capability of the hydrophobic drug-loaded system can be verified by loading and studying dexamethasone, betamethasone, etc. Furthermore, it is also recommended to load hydrophilic drugs in PLC7030 and study the release behaviour. Hydrophilic drugs for glaucoma-associated treatment can be timolol maleate, valproic acid, mitomycin C or protein like Avastin.

7.2.3 Multi-layers design to achieve multiple drug release

By employing the multi layer concept in designing the drug delivery device, it is possible to load different drugs in different layers. By determining the partition coefficient of each drug in every layer of the film, and the diffusion coefficient of the drug through that layer, the drug release from a multi-layer system can be evaluated. Mathematical model for multi-drug release from multi-layer system can be generated thereafter. If the partition coefficient of drug in each layer can be well monitored, and degradation behaviour of materials in each layer is controllable, an all-in-one drug release device can be developed, which will be potentially solving many problems clinically.

References

1. Hitchings RA and Grierson.I. (1983), Clinico pathological correlation in eyes with failed fistulizing surgery. *Transactions of the ophthalmological societies of the United Kingdom*, 103 (Part 1), 84-88.
2. Skuta, G.L. and R.K. Parrish (1987), Wound healing in glaucoma filtering surgery. *Surv Ophthalmol*, 32, 149-170.
3. Raizman, M. (1996), Corticosteroid therapy of eye disease. Fifty years later. *Arch Ophthalmol*, 114, 933-937.
4. Ghate, D. and H.F. Edelhauser (2006), Ocular drug delivery. *Expert Opin Drug Deliv*, 3, 275-287.
5. Barar, J., A.R. Javazadeh, and Y. Omid (2008), Ocular novel drug delivery: impacts of membranes and barriers. *Expert Opin Drug Deliv*, 5, 567-581.
6. Souto, E.B., *et al.* (2010), Feasibility of lipid nanoparticles for ocular delivery of anti-inflammatory drugs. *Curr Eye Res*, 35, 537-552.
7. Johansen, S., RaskPedersen E., and Prause J.U. (1996), A bioavailability comparison in rabbits after a single topical ocular application of prednisolone acetate formulated as a high-viscosity gel and as an aqueous suspension .1. . *Acta Ophthalmologica Scandinavica*, 74, 253-258.
8. Kent, A.R., *et al.* (1998), The efficacy and safety of diclofenac 0.1% versus prednisolone acetate 1% following trabeculectomy with adjunctive mitomycin-C. *Ophthalmic Surg Lasers*, 29, 562-569.
9. Gaudana, R., *et al.* (2009), Recent perspectives in ocular drug delivery. *Pharm Res*, 26, 1197-1216.
10. Beeley, N.R., *et al.* (2006), Development, implantation, in vivo elution, and retrieval of a biocompatible, sustained release subretinal drug delivery system. *J Biomed Mater Res A*, 76, 690-698.
11. Okabe, J., *et al.* (2003), Biodegradable intrascleral implant for sustained intraocular delivery of betamethasone phosphate. *Invest Ophthalmol Vis Sci*, 44, 740-744.
12. Jeong, S.I., *et al.* (2004), In vivo biocompatibility and degradation behavior of elastic poly(l-lactide-co-ε-caprolactone) scaffolds. *Biomaterials*, 25, 5939–5946.
13. Gopferich, A. (1997), Polymer bulk erosion. *Macromolecules*, 30, 2598-2604.

14. Tamada, J. and R. Langer (1993), Erosion kinetics of hydrolytically degradable polymers. *Proceedings of the National Academy of Sciences*, 90, 552-556.
15. Duong-Hong, D., *et al.* (2010), Fully biodegradable septal defect occluder-a double umbrella design. *Catheter Cardiovasc Interv*, 76, 711-718.
16. Beeley, N.R., *et al.* (2005), Fabrication, implantation, elution, and retrieval of a steroid-loaded polycaprolactone subretinal implant. *J Biomed Mater Res A*, 73, 437-444.
17. Frank A., *et al.* (2006), Some Insight into Hydrolytic Scission Mechanisms in Bioerodible Polyesters. *Journal of Applied Polymer Science*, 102, 3111-3117.
18. Klose, D., *et al.* (2008), PLGA-based drug delivery systems: Importance of the type of drug and device geometry. *International Journal of Pharmaceutics*, 354, 95-103.
19. Frank, A., S.K. Rath, and S.S. Venkatraman (2005), Controlled release from bioerodible polymers: effect of drug type and polymer composition. *J Control Release*, 102, 333-344.
20. Wang, X., *et al.* (2006), Controlled release of sirolimus from a multilayered PLGA stent matrix. *Biomaterials*, 27, 5588-5596.
21. Lewis, K.J., W.J. Irwin, and S. Akhtar (1998), Development of a sustained-release biodegradable polymer delivery system for site-specific delivery of oligonucleotides: characterization of P(LA-GA) copolymer microspheres in vitro. *J Drug Target*, 5, 291-302.
22. Barocas, V.H. and R.K. Balachandran (2008), Sustain transscleral drug delivery. *Expert Opin Drug Deliv*, 5, 1-10.
23. Ogura, Y. (2001), Drug delivery to the posterior segments of the eye. *Advanced Drug Delivery Reviews*, 52, 1-3.
24. Kunou, N., *et al.* (1995), Controlled intraocular delivery of ganciclovir with use of biodegradable scleral implant in rabbits. *Journal of Controlled Release*, 37, 143-150.
25. Weir, N.A., *et al.* (2004), Degradation of poly-L-lactide. Part 1: in vitro and in vivo physiological temperature degradation. *Proceedings of the Institution of Mechanical Engineers, Part H: Journal of Engineering in Medicine* 218-307.
26. Danmark, S., *et al.* (2011), In vitro and in vivo degradation profile of aliphatic polyesters subjected to electron beam sterilization. *Acta Biomaterialia*, 7, 2035-2046.

27. Gupta, C. and A. Chauhan (2010), Drug transport in HEMA conjunctival inserts containing precipitated drug particles. *Journal of Colloid and Interface Science* 347, 31-42.
28. Jose A. Cardillo, *et al.* (2010), Subconjunctival delivery of antibiotics in a controlled-release system-a novel anti-infective prophylaxis approach for cataract surgery. *Arch Ophthalmol*, 128, 81-87.
29. Chetoni, P., *et al.* (2007), Liposome-encapsulated mitomycin C for the reduction of corneal healing rate and ocular toxicity. *Journal of Drug Delivery Science and Technology*, 17, 43-48.
30. Lavik, E., M.H. Kuehn, and Y.H. Kwon (2011), Novel drug delivery systems for glaucoma. *Eye*, 25, 578-586.
31. Gupta, H., *et al.* (2011), Biodegradable levofloxacin nanoparticles for sustained ocular drug delivery. *Journal of Drug Targeting*, 19, 409-417.
32. Klose, D., *et al.* (2010), Drug release from PLGA-based microparticles: Effects of the "microparticle:bulk fluid" ratio. *International Journal of Pharmaceutics* 383, 123-131.
33. Kesavan, K., *et al.* (2011), Newer approaches for optimal bioavailability of ocularly delivered drugs: review. *Current Drug Delivery*, 8, 172-193.
34. Baudouin, C., *et al.* (2010), Preservatives in eyedrops: The good, the bad and the ugly. *Progress in Retinal and Eye Research*, 29, 312-334.
35. Ranne, T.T., *et al.* (2007), In vivo behavior of poly(epsilon-caprolactone-co-DL-lactide)/bioactive glass composites in rat subcutaneous tissue *Journal of Bioactive and Compatible Polymers* 22, 249-264.
36. Fukuzaki, H., *et al.* (1990), In vivo characteristics of low molecular weight copolymers composed of glycolic acid and various dl-hydroxy polyester biodegradable carriers for drug delivery systems. *Biomaterials*, 11, 441-445
37. Kansara, V., Budda B., and Mitra A.K. (2007). Advancements in ocular drug delivery, In B.O. Mashkevich(Ed. *Drug Delivery Research Advances* (pp. 1-37). New York: Nova Science Publishers, Inc.
38. Ranta, V.P. and A. Urtti (2006), Transscleral drug delivery to the posterior eye: Prospects of pharmacokinetic modeling. *Advanced Drug Delivery Reviews*, 58, 1164-1181.
39. Bores, L.D. (2002) *Ocular anatomy*. [On-line], Available: http://www.e-sunbear.com/anatomy_03.html

40. VisionRx, LLC. (2002) *Acute narrow angle glaucoma*. Available: http://www.visionrx.com/library/enc/enc_anaglaucoma.asp
41. Schacknow, P.N. and J.R. Samples (Ed). (2010). *The glaucoma book-a practical, evidence-based approach to patient care*. Chapter 1. Glaucoma in the Twenty-First Century, Ed. R.L.a.I. Goldberg, New York: Springer.
42. Haddrill, M. (2011) *Glaucoma surgery*. Available: <http://www.allaboutvision.com/conditions/glaucoma-surgery.htm>
43. Zhang, W., M.R. Prausnitz, and A. Edwards (2004), Model of transient drug diffusion across cornea. *J Control Release*, 99, 241-258.
44. Johansen, S., E. Rask Pedersen, and J.U. Prause (1996), An ocular bioavailability comparison in rabbits of prednisolone acetate after repeated topical applications formulated as a high-viscosity gel and as an aqueous suspension. *Acta Ophthalmol Scand*, 74, 259-264.
45. Marmor, M., A.Negi, and D. Maurice. (1985), Kinetics of macromolecules injected into the subretinal space. *Exp Eye Res.*, 40, 687-696.
46. Skuta, G.L. and R.K.I. Parrish (1987), Wound healing in glaucoma filtering surgery. *Surv Ophthalmol*, 32, 149-70.
47. Klink, T., *et al.* (2006), Postoperative care after glaucoma filtration surgery. *Ophthalmology*, 113, 815-826.
48. Uusitalo, H., *et al.* (2006), Improved systemic safety and risk-benefit ratio of topical 0.1% timolol hydrogel compared with 0.5% timolol aqueous solution in the treatment of glaucoma. *Graefes Arch Clin Exp Ophthalmol*, 244, 1491-1496.
49. Tan, D.T., *et al.* (1999), Randomized clinical trials of a new dexamethasone delivery system (Surodex) for treatment of post-cataract surgery inflammation. *Ophthalmology*, 106, 223-231.
50. Kodama, M., *et al.* (2003), Effect of a new dexamethasone-delivery system (Surodex) on experimental intraocular inflammation models. *Graefe's Arch Clin Exp Ophthalmol*, 241, 927-933.
51. Jaffe, G.J., P. Ashton, and P.A. Pearson (Ed). (2006). *Intraocular drug delivery*. Biodegradable Systems, Ed. Y.O. Hideya Kimura, New York: Taylor & Francis Group LLC.
52. DeCampos, *et al.* (2003), The effect of a PEG versus a chitosan coating on the interaction of drug colloidal carriers with the ocular mucosa. *Eur J Pharm Sci*, 20, 73-81.

53. Natarajan, J.V., *et al.* (2011), Sustained release of an anti-glaucoma drug: demonstration of efficacy of a liposomal formulation in the rabbit eye. *PLoS ONE*, 6, e24513.
54. Göpferich, A. (1996), Mechanisms of polymer degradation and erosion. *Biomaterials*, 17, 103-114.
55. Li, S. and M. Vert (Ed). (1999). *Biodegradable polymers: Polyesters*. Encyclopedia of Controlled Drug Delivery, Ed. Mathiowitz, (pp.71-93). New York: John Wiley & Sons.
56. Dexamethasone ophthalmic - Oculex: Surodex(R) (2002),. *Drugs in R&D*, 3, 152-153.
57. Thomson, H., *et al.* (2011), Optimisation of polymer scaffolds for retinal pigment epithelium (RPE) cell transplantation *British Journal of Ophthalmology* 95, 563-568.
58. Tamai, H., *et al.* (2000), Initial and 6-month results of biodegradable poly-l-lactic acid coronary stents in humans. *Circulation*, 102, 399-404.
59. Tsuji, H. (2008). *Degradation of poly (Lacide)-based biodegradable materials*. New York: Nova Science Publishers, Inc.
60. Domb, A.J., *et al.* (2002). Biodegradable polymers ad drug carrier systems, In S. Dumitriu(Ed. *Polymeric Biomaterials* (pp. 91-112). New York: Marcel Dekker
61. Amecke, B., D. Bendix, and G. Entenmann (1995). Synthetic resorbable polymers based on glycolide, lactides, and similar monomers, In D.L. Wise, et al.(Eds), *Encyclopedic handbook of biomaterials and bioengineering, part A: Materials* (pp. 977-1007). New York: Marcel Dekker
62. Szycher, M. (Ed). (1991). *Synthetic bioabsorbable polymers in high performance biomaterials*. Ed. T. Barrows, (pp.243-257). Technomic: Lancaste.
63. Lu, X.L., W. Cai, and Z.Y. Gao (2008), Shape-memory behaviors of biodegradable poly(L-lactide-co- ϵ -caprolactone) copolymers. *Journal of Applied Polymer Science*, 108, 1109-1115.
64. Cohn, D. and A.H. Salomon (2005), Designing biodegradable multiblock PCL/PLA thermoplastics elastomers. *Biomaterials*, 26, 2297-2305.
65. Burkersroda, F.v., S. Luise, and G. Achim (2002), Why degradable polymers undergo surface erosion or bulk erosion. *Biomaterials*, 23, 4221-4231.
66. Comyn, J. (Ed). (1985). *Polymer permeability*. London and New York: Elsevier Applied Science Publishers Ltd.

67. Fick, A. (1995), On liquid diffusion (reprinted from the London, Edinburgh, and Dublin Philosophical Magazine and Journal of Science, Vol 10, pg 30, 1855). *Journal of Membrane Science*, 100, 33-38.
68. Crank, J. (Ed). (1975). *The mathematics of diffusion*. Second ed., New York: Oxford University Press.
69. Ochoa-Martinez, C.I., H.S. Ramaswamy, and A.A. Ayala-Aponte (2009), Suitability of Crank's solutions to Fick's Second Law for water diffusivity calculation and moisture loss prediction in osmotic dehydration of fruits. *Journal of Food Processing Engineering*, 32, 933-943.
70. Baker, R. (1987). *Controlled release of biological active agents*. New York: John Wiley & Sons.
71. Paul, D.R. and S.K. McSpaden (1976), Diffusional release of a solute from a polymer matrix. *Journal of Membrane Science*, 1, 33-48.
72. Siepmann, J. and A. Gopferich (2001), Mathematical modeling of bioerodable, polymer drug delivery systems. *Advanced Drug Delivery Reviews*, 48, 229-247.
73. Charlier, A., B. Leclerc, and G. Couarraze (2000), Release of mifepristone from biodegradable matrices: experimental and theoretical evaluations *International Journal of Pharmaceutics*, 200, 115-120.
74. Arifin, D.Y., L.Y. Lee, and C.-H. Wang (2006), Mathematical modeling and simulation of drug release from microspheres: Implications to drug delivery systems. *Advanced Drug Delivery Reviews*, 58, 1274-1325.
75. Rothstein, S.N., W.J. Federspiel, and S.R. Little (2009), A unified mathematical model for the prediction of controlled release from surface and bulk eroding polymer matrices. *Biomaterials*, 30, 1657-1664.
76. Lao, L.L., S.S. Venkatraman, and N.A. Peppas (2008), Modeling of drug release from biodegradable polymer blends. *Eur J Pharm Biopharm*, 70, 796-803.
77. Lao, L.L., S.S. Venkatraman, and N.A. Peppas (2009), A novel model and experimental analysis of hydrophilic and hydrophobic agent release from biodegradable polymers *Journal of Biomedical Materials Research Part A*, 90A, 1054-1065.
78. Chen, Y., S. Zhou, and Q. Li (2011), Mathematical modeling of degradation for bulk-erosive polymers: Applications in tissue engineering scaffolds and drug delivery systems. *Acta Biomaterialia*, 7, 1140-1149.
79. Panagiotis, A.T. (Ed). (2008). *Animal models in eye research*. (pp.184-204). Elsevier Ltd.

80. See, J.L.S., *et al.* (2007), Changes in anterior segment morphology in response to illumination and after laser iridotomy in Asian eyes: an anterior segment OCT study. *British Journal of Ophthalmology*, 91, 1485-1489
81. Singh, M., *et al.* (2007), Imaging of trabeculectomy blebs using anterior segment optical coherence tomography. *Ophthalmology*, 114, 47-53.
82. Ramos, J.L., Y. Li, and D. Huang (2009), Clinical and research applications of anterior segment optical coherence tomography - a review. *Clinical & Experimental Ophthalmology*, 31, 81-89.
83. Huizinga, A., *et al.* (1989), Local variation in absolute water content of human and rabbit eye lenses measured by raman microspectroscopy. *Experimental Eye Research*, 48, 487-496.
84. Cordeiro, M.F., J.A. Gay, and P.T. Khaw (1999), Human anti-transforming growth factor-beta2 antibody: a new glaucoma anti-scarring agent. *Invest Ophthalmol Vis Sci*, 40, 2225-34.
85. Li, S.M. and S. McCarthy (1999), Influence of crystallinity and stereochemistry on the enzymatic degradation of poly(lactide)s. *Macromolecules*, 32, 4454-4456.
86. Pitt, C.G., *et al.* (1981), Aliphatic polyesters. I. The degradation of poly(ϵ -caprolactone) in vivo. *Journal of Applied Polymer Science*, 26, 3779-3787.
87. Kranz, H., *et al.* (2000), Physicomechanical properties of biodegradable poly(D,L-lactide) and poly(D,L-lactide-co-glycolide) films in the dry and wet states. *Journal of Pharmaceutical sciences*, 89, 1558-1566.
88. Zhang, Y., *et al.* (1997), Effects of metal salts on poly(DL-lactide-co-glycolide) polymer hydrolysis. *Journal of Biomedical Materials Research*, 34, 531-538.
89. Steele, T.W.J., *et al.* (2011), The effect of polyethylene glycol structure on paclitaxel drug release and mechanical properties of PLGA thin films *Acta Biomaterialia*, 7, 1973-1983.
90. Zhu, Y., *et al.* (2006), Protein bonding on biodegradable poly(L-lactide-co-caprolactone) membrane for esophageal tissue engineering. *Biomaterials*, 27, 68-78.
91. Perego, G., *et al.* (1994), Preparation of a new nerve guide from a poly(l-lactide-co-6-caprolactone) *Biomaterials*, 15, 189-193.
92. Lee, V.H., R. Stratford, and W.M. Kim (1983), Age-related changes in esterase activity in rabbit eyes. *International Journal of Pharmaceutics*, 13, 183-195.

93. Houchin, M. and E.M. Topp (2008), Chemical degradation of peptides and proteins in PLGA: a review of reactions and mechanisms. *Journal of Pharmaceutical Sciences*, 97, 2395-2404.
94. Grizzi, I., *et al.* (1995), Hydrolytic degradation of devices based on poly(-lactic acid) size-dependence. *Biomaterials*, 16, 305-311.
95. Witt, C. and T. Kissel (2001), Morphological characterization of microspheres, films and implants prepared from poly(lactide-co-glycolide) and ABA triblock copolymers: is the erosion controlled by degradation, swelling or diffusion? *European Journal of Pharmaceutics and Biopharmaceutics*, 51, 171-181.
96. Antheunis, H., *et al.* (2010), Autocatalytic equation describing the change in molecular weight during hydrolytic degradation of aliphatic polyesters. *Biomacromolecules*, 11, 1118-1124.
97. Lee, V.H.L., *et al.* (1985), Ocular esterase composition in albino and pigmented rabbits-possible implications in ocular prodrug design and evaluation *Current Eye Research*, 4, 1117-1125.
98. Çokuğraş, A.N. (2003), Butyrylcholinesterase: structure and physiological importance. *Turkish Journal of Biochemistry*, 28, 54-61.
99. Elias, H.G. (1997). *An introduction to polymer science*. New York: VCH mbH.
100. Malin, M., *et al.* (1996), Biodegradable lactone copolymers .2. Hydrolytic study of epsilon-caprolactone and lactide copolymers *Journal of applied polymer science* 59, 1289-1298
101. Duda, J.L., *et al.* (1982), Prediction of diffusion-coefficients for polymer-solvent systems. *Aiche Journal*, 28, 279-287.
102. Yoon, J.S., *et al.* (2000), Diffusion coefficient and equilibrium solubility of water molecules in biodegradable polymers. *Journal of Applied Polymer Science*, 77, 1716-1722.
103. Candia, O.A., L.J. Alvarez, and A.C. Zamudio (2006), Regulation of water permeability in rabbit conjunctival epithelium by anisotonic conditions. *American Journal of Physiology-Cell Physiology*, 290, 1168-1178.
104. Candia, O.A. and L.J. Alvarez (2008), Fluid transport phenomena in ocular epithelia. *Progress in Retinal and Eye Research*, 27, 197-212
105. Li, Y., *et al.* (2001), Rabbit conjunctival epithelium transports fluid, and P2Y22 receptor agonists stimulate Cl⁻ and fluid secretion. *American Journal of Physiology-Cell Physiology*, 281, 595-602.

106. Peng, Y., *et al.* (2011), Biocompatibility and biodegradation studies of subconjunctival implants in rabbit eyes. *PLoS ONE*, 6, e22507.
107. Huuskonen, J., M. Salo, and J. Taskinen (1998), Aqueous solubility prediction of drugs based on molecular topology and neural network modeling. *Journal of Chemical Information and Computer Sciences*, 38, 450-456.
108. Ctierke, T.D. and W.Y. Hsu (1982), The cluster-network of ion clustering in perfluorsulfonated membranes. in *Perfluorinated Ionomer Membranes*. Washington DC: American Chemical Society.
109. Heller, J. and R.W. Baker (1980). Theory and practice of controlled drug delivery from bioerodible polymers, In R.W. Baker(Ed. *Controlled Release of Bioactive Materials* (pp. 1). New York: Academic
110. Thom J. Zimmerman, K.S.K. (Ed). (2001). *Clinical pathways in glaucoma*. (pp.457-481). Thieme New York.
111. Johansen, S., E. RaskPedersen, and J.U. Prause (1996), An ocular bioavailability comparison in rabbits of prednisolone acetate after repeated topical applications formulated as a high-viscosity gel and as an aqueous suspension. *Acta Ophthalmologica Scandinavica*, 74, 259-264.
112. Ang, M., *et al.* (2011), Evaluation of sustained release of PLC-loaded prednisolone acetate microfilm on postoperative inflammation in an experimental model of glaucoma filtration surgery. *Current Eye Research*, 36, 1123-1128.
113. Rothstein, S.N., W.J. Federspiel, and S.R. Little (2008), A simple model framework for the prediction of controlled release from bulk eroding polymer matrices. *Journal of Materials Chemistry*, 18, 1873-1880.
114. Pitt, C.G. (1990). Poly- ϵ -caprolactone and its copolymers, In M. Chasin and R. Langer(Eds), *Biodegradable Polymers as Drug Delivery Systems* (pp. 71-120). New York: Marcel Dekker
115. Ohtori, A. and K. Tojo (1994), In-vivo in-vitro correlation of intravitreal delivery of drugs with the help of computer simulation. *Biological & pharmaceutical Bulletin*, 17, 283-290.
116. Tojo, K. and A. Isowaki (2001), Pharmacokinetic model for in vivo / in vitro correlation of intravitreal drug delivery. *Advanced Drug Delivery Reviews*, 52, 17-24.

117. Lee, Y.-C. and S.H. Yalkowsky (1999), Ocular devices for the controlled systemic delivery of insulin: in vitro and in vivo dissolution. *International Journal of Pharmaceutics*, 181, 71-77.